DANISH METEOROLOGICAL INSTITUTE

SCIENTIFIC REPORT

01-01

Northern Polar Cap magnetic activity index PCN: Effective area, universal time, seasonal and solar cycle variations

By

V. O. Papitashvili, L. I. Gromova, V. A. Popov, and O. Rasmussen

COPENHAGEN 2001

Danish Meteorological Institute, Solar-Terrestrial Physics Division,
Lyngbyvej 100, DK-2100 Copenhagen Ø, Denmark

ISSN-Nr. 0905-3263
ISSN-Nr. 1399-1949 (Online)
ISBN-Nr. 87-7478-432-3

Northern Polar Cap magnetic activity index PCN: Effective area, universal time, seasonal and solar cycle variations

V. O. Papitashvili [1,2], L. I. Gromova [3], V. A. Popov [3], and O. Rasmussen [1]

[1] *Solar-Terrestrial Division, Danish Meteorological Institute, Copenhagen, Denmark*

[2] *Space Physics Research Laboratory, University of Michigan, Ann Arbor, Michigan, U.S.A.*

[3] *Institute of Terrestrial Magnetism, Ionosphere and Radio Wave Propagation, Moscow, Russia*

Abstract

In this study, we investigated the effective area and various variations (universal time, seasonal, and solar cycle) of the northern polar cap magnetic activity index PCN. These variations are also studied in the parameters used for derivation of the index: preferred directions of the transpolar ionospheric current and normalization coefficients (slope and intercept) obtained from correlation analyses of ground geomagnetic observations at Qaanaaq (former Thule, THL, Greenland) with the "merging" interplanetary electric field. Currently PCN is calculated from a set of above-mentioned coefficients obtained for years 1977–1980 and combined monthly to increase statistics.

We analyzed solar cycle variations in the preferred directions and normalization coefficients obtained for Qaanaaq from 1965 to 1998 (i.e., for all years with available interplanetary data) combining data monthly for three consecutive years and using a 3-year "moving window". The obtained results show that the solar cycle effect is clearly seen in the studied parameters amounting from 20% to 40% of the magnitude. We also calculated similar sets of coefficients and computed the "station-based" indices (using 20-sec geomagnetic field observations from 1991 to 1999 and combining data monthly for three consecutive years) for most of high-latitude Greenlandic magnetometers located at the west and east coasts. We found that the behavior of these coefficients and PCN_{sta} indices are somewhat similar for the northernmost stations through an entire UT day; however, only 3–4 stations equatorward of Qaanaaq (that is, Savissivik, Kullorsuaq, Upernavik, and Nord) produce comparable (to PCN_{THL}) index. The PCN_{THL} and PCN_{SVS} are almost identical, but other listed stations produce the PCN_{THL}-like index only during wintertime or over few nighttime hours. However, to be on sure ground with the PCN routine calculations, we recommend limiting the PCN index effective area to a circular area of 20° in diameter, centered at the northern corrected geomagnetic pole. In case the geomagnetic data from Qaanaaq are inadvertently lost, we recommend using only the data recorded at the Greenland West Coast station Savissivik as a backup for the standard PCN replacement.

Content

1. Introduction

The International Association of Geomagnetism and Aeronomy (http://www.ngdc.noaa.gov/IAGA/) officially supports (through the International Service of Geomagnetic Indices, http://www.cetp.ipsl.fr/~isgi/homepag1.htm) a number of indices suggested for appropriate rating of global geomagnetic activity; that rating is needed for scientific studies as well as for a number of practical applications. For example, the IAGA 3-hr Kp index rates the planetary geomagnetic activity; the hourly Dst index follows dynamics of the magnetospheric ring current identifying magnetic storms; the 1-min "auroral electrojet" indices AE, AL, and AU characterize geomagnetic activity at auroral latitudes indicating development of magnetic substorms in the northern hemisphere.

Fairfield [1968] found that geomagnetic activity in the northern polar cap (defined as a maximum perturbation in the horizontal magnetic field components measured at the magnetic observatories Alert, Mould Bay, and Resolute Bay) sometimes increases slightly before changes in the AE index. He suggested that this "magnetic activity magnitude" might be a better indicator of the overall high-latitude magnetic activity since it is less likely to be affected by spatial variations; in contrary to the uneven spatial distribution of AE stations. Although this approach has been used in some studies [e.g., *Kokubun et al.,* 1972], the index has never been derived routinely. Later *Saroso et al*. [1992], *Maclennan et al.* [1997], and *Ballatore et al.* [1998; 1999] introduced the AE-like index derived from magnetic disturbances recorded near −80° of corrected geomagnetic latitude (http://nssdc.gsfc.nasa.gov/space/cgm) [*Gustafsson et al*., 1992].

Troshichev et al. [1979, 1988] introduced the polar cap (PC) magnetic activity index widely used today, which is derived from geomagnetic data recorded at a single near-pole station. A major motivation for developing this index was to quantify magnetic disturbances caused by a sunward, transpolar portion of the standard two-cell ionospheric Hall current system, in other words, the ionospheric DP2 non-substorm current system. Therefore, the PC index can be regarded as a measure of high-latitude, transpolar convection electric fields generated by coupling of the solar wind and interplanetary magnetic field (IMF) with the Earth's magnetosphere.

Vennerstrøm et al. [1991] suggested another possible source of the near-pole magnetic disturbances: a distant effect of field-aligned currents (FAC) located at the poleward boundary of the auroral oval. They hypothesized that because during summer the ionospheric conductivity in the sunlit, near-pole area is mainly produced by the solar ultraviolet radiation, a dominant source of the near-pole ground magnetic disturbances would be the ionospheric Hall currents. However, the magnetic effect from the distant field-aligned currents can dominate in the dark, winter hemisphere because conductivity becomes too low to support any substantial ionospheric current. *Vassiliadis et al.* [1996] and *Chun et al.* [1999] also refer to such additional contributions to the PC index.

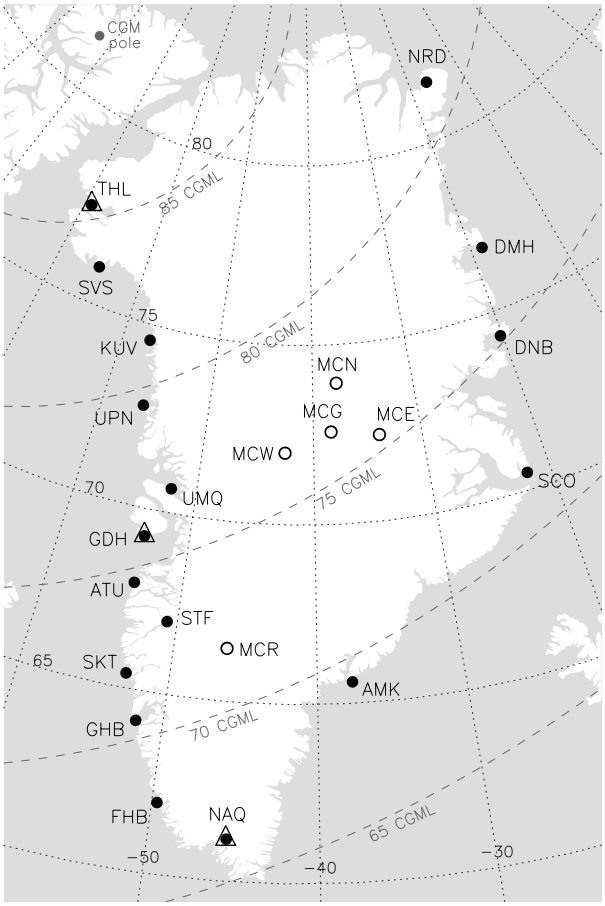

Figure 1. The standard magnetic observatories (triangles) and a number of variation stations deployed in Greenland by DMI (filled circles) and SPRL, University of Michigan (open circles). *Courtesy of Jurgen Watermann*

Because of apparent differences in ionospheric conductivities of the winter and summer polar caps, two standard magnetic observatories, Thule (THL, now Qaanaaq, **Figure 1**) in Greenland and Vostok (VOS) in Antarctica, were suggested for simultaneous derivation of the PCN and PCS indices [e.g., *Troshichev et al*., 1991; *Vennerstrøm et al.,* 1994]. Initially the time resolution was proposed to be 15-min; recently the resolution was increased to 1-min. The PCN index from Qaanaaq (Thule) is now routinely available from the Danish Meteorological Institute (DMI, Copenhagen, http://www.dmi.dk/projects/wdcc1/pcn/pcn.html); the Russian Arctic and Antarctic Research Institute (AARI, St. Petersburg, http://www.aari.nw.ru/clgmi/geophys/pc_Data_2.html) produces the PCS index from Vostok. In 1999, the International Association of Geomagnetism and Aeronomy adopted the PC index as the official IAGA index for measuring of magnetic activity in the polar caps and recommended continuing its derivation for the northern and southern polar caps [*Troshichev et al.*, 2001; http://www.cetp.ipsl.fr/~isgi/homepag1.htm].

However, since the first inception of PC index, geomagnetic data from few more stations in the near-pole regions have become available. **Table 1** lists magnetic stations that are located above 80° CGM latitudes in both the northern and southern polar caps; two stations, Eureka and Concordia, are located near the corresponding corrected geomagnetic poles. Geomagnetic data from all these stations can be utilized to investigate morphology and dynamics of the near-pole ionospheric currents, as well as in validating the PC_{sta} index calculated from data recorded at different stations.

Therefore, the main goal of our study was three-fold. First, we investigated the PCN index currently derived from 1-min digital geomagnetic data recorded at the standard magnetic observatory Qaanaaq (Thule). This index is routinely calculated at DMI since the end of 1980s using computer codes and normalization coefficients developed by *Vennerstrøm* [1991]. Although a number of various studies of PC index have been undertaken, here we address the universal time (UT), seasonal, and solar cycle effects in the routinely calculated index PCN.

Table 1. Near-pole geomagnetic stations in the northern and southern polar caps

Epoch 2000 Station name	Code	CGM/Geocentric Lat.°	CGM/Geocentric Long.°	MLT Noon	Epoch 2000 Station name	Code	CGM/Geocentric Lat.°	CGM/Geocentric Long.°	MLT Noon
Eureka	EUR	88.48 80.00	327.93 274.10	18:48	Concordia	CRD	−88.73 −75.10	56.61 123.40	00:51
Alert	ALE	87.06 82.50	99.79 297.65	09:44	AGO P5	AP5	−86.74 −77.24	30.82 123.52	14:47
Qaanaaq	THL	85.30 77.47	33.93 290.77	15:01	AGO P6	AP6	−84.85 −69.51	214.84 130.03	02:29
Savissivik	SVS	83.55 76.02	34.83 294.90	14:48	Vostok	VOS	−83.44 −78.46	55.20 106.83	13:00
Resolute Bay	RES	83.37 74.69	319.47 265.11	19:16	Casey	CSY	−80.72 −66.28	156.48 110.53	06:29
Kullorsuaq	KUV	81.16 74.57	43.60 302.82	14:09	Dumont d'Urville	DRV	−80.47 −66.67	235.57 140.02	00:56
Mould Bay	MBC	81.03 76.32	273.37 240.64	22:21	AGO P1	AP1	−80.13 −83.86	17.45 129.61	15:43
Nord	NRD	81.02 81.60	104.97 343.33	09:20	Terra Nova	TNB	−80.03 −74.69	307.20 164.12	20:09

Second, we investigated the UT, seasonal and solar cycle variations in the index's normalization coefficients (slopes and intercepts) obtained from correlations of Thule's magnetometer data with the interplanetary parameters for each UT hour through the 20–22 solar activity cycles (1965−1998). We also developed a new computer code for the PCN calculations where the solar cycle effect is taken into account.

Third, utilizing an approach applied to the geomagnetic data from Qaanaaq (THL), we calculated the "station-based" PCN_{sta} index from the data recorded at all Greenland West Coast magnetometers, stretched along ~40° geomagnetic meridian from 86° to 66° CGM latitudes (see http://www.dmi.dk/projects/chain/ for geographic and geomagnetic coordinates of these stations). This allowed us to determine with greater spatial resolution a boundary between the areas where the PCN index stably preserves a value and where the PCN index becomes invalid. The obtained results might be helpful in defining robustness and reliability of the PCN index for immediate benefits of various practical applications, especially in the light of recently introduced "space weather" initiatives.

2. Method

An algorithm used to derive the PC index is based on a statistical analysis of relationships between variations in the interplanetary parameters and ground geomagnetic perturbations observed near the corrected geomagnetic pole. Since any near-pole station is located under the sunward, transpolar portion of two-cell ionospheric current system DP2, the observed magnetic perturbation vectors ΔF point approxi-

mately towards dusk while DP2 is not significantly distorted by some other current sources. The direction of DP2 transpolar current is slightly skewed with respect to a noon-midnight meridian due to gradients in the ionospheric conductivity between the auroral zone and polar cap [e.g., *Papitashvili et al.,* 1994].

Troshichev and Andrezen [1985] have shown that ground geomagnetic disturbances measured at a single near-pole station highly correlate ($r > 0.8$) with the "merging" interplanetary electric field E_m constantly applied to the Earth's magnetosphere [*Kan and Lee,* 1979]:

$$E_m = V_{SW}\, B_T \sin^2(\theta/2) = V_{SW}\, (B_y^2 + B_z^2)^{1/2} \sin^2(\theta/2) \qquad (1)$$

Here V_{SW} is the solar wind velocity, B_y and B_z are the IMF azimuthal and vertical components, respectively, and θ is the IMF "clock-angle" measured between the Earth's magnetic field vector and B_T.

Following *Vennerstrøm* [1991], we write the transverse magnetic perturbation at the Earth's surface caused by the DP2 transpolar current as:

$$\Delta F_{PC} = \Delta H \sin\gamma \pm \Delta D \cos\gamma \qquad (2)$$

where $\gamma = \lambda \pm D_E + \varphi + UT\cdot 15°$. Here ΔH and ΔD are deviations in the ground horizontal H and D magnetic field components from the pre-selected "quiet level", D_E is the station's average declination angle, λ is its geographical longitude, and φ is the UT-dependent angle between the DP2 transpolar current and the noon-midnight meridian. The signs "+"and "–" are used for data from Vostok and Qaanaaq, respectively. For Qaanaaq, an appropriate daily "quiet level" is deduced from interpolation between the magnetic field's absolute values determined at nighttime hours of quiet winter days in the two consecutive years [*Vennerstrøm et al.,* 1994]. The "quiet level" for Vostok is determined from quiet days for the examined month [*Troshichev et al.,* 2001].

The "optimal direction" angle φ is obtained through a correlation analysis relating E_m and horizontal magnetic perturbations projected on various directions; such the direction where correlation is maximal is then used for the index derivation during a given UT day; it was found that these optimal directions vary with UT and season. The projected horizontal perturbation ΔF_{PC} should be normalized with respect to E_m:

$$\Delta F_{PC} = \alpha\cdot E_m + \beta \qquad \text{and} \qquad PC = (\Delta F_{PC} - \beta) / \alpha\cdot\eta \qquad (3)$$

Here α (slope) and β (intercept) are functions of magnetic local time (MLT) and month, $\eta = 1$ mV/m is a normalization coefficient required to make the PC index dimensionless.

The PCN index is currently calculated from a set of 12 (months) by 24 (hourly) values of the coefficients α and β, and angles φ. These coefficients were independently determined for Thule and Vostok combining data monthly over four years 1977–1980, that is, for a period with good coverage by the IMF and solar wind data. As an example, **Figure 2** (left panel) shows optimal directions obtained at Vostok

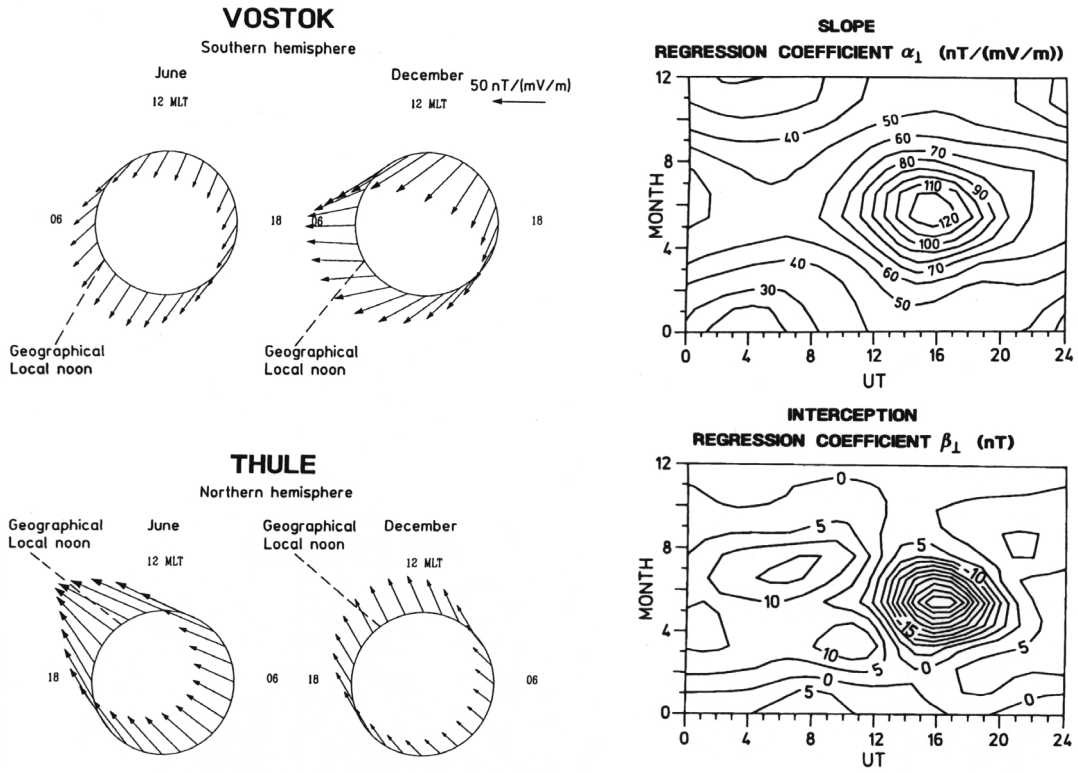

Figure 2. Left panel: The CGM latitude – MLT diagram of optimal directions for June and December, obtained from Eqs. (2–3) at Vostok and Thule. Right panel: Dependence of the regression coefficients α and β on the UT hour and month obtained from Eq. (3) for Thule. [After *Vennerstrøm et al.,* 1994].

and Thule for June and December, respectively, where the vectors' magnitude equals to $\Delta F = \alpha + \beta$, being normalized to E_m = 1 mV/m. The contour plots of coefficients α and β obtained for Thule as a function of the month and UT hour are shown in the right panel of **Figure 2.**

As seen from the latter plot, the magnetic disturbances at Thule correlate better with E_m during near-noon MLT hours (1300–1900 UT) in summer. However, during summer the sunward (reverse) ionospheric convection caused by the northward orientation of IMF can significantly distort the DP2 system, sometime reversing the sign of PC index from positive to negative values; this affects the PC index capabilities in estimating variations of E_m. *Troshichev et al.* [1988] and *Vennerstrøm et al.* [1991] showed that the PC and AE indices correlate better during winter and equinoctial months, though the ionospheric conductivity in the center of the dark polar cap is reduced. Considering these facts, it was suggested to derive the PCN and PCS indices simultaneously from geomagnetic data of Thule and Vostok.

3. Initial analysis

A small data file with carefully defined winter quiet levels for all geomagnetic field components at Thule is maintained by DMI being updated every year (`qwdthl.dat`, see **Table 2** where this file is printed as it is). These data are used for linear interpolation of the quiet level (between January 1 of two

consecutive years) to a given UT day, needed for calculations of ΔF in Eq. (2). Since more than ten years passed when *Vennerstrøm* [1991] worked on her thesis at DMI, we were unable to locate the original 15-min datasets and computer codes used for correlations of the ground and interplanetary data. However, the hourly averaged, smoothed set of normalization coefficients (described in the previous section) is still available at DMI (`coef24g3.dat`, http://web.dmi.dk/projects/wdcc1/pcn/coef24g3.txt). These two DAT files are essential for the routine, day-to-day calculations of the PCN index.

During the decade, the FORTRAN code `pcday.for` developed by Susanne Vennerstrøm has been used for computations of the 15-min PCN index from 1-min Thule standard magnetic observatory data under the MS DOS computer operation system. As we began our study, we decided to modify this code for continuing production of the standard 15-min PCN index, but also for increasing the PCN index resolution to 1-minute; to match the latter with the southern PCS index derived at AARI (http://www.aari.ru/clgmi/geophys/pc_Data_2.html). However, in February 2000, we discovered a minor typo in the used code `pcday.for` – the round-o'clock loop (where the hourly normalization coefficients are interpolated through a UT day to obtain 15-min resolution) was fixed in the code to the last UT hour. This typo forced only a single value of each parameter (that is, the optimal direction angle, slope, and intercept) to be taken for calculations of the index through the entire UT day, causing introduction of an artificial UT variation in the calculated PCN index values for 1975–1999 and for the first two months of the year 2000.

Table 2. Winter quiet levels for various geomagnetic components selected for Thule from 1973 to 2001

Year	D°	I°	H, nT	X, nT	Y, nT	Z, nT	T, nT	
1973.0	282.250	86.018	3936	835	-3846	56543	56680	
1974.0	282.550	86.024	3934	855	-3840	56596	56733	
1975.0	282.917	86.030	3931	879	-3832	56638	56774	
1976.0	283.333	86.034	3929	906	-3823	56664	56800	
1977.0	283.800	86.036	3928	937	-3815	56681	56817	
1978.0	284.333	86.038	3926	972	-3804	56690	56826	
1979.0	284.833	86.037	3927	1005	-3796	56691	56827	
1980.0	285.267	86.033	3930	1035	-3791	56676	56812	
1981.0	285.667	86.032	3930	1061	-3784	56655	56791	
1982.0	286.033	86.034	3927	1085	-3774	56640	56776	
1983.0	286.350	86.035	3925	1105	-3766	56622	56758	
1984.0	286.667	86.038	3919	1124	-3754	56582	56718	
1985.0	286.983	86.046	3909	1142	-3739	56555	56690	
1986.0	287.300	86.054	3899	1159	-3723	56520	56654	
1987.0	287.700	86.062	3888	1182	-3704	56486	56620	
1988.0	288.067	86.071	3878	1203	-3687	56465	56598	
1989.0	288.450	86.073	3875	1226	-3676	56447	56580	
1990.0	289.050	86.084	3863	1261	-3651	56430	56562	
1991.0	289.417	86.089	3856	1282	-3637	56400	56532	
1992.0	289.917	86.090	3855	1313	-3624	56395	56527	
1993.0	290.467	86.089	3853	1347	-3610	56362	56494	
1994.0	291.083	86.093	3848	1384	-3590	56350	56481	
1995.0	291.850	86.090	3850	1433	-3573	56335	56466	
1996.0	292.567	86.097	3842	1474	-3548	56315	56446	
1997.0	293.433	86.090	3848	1530	-3531	56304	56435	
1998.0	294.333	86.088	3850	1586	-3508	56300	56431	
1999.0	295.333	86.077	3862	1652	-3491	56310	56442	
2000.0	296.333	86.060	3878	1720	-3476	56310	56443	
2001.0	297.333	86.049	3890	1786	-3456	56315	56449	preliminary

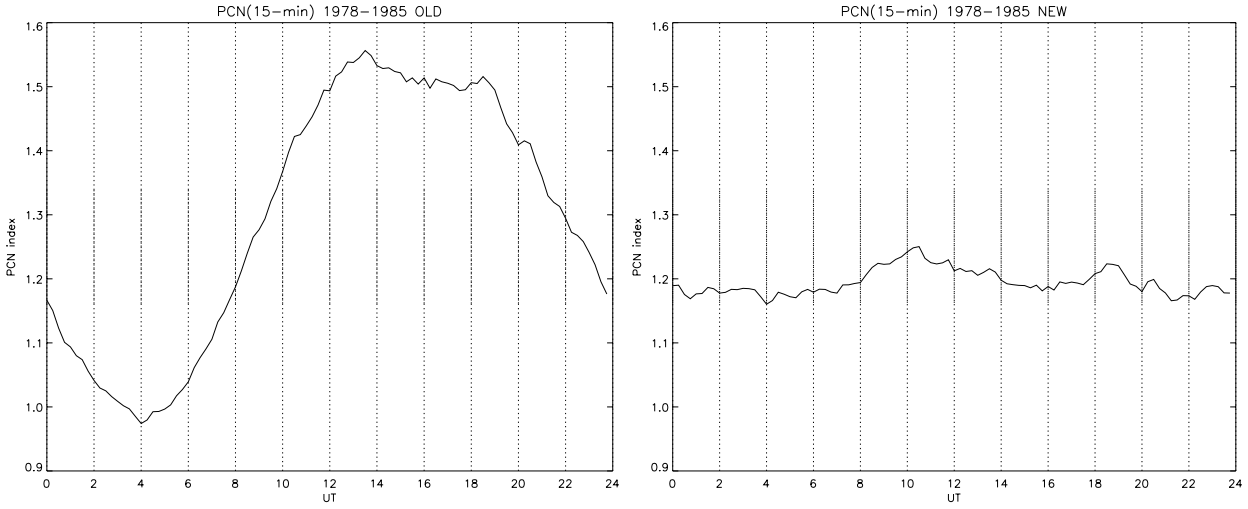

Figure 3. The universal time (UT) variation of PCN index averaged for 1978–1985. Left panel – the averaged old PCN index (*courtesy of Kalevi Mursula*), calculated with a minor typo in the computer code; right panel – the averaged new PCN index calculated after the typo was corrected.

Dr. Kalevi Mursula (University of Oulu, Finland) brought to our attention a graph where the PCN index, being averaged over eight years, from 1978 to 1985, shows a pronounced UT variation. **Figure 3** (left panel) shows that graph; one can see there that the UT variation accounts for ~50% of the average index magnitude. Although this UT variation was not obviously seen in the PCN daily or monthly graphs [e.g., *Troshichev et al.,* 1991; *Vennerstrøm et al.,* 1994], we guessed that the above-mentioned typo in the computer code caused this variation. Therefore, we recalculated the PCN index time series from 1975 to 2000, using the new, corrected code `pcday.for`. **Figure 3**, right panel, shows the recalculated PCN index averaged for the same eight years, 1978–1980. As seen, the UT variation is now eliminated; the daily averaged mean of PCN_{1978_1980} is ~1.20 and the index varies less than 10% of the total magnitude.

In **Figure 4** (top left panel), we plot a yearlong time-series of optimal directions (as the azimuth from magnetic north) and normalization coefficients (slope and intercept) from the file `coef24g3.dat` (note that we mark below all plots as "DMI" if calculations are made by using this file of normalization coefficients). The bottom left panel shows same parameters plotted in the CGM Latitude–MLT coordinates for each month. Here we remind the reader again that these parameters were obtained by *Vennerstrøm* [1991] for Thule by correlating the 15-min averaged ground horizontal magnetic disturbances ΔF with the 15-min averaged "merging" interplanetary electric fields E_m, combined monthly over four years 1977–1980. It seems that the obtained 15-min coefficients α and β were then averaged over an hour and smoothed by a 3-point "moving window" through entire year. This set of 12 (months) by 24 (hourly) normalization coefficients is used at DMI for routine calculations of PCN index from 1975 to present (see details at http://web.dmi.dk/projects/wdcc1/pcn/pcn.html).

Figure 4 (top left panel) shows that daily variations in the optimal directions are of the same order through the entire year. The slope shows UT variations that change significantly through the year having a

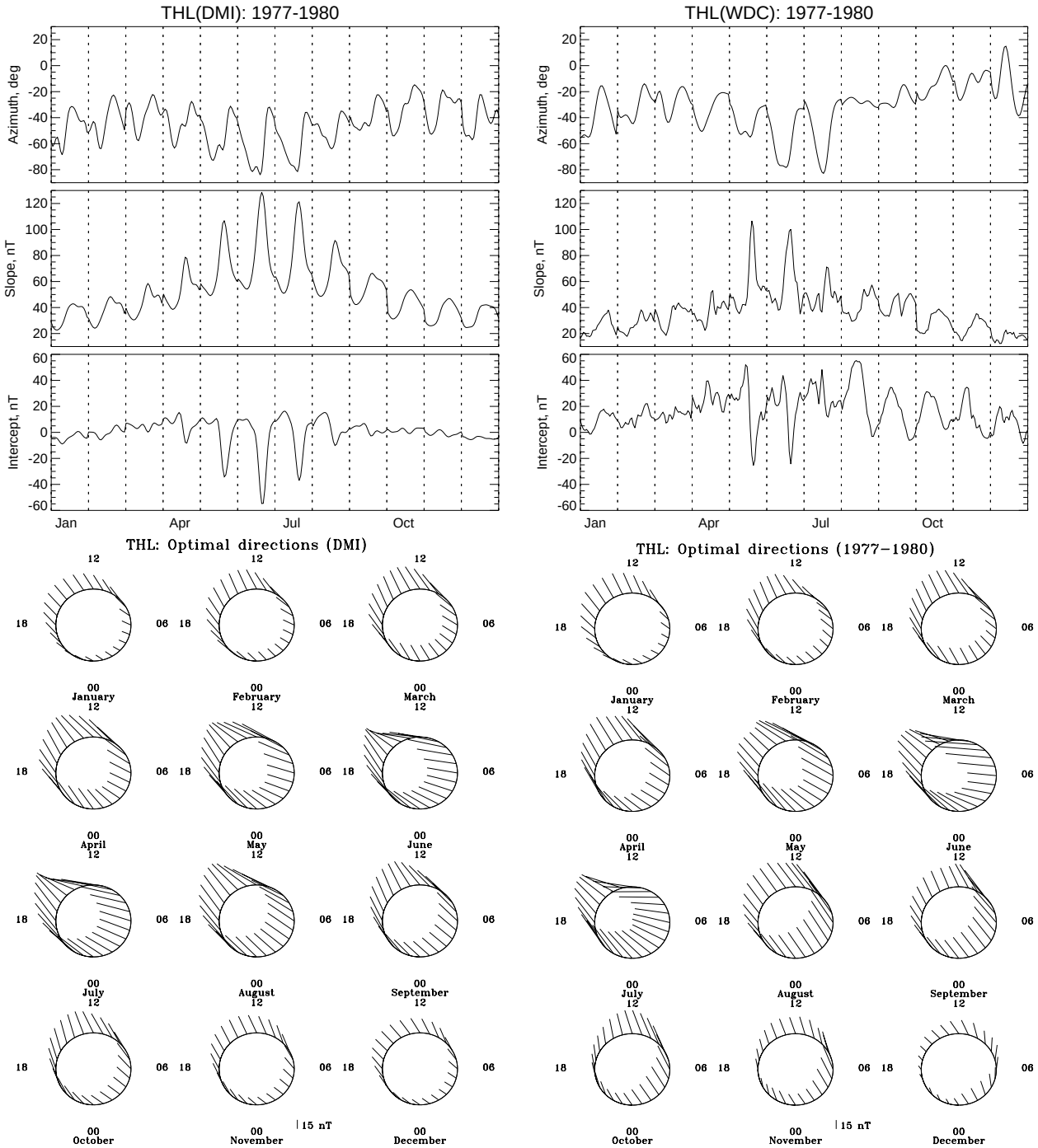

Figure 4. Time series of the optimal direction angle (azimuth from magnetic north), slope, and intercept for Thule (top row) obtained by *Vennerstrøm* [1991] from a set of 15-min data combined monthly for 1977–1980 (left panel) and recalculated for this study from Thule's absolute hourly means and corresponding quiet level interpolated between two consecutive winters (right panel). The bottom row shows same data plotted as the CGM Latitude–MLT diagrams of magnetic disturbance vectors ΔF along the optimal directions at each MLT = UT − 3 hour. The vector magnitude $\Delta F = \alpha + \beta$ is normalized to $E_m = 1$ mV/m (see text for details).

maximum in summer; daily variations are also seen in the intercept parameter but only during summer months. Changes in the ΔF response (i.e., slope) with a season are caused by an increase of ionospheric conductivity in the sunlit polar cap during summer months; however, the cause of a huge increase in the UT variation of intercept during summer months is still unclear to us. One can see that the intercept values maintain near-zero level in winter and equinox, but the intercept values change almost to –60 nT through the UT day between May and August.

Unfortunately, as we mentioned above, in re-developing a set of computer codes for this study, we were unable to locate the original set of geomagnetic data from Thule and corresponding 15-min IMF dataset for 1977-1980 used specifically for obtaining the file `coef24g3.dat`. Therefore, we recalculated optimal direction angles and normalization coefficients (slope and intercept) following the method developed by *Vennerstrøm* [1991] and described here in **Section 2**, but correlating hourly means of the ground and interplanetary data combined monthly for the same years 1977–1980. In our analysis, we used absolute 1-hr means of geomagnetic field components H and D from Thule (obtained through the DMI's World Data Center for Geomagnetism in Copenhagen) and utilized the same data file `qwdthl.dat` (**Table 2**) for interpolation of quiet levels through a given year. The obtained magnetic disturbances ΔF were correlated with the interplanetary electric field E_m calculated from the NSSDC OMNI dataset [*Cousens and King*, 1986; http://nssdc.gsfc.nasa.gov/omniweb/]. The right panel in **Figure 4** shows our newly calculated parameters in the same format as for the file `coef24g3.dat` (note that we mark below all plots as "WDC" if calculations are made by using this new, "hourly mean" technique).

The most striking observation here is that the polar diagrams of optimal directions and normalization coefficients are almost identical on both the left and right bottom plots, but the time series (top row) show some differences. The vectors' azimuths, obtained from these two techniques, behave similarly, mainly pointing in the same direction and showing UT variations of comparable magnitude. Seasonal variations in the slope parameter are also similar on both panels, showing comparable responses in the magnitude but somewhat less significant UT variations during summer months. The most different feature in these plots is the intercept parameter; its new average level differs by ~20 nT from the old calculations and the newly obtained values show recognizable UT variations not only during the summer months but rather through the entire year. Nevertheless, the bottom row of dial plots boldly shows that there is not much difference in the combined responses (that is, slope plus intercept as required by Eq. 3) of the ground geomagnetic field to the changes in E_m obtained ten years ago and in this study.

Therefore, we conclude that our attempt in obtaining correlations of the ground magnetic data from Thule with the interplanetary parameters by using hourly means (combined monthly for three consecutive years) is a valid approach. This allowed us to expand the PCN study in time through the solar cycles 21–23 (1975–1999) and spatially over the west and east coast chains of Greenland magnetometers.

4. Analysis of the current PCN index

4.1 PCN universal time variations

As seen in **Figure 3** (right panel), currently available time series of the PCN index do not show the UT variation if averaged over eight years. However, we note that the averaging procedure used for this plot mixes all (positive and negative) PCN values together, which we believe has no physical sense. As shown in **Section 2**, different physical mechanisms cause the standard (positive PCN) and reverse (negative PCN) currents over the station in the polar ionosphere [e.g., *Troshichev et al.*, 2000]. The positive PCN index is a measure of the dawn-dusk ionospheric electric fields, related to the southward IMF conditions; the negative PCN values are mainly recorded during northward IMF conditions.

Figure 5 shows the UT variation plot where we averaged the PCN index over 25 years, from 1975 through 1999. Here we did the averaging separately for all its positive values (bold solid line) and for all its negative values (thin bottom line). In addition, we split PCN for the quiet ($0 \le$ PCN ≤ 2.5) and disturbed (PCN > 2.5) conditions (see the corresponding thin lines on the plot).

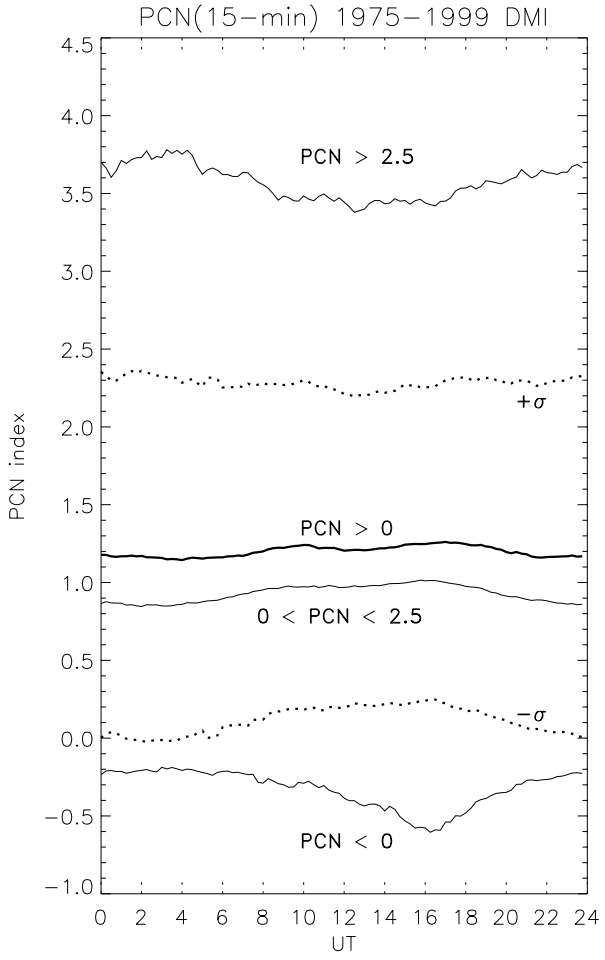

Figure 5. The UT variation of PCN index averaged in every 15-min interval over 1975–1999 for all positive values (bold solid line); the $\pm\sigma$ standard deviation is shown by two dotted lines. Three thin lines show the averaged PCN index within the corresponding ranges.

This plot can be compared with the UT variation in the auroral electrojet indices AL and AU, investigated by *Ahn et al*. [2000a, Figure 1]; one can see that AL/AU indices do not show the UT variation during quiet times. The AL index shows the pronounced UT variation for disturbed times, where occurrences of higher activity peak near 1200–1800 UT. **Figure 5** shows slightly higher positive PCN values (bold solid curve) over the same time interval 1000–1800 UT; the negative PCN curve dips near magnetic noon (1500 UT). However, the averaged "disturbed time" PCN values are lower during the magnetic daytime; they insignificantly increase in the magnetic pre-midnight sector responding to the closure, trans-polar currents of the DP1 magnetic substorm activity.

The daily average of all positive PCN values is ~1.2 with a standard deviation $\sigma \approx \pm 1.1$. This average value is close to the "quiet time" PCN ≈ 0.95; the "disturbed" PCN values vary insignificantly near ~3.6. All three curves show little variations (less than 10%) over a UT day. The average negative PCN values stand aside, showing that during certain conditions (mainly when IMF is northward) the transpolar current over Thule can be reversed. This reversed current is less extended to the nightside and can be narrow; this induces the recognizable UT variation (from –0.2 to –0.6) with a peak near magnetic noon. The latter reflects the enhanced ionospheric convection at the dayside during northward IMF.

We note that the PC index differs principally from the family of AE indices. The PC index shows a rate of the direct electrodynamic energy inflow into the magnetosphere and farther down to the ionosphere and neutral atmosphere, whereas the auroral electrojet indices rather measure the energy releases previously deposited in the magnetospheric tail and then downloaded into the auroral ionosphere in a form of magnetic substorms. Correlations between the PCN and auroral electrojet indices were thoroughly studied by *Vennerstrøm et al.* [1991] and it turned out that the PCN index correlates better with AE and AL rather than with AU indices; the coefficient of linear correlation equal 0.8–0.9 in winter and to 0.6–0.8 in summer. *Takalo and Timonen* [1998] analyzed relationships between the PCN and AE indices in detail, where AE was derived from PCN for 7.5-min ahead of time; the corresponding correlation coefficient was 0.91 at the best. This can be related to a larger contribution to the transpolar current from the westward auroral electrojet during magnetic substorms.

Vassiliadis et al. [1996] found that good correlation between the PCN and AE indices could be utilized in developing a predictive scheme for estimates of the auroral electrojet intensity solely from the PCN index. The linear moving-average filters reproduce the observed AL with correlation of 88% and AU with 75%; while the linear autoregressive moving-average (ARMA) models based on the PCN index produce single-step predictions with 98% and 97% correlation with AL and AU, respectively. For the long-term prediction, the linear PCN-based ARMA model has an asymptotic prediction error that is at least 25% more accurate than prediction of AE-index from the IMF. *Vassiliadis et al*. [1996] obtained the following relationships between these indices for winter months: AL (nT) = $-98.8 \cdot$ PCN + 20.7 and AU (nT) = $34.1 \cdot$ PCN + 22.2. Utilizing these relationships, we estimate the selected ranges of activity for PCN (as indicated in **Figure 5**) as the following: (a) quiet time, -225 nT < AL < -20 nT, $0 \le$ PCN ≤ 2.5); (b) disturbed time, AL < -225 nT, PCN > 2.5).

4.2 PCN seasonal variations

To continue comparisons with the family of AE indices, we investigated the seasonal variation in the PCN index. **Figure** 6 shows this variation, averaged daily over years 1975–1999 (thin lines) separately for the positive and negative PCN values. Doing that averaging, we calculated the standard deviations for

every day; then we averaged the daily means and the corresponding deviations monthly. The monthly averages (obtained from the corresponding daily means) are over-plotted in **Figure 6** as thick curves. As seen, the positive PCN index values show a broad minimum of geomagnetic activity in the northern polar cap during summer months (July–August), with a little enhancement near solar solstice in June. The geomagnetic activity maximums are seen during February–March and October–November; it seems that these peaks correspond to the annual variation of occurrences of geomagnetic storms [see Figure 2 in *Russell and McPherron*, 1973], rather than to the semiannual variation of global geomagnetic activity explained as the well-known Russell–McPherron effect. The latter predicts maximums in early April and early October from favorable orientation of the Earth's rotation axis relative to the solar wind flow direction. The negative PCN index peaks near summer solstice (May–June) when the ionospheric conductivity enhances at high latitudes.

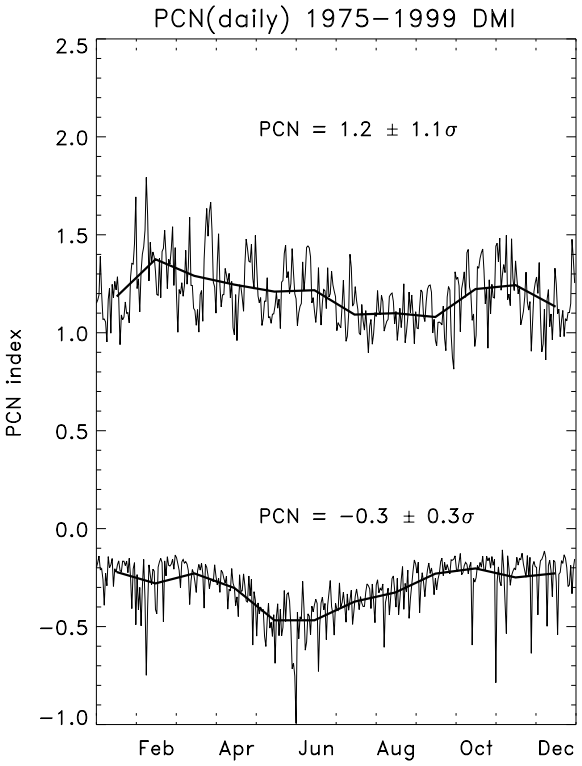

Figure 6. The PCN seasonal variation obtained from daily-averaged means over years 1975–1999 separately for the positive (top) and negative (bottom) values.

The comparison of **Figure 6** with the seasonal variation in AE index [*Ahn et al.,* 2000b, Figures 1 and 4] shows that behaviors of these two indices are quite different. The monthly AE index peaks slightly in April, the AU index – in June, and only the AL index shows a weak semiannual variation, which peaks in April and September–October, in agreement with the Russell–McPherron effect. From these results, we conclude that geomagnetic activity in the polar caps is mainly controlled by the "directly-driven" processes in the solar wind-magnetosphere-ionosphere coupling, which occur all the time because the varying IMF and solar wind encounter continuously the Earth's magnetosphere. From the obtained semiannual variation in PCN, we conclude that the "directly-driven" processes may play a significant role in the storm-driven events; this distinct the polar cap magnetic activity from the (mainly) substorm-driven activity in the auroral zones.

4.3 PCN solar cycle variations

Figure 7 shows the solar cycle variation in the PCN index, plotted separately for the positive and negative values. One can see two distinctive maximums (1981–1982 and 1989–1991) in the positive PCN

index time series; the corresponding minimums are observed in 1976–1977, 1986–1987, and 1996–1997. The second major maximum is double-peaked, although two additional, smaller maximums are also seen in 1978–1979 and 1994–1995. The beginning of 23rd cycle is seen with the rise of PCN in 1998–1999.

According to the 27-day averaged sunspot numbers plot [e.g., *Papitashvili et al.*, 2000], the 21st solar cycle started in 1976 (minimum) and reached the maximum in 1980. The next, 22nd cycle began in 1985–1986, reaching maximum in 1989–1991; the sunspot numbers also show that this maximum was double-peaked. From **Figure 7**, we see that the index follows the solar activity cycle, showing higher activity in the northern polar cap during the solar cycle maximums ($PCN_{max} \sim 1.6$); the minimum activity is achieved during the solar minimums ($PCN_{min} \sim 0.8$). Thus, the solar cycle effect in PCN accounts for ±30% of its 25-year long average value $PCN_{av} \sim 1.2–1.3$.

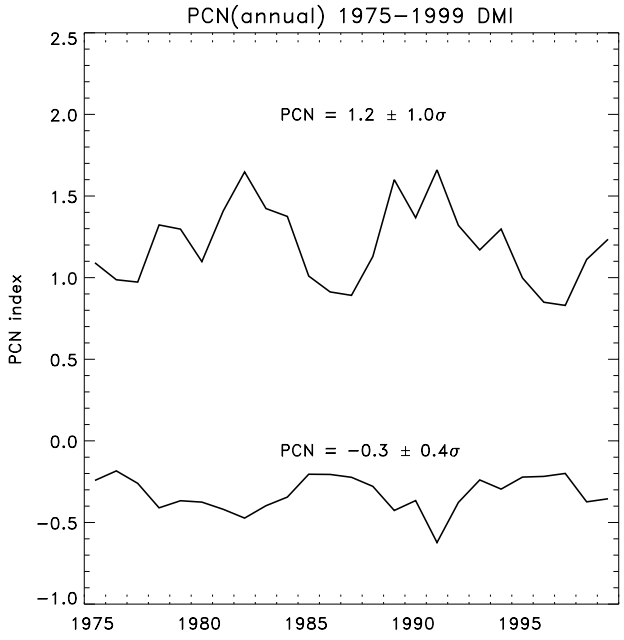

Figure 7. The solar cycle variation in the annual PCN index.

Referring to the study undertaken by *Ahn et al.* [2000b], we can compare the solar cycle variations in PCN and the family of AE indices. Figure 3 in the cited paper shows clearly that all the AE, AL, AU, and even *aa* indices have the solar cycle variation, peaking near solar activity maximums; very similar to what we see in **Figure 7** for the PCN index. To be on sure ground in our solar cycle variation study, we show in **Figure 8** the results of our analysis of the PCN solar cycle variations for each UT hour. To our satisfaction, all the detected peaks and general behavior are repeated in these plots, confirming results shown in **Figure 7**.

However, we remember that the current PCN index has been calculated using the series of normalization coefficients obtained for 1977–1980 (see **Section 3**); these coefficients are now applied to the Thule geomagnetic data every year including 2001. Although we know that the solar wind interaction with the Earth's magnetosphere does not depend much on the solar activity cycle [e.g., *Papitashvili et al.*, 1994], the obtained results shown in **Figure 7** and **Figure 8** raise an important question: What if these coefficients will be obtained for every year and then investigated for their behavior with the solar cycles? If these coefficients would have their solar cycle variation, does it mean that the solar cycle effect in PCN could be eliminated if the "solar-cycle-related" coefficients will be used for in calculating the index? We investigate these issues below in an attempt to obtain suitable answers.

5. Analysis and correction of PCN for solar cycle effects

5.1 Solar cycle effects in normalization coefficients

As we have shown in **Figure 4** (right bottom panel), the CGM Lat.–MLT monthly diagrams of the magnetic disturbance vector ΔF obtained in this study from the absolute geomagnetic field observations at Thule for 1977–1980 are almost identical to the corresponding diagrams plotted from the file `coef24g3.dat` (**Figure 4**, left bottom panel). Although the graphs at the top panels in this figure do not match exactly (showing good agreement nevertheless), we decided to obtain a complete set of normalization coefficients for every year from 1965 to 1998, years with all available digital geomagnetic data from Thule and the corresponding set of hourly IMF parameters [*King and Papitashvili*, 1994; http://nssdc.gsfc.nasa.gov/omniweb/]. Similar to the period 1977–1980 (**Section 3**), we combined geomagnetic and IMF data monthly for three consecutive years and used the 3-year moving window in calculating the normalization coefficients and optimal directions for every year in the period from 1966 to 1997. Note that in this way we are unable to calculate coefficients for the start (1965) and end (1998) years.

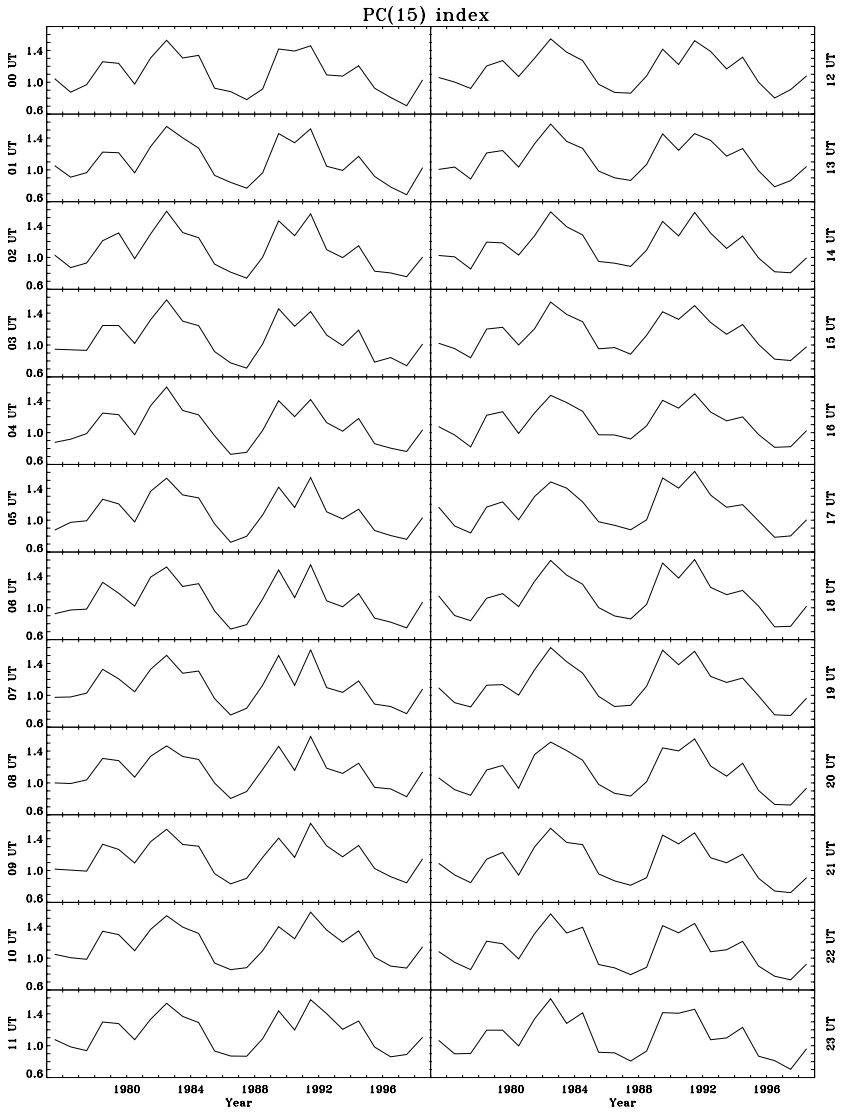

Figure 8. The solar cycle variation of the current 15-min PCN index averaged over 1975–1999 for every UT (MLT+3) hour.

Figures A1–A16 in **Appendix A** show annual time series of the normalization coefficients as well as the "dial plot" diagrams for the entire dataset from 1966 to 1997. The first and most obvious observation here is that these plots are very similar to the plots in **Figure 4**; however, their close inspection for years

1977, 1978, 1979, and 1980 (**Figures A6–A8**) reveals that, even over this short time interval, the direction and magnitude of the vectors can be different.

This difference is understandable because different geomagnetic and IMF datasets are involved in the correlations from "year-to-year", but it also suggests that combining data monthly over the three or four years intervals may produce slightly different sets of coefficients. Therefore, we think that the proposed (in this study) approach in combining three years of data monthly is robust and the obtained set of nor-

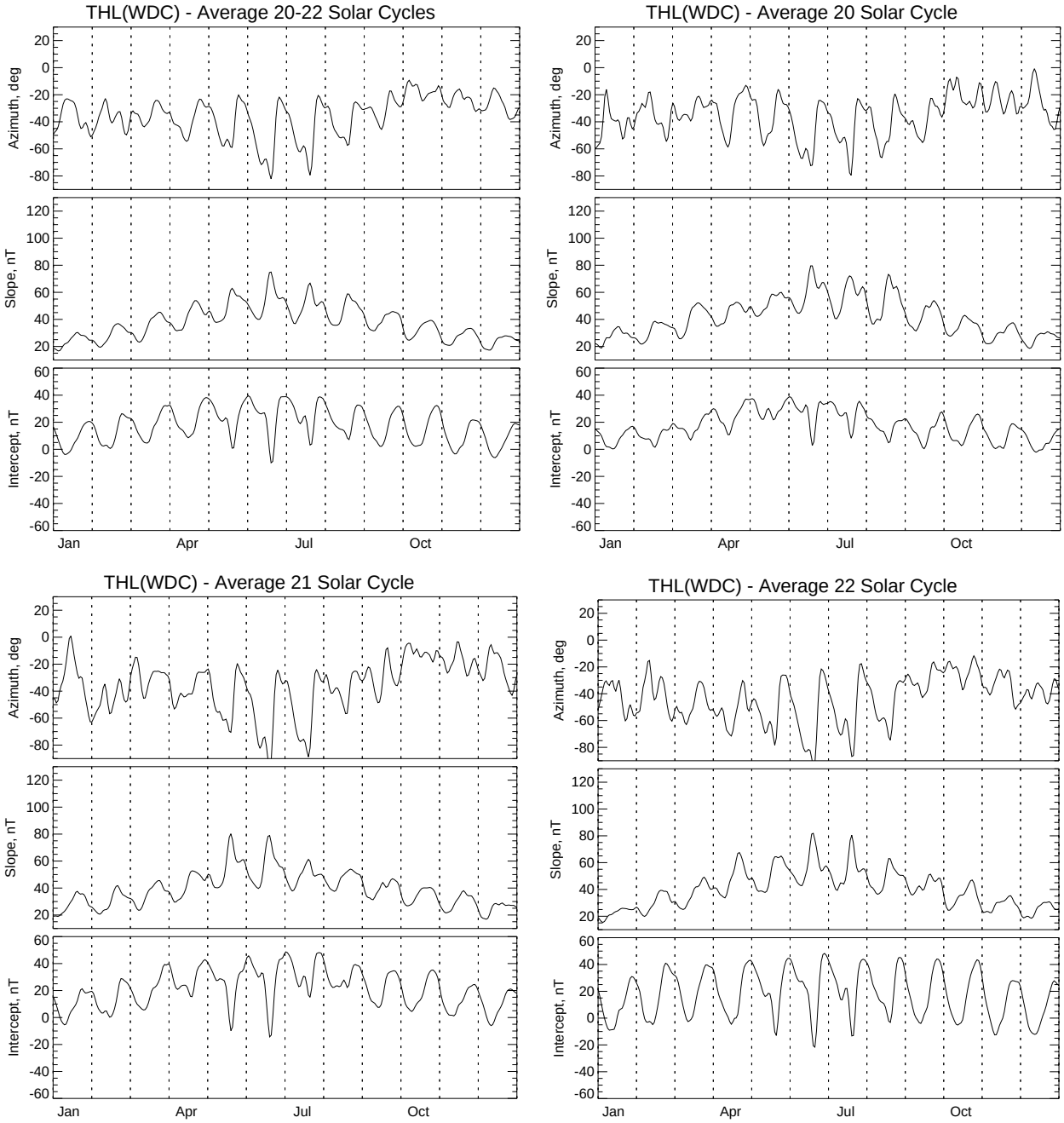

Figure 9. The same as in **Figure 4** (top panel) but averaged over years 1966–1997 (top left), 1966–1976 (top right), 1977–1986 (bottom left), and 1987–1997 (bottom right).

malization coefficients allows us to study solar cycle effects in the solar wind-magnetosphere interaction.

Close inspection of the plots in **Appendix A** reveals that the behavior of optimal directions changes insignificantly over three solar cycles; this regime is also understandable because this direction depends on orientation of the Earth geomagnetic and rotation axes regarding the solar wind velocity vector. Although this mutual orientation changes in a course of a year, there are no changes in the "day-to-day" orientation with years. However, the general behavior of normalization coefficients (slope and intercept) is different; most surprising is that the daily variation in the intercept parameter increases significantly from 1960s to 1990s; it seems that the slope parameter behavior does not change much over three decades.

To illustrate this behavior better, we show in **Figure 9** the averaged time series of normalization coefficients over the entire time interval 1966–1997, as well as separately for 20–22 solar activity cycles, that is, averaging the coefficients over 1966–1976, 1977–1986, and 1987–1997, respectively. Here one can clearly see that the average response on the ground geomagnetic field at Thule (slope) is almost the same during all three solar cycles. However, the intercept parameter increases in magnitude and shapes into a more regular daily variation; this increase accounts for almost 30% of the intercept's daily magnitude. We note that our results do not match exactly with the corresponding time series obtained about a decade ago and shown in **Figure 4** (top left panel); more studies are needed to understand that difference and to explain the intercept's magnitude increase which seems to be irrespective of the solar cycle phase.

In **Figure 10**, we show the same time series but averaged over three years near the solar cycles' minimums (1975–1977, 1985–1987, 1995–1997) and maximums (1968–1970, 1979–1981, 1990–1992). What

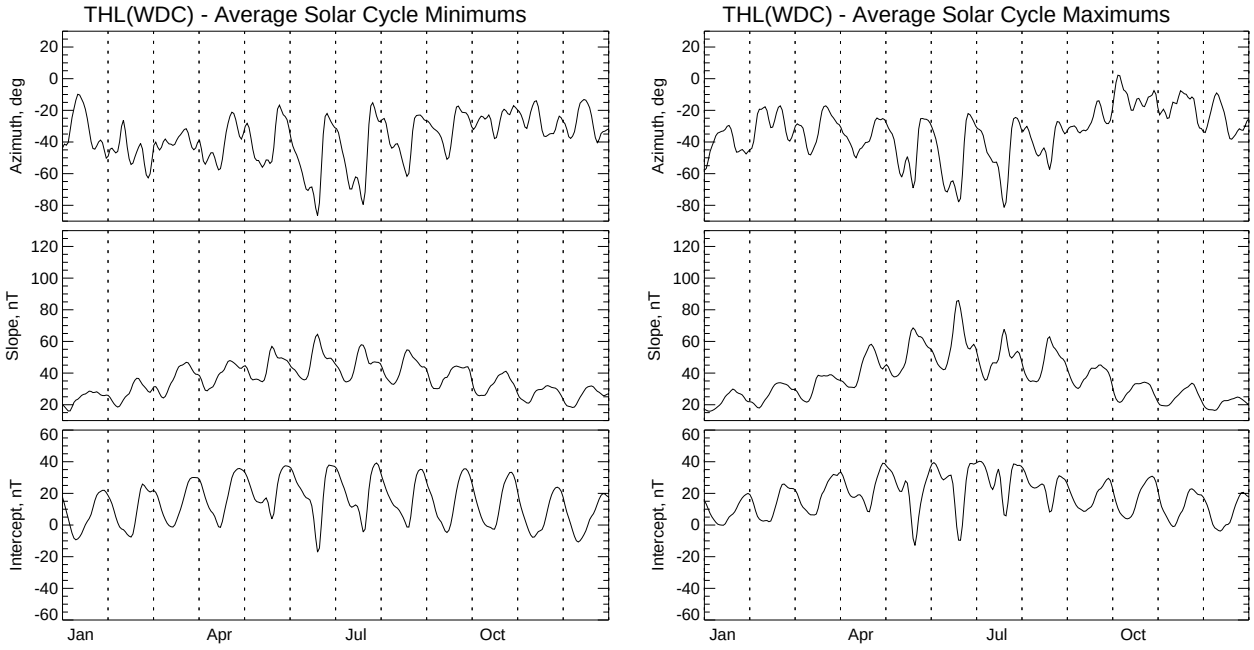

Figure 10. The same as in **Figure 9** but averaged (by three consecutive years) over the 20–22 solar cycles' minimums (left) and maximums (right).

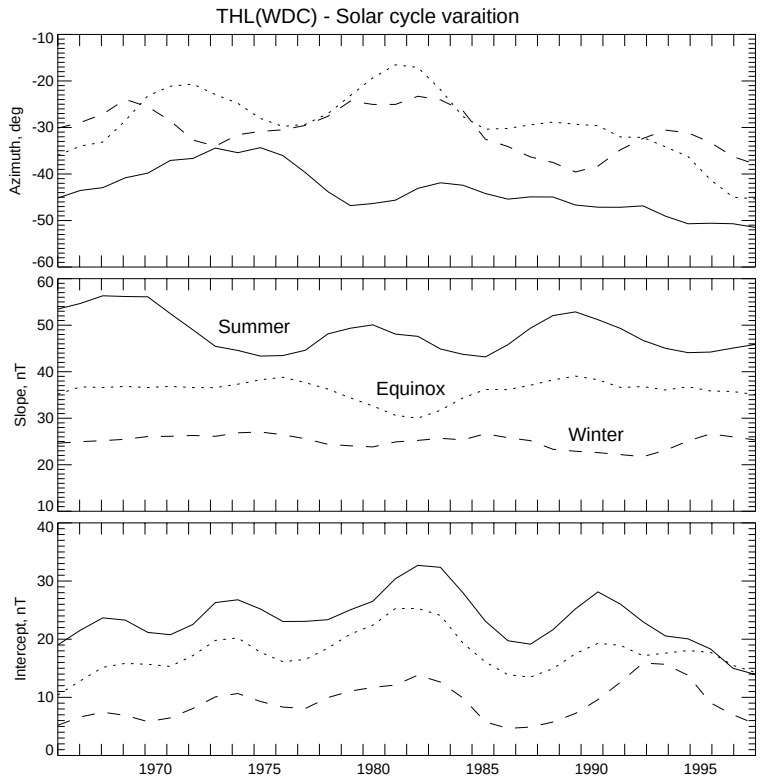

Figure 11. The solar cycle variation of the PCN normalization coefficients averaged by seasons.

What surprises us here is that the intercept's daily variation becomes more regular during the solar cycle minimums than during the corresponding maximums, showing clearly an increase of the daily variation magnitude during summer months in the "maximums" plot. The important increase is seen in the geomagnetic field response (slope) from the solar cycle minimums to maximums; we believe that this is a solar cycle effect in the ionospheric conductivity during summer.

In **Figure 11**, we re-plotted the normalization coefficients over three decades averaged by the year's season (Summer: May–August; Equinox: March, April, September, October; and Winter: December–February). As seen, all three parameters exhibit the solar cycle variation, though not exactly in concert. However, the slope (the most important parameter of the ionospheric response to the solar wind-magnetosphere interaction) shows almost no cycle variations during winter and equinox; the "summer" solar cycle variations accounts for about 20% of the magnitude. The intercept parameter exhibits clear variations with the solar cycle (up to 40–50%); the azimuths vary similarly.

Thus, we conclude that the normalization coefficients (slope, intercept, and optimal direction), needed for calculations of the PCN index, reveal recognizable solar cycle variations, which may affect the PCN values calculated routinely.

5.2 UT variation in the "corrected" PCN index

We calculated the new, "corrected" PCN index, utilizing the coefficients obtained by the 3-year moving window from Thule's geomagnetic data held at the World Data center for Geomagnetism in Copenhagen. This index is marked as PCN(WDC) in all follow-on plots, which we repeated in the same way as we did in **Section 4** to find out if this "corrected" index differs from the one currently calculated at DMI.

Figure 12 shows the UT variation of the new PCN(WDC) index; this plot should be compared with **Figure 5**. From these comparisons, one can see that the new index is ~25% larger than the current one and exhibits a weak UT variation (of the order of 25% of the average daily magnitude) with the maximum

over the pre-non MLT hours. This suggests that correction for the solar cycle effects in the normalization coefficients made the index more responsive to changes in the IMF; at the same time, the index became more sensible to limitations in the extent of the transpolar ionospheric current over Thule. **Table 1** shows that Thule is located at 85.3° CGM latitude (~520 km from the CGM pole). If we assume a radius for the observatory's "field-of-view" of the ionosphere as 3-4 ionospheric altitudes (~120 km), we can estimate that the width of an "ideal" midnight-noon transpolar current should be equal to ~1000 km. Thus, the UT variation should not be seen in Thule's data if that current is uniform over the area confined within the CGM 10° co-latitude.

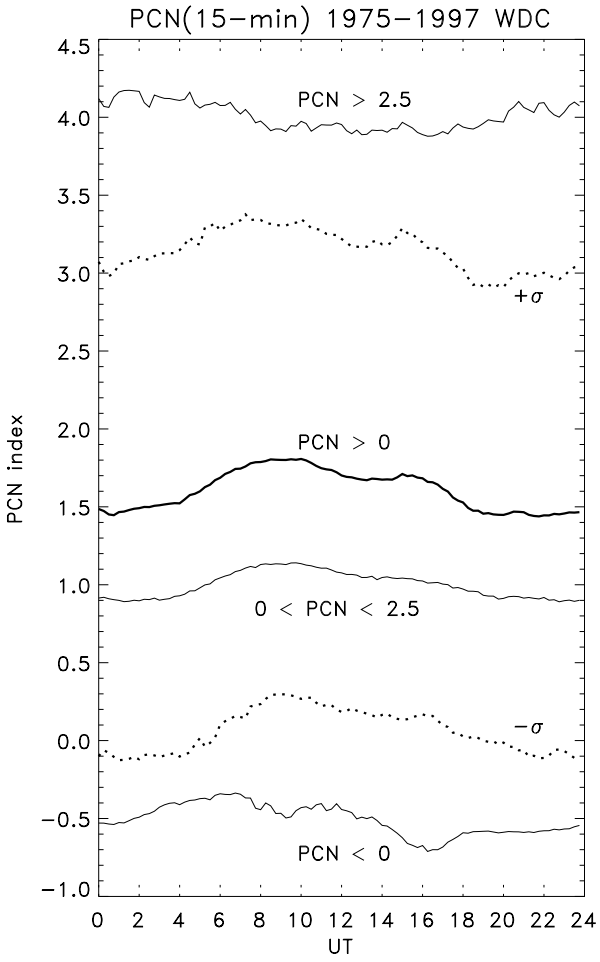

Figure 12. The UT variation of the PCN(WDC) index calculated from the coefficients shown in **Appendix**, plotted in the same format as in **Figure 5**.

However, the IZMEM model (*Papitashvili et al.*, 1994; http://www.sprl.umich.edu/mist/limie.html) shows that such the uniform current may exist only when the IMF is purely southward. As soon as the IMF B_y component exceeds ±1 nT, the current's flow becomes distorted and non-uniform. Thus, we believe that geomagnetic variations at Thule should exhibit the weak UT variation even if the IMF conditions would be stable over the entire 24-hour interval.

5.3 Seasonal and solar cycle variations in the "corrected" PCN index

Figure 13 shows seasonal variations of PCN(WDC), which are almost identical to the variations shown in **Figure 6**. We only note that the Fall maximum in the positive PCN(WDC) index is now slightly shifted to November; seasonal variations in the negative PCN(WDC) index are almost the same as in the current PCN(DMI) time series, except the absolute magnitude is higher in the former index. Same conclusions can be made from the comparison of solar cycle variations in the current and new indices shown in **Figure 7** and **Figure 14**, respectively. All peaks are in the same place, however, the amplitude of the solar cycle variation is larger by ~25% in the "corrected" PCN index.

Thus, we conclude that the new procedure proposed here might be better suited for routine calculations of the PCN index because it accounts for the solar cycle variations in the normalization coefficients.

The "corrected" PCN(WDC) index is more responsive to the changing IMF conditions, showing larger magnitudes for both the positive and negative PCN values. This requires further and detailed study, however, we may recommend reassessing the current routine procedure by introducing a new set of normalization coefficients obtained for every year of the past and current solar cycles. In this way, the preliminary index values can be obtained by using the normalization coefficients for a previous year; then the final PCN index (for the previous year) can be recalculated as the definitive geomagnetic data become available from Qaanaaq for the current year

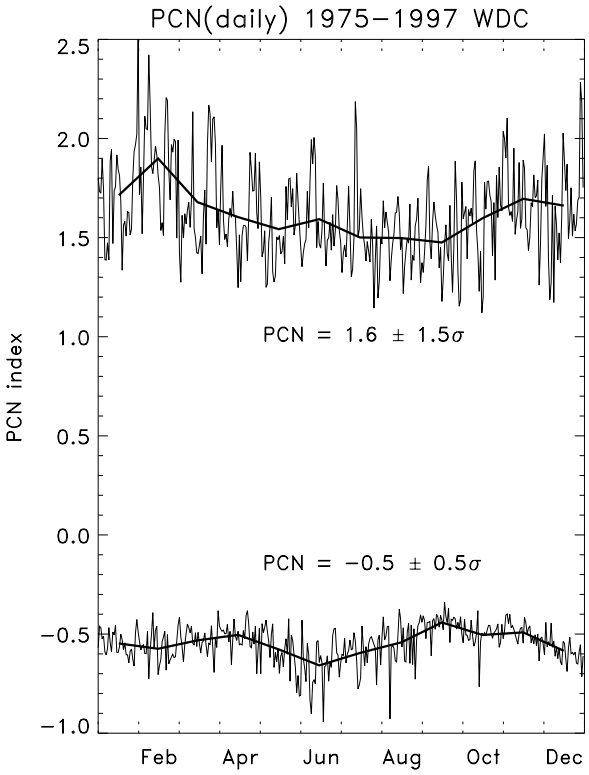

Figure 13. Seasonal variations of the PCN(WDC) index obtained from daily-averaged values over years 1975–1997 for the positive (top) and negative (bottom) index values.

6. Analysis of an effective area for the standard PCN index

For this analysis, we utilized the same set of pre-defined normalization coefficients obtained for Thule (i.e., file `coef24g3.dat`, see Section 3) in calculating the 15-min PCN_{sta} indices from geomagnetic data obtained at Qaanaaq, Savissivik, and Kullorsuaq through 1998 [*Papitashvili and Rasmussen*, 1999]. According to **Figure 1** and **Table 1**, one can see that these stations are located approximately along the same geomagnetic meridian and they span geomagnetic latitudes from 85.3° to 81.2°. **Figure 15** shows for the comparison the PCN_{sta} time series derived from THL, SVS, and KUV for May 1–15, 1998. As seen, all three series show similar behavior, though some differences are recognizable when the PCN_{sta} indices experience sharp negative excursions. Nevertheless, it seems that all three stations can produce the PC_{THL}–like index.

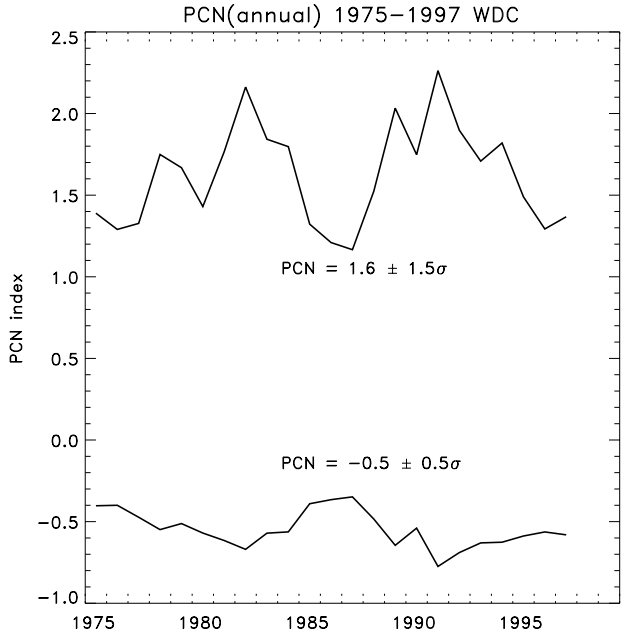

Figure 14. Solar cycle variations in the PCN(WDC) index.

We calculated and then correlated the PCN_{sta} times series from THL and SVS for 1998. **Figure 16** shows these results plotted separately for winter, equinox, and summer. The dashed lines indicate 45° slopes; the solid lines (plotted within a range of fitted ~11,000 points for every season) represent the regression equations shown at the left, top corner of each plot.

As seen, the correlation coefficients between the two PCN_{sta} series are 0.96 in average and the slope of solid straight lines is almost 45°. The best correlation is achieved during winter; the points increasingly scatter through equinox and summer. These results clearly show that the PCN index is stable between THL and SVS; therefore, almost identical PCN_{sta} indices can be produced using geomagnetic data from these two stations.

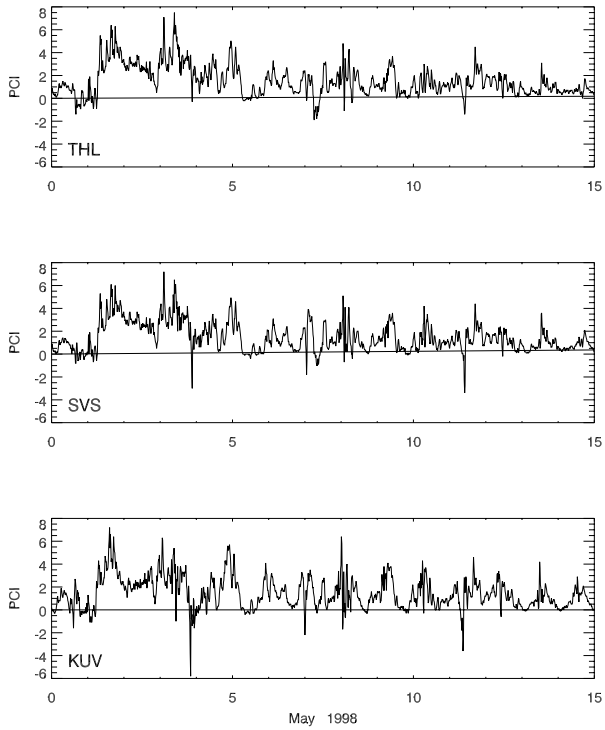

Figure 15. The $PCN(DMI)_{sta}$ indices derived from THL, SVS, and KUV for May 1–15, 1998.

Figure 17 shows results of similar correlations between THL, SVS, and KUV, plotted for three months (April–June 1998) in transition from equinox to summer (this interval was limited by the available data from KUV). The top row shows correlation between THL and SVS, the middle row – between THL and KUV, and the bottom row – between SVS and KUV. The correlation between THL and SVS for these three months almost repeats the results shown on **Figure 16** in the distribution of points (~2,800 for each month), as well as for the obtained numbers. However, correlation becomes poorer ($r \sim 0.5$) as we compare THL and KUV: the slope of the linear re-

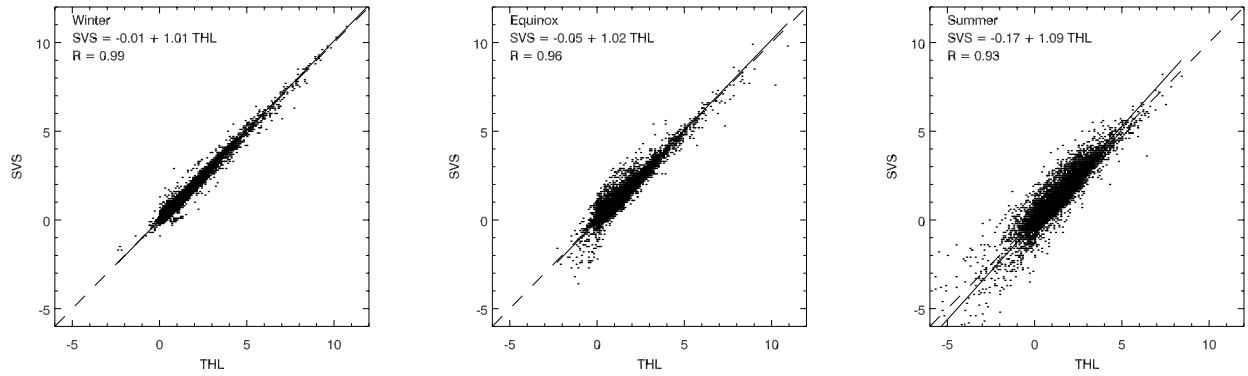

Figure 16. Correlation of the $PCN(DMI)_{sta}$ indices obtained from THL and SVS for winter, equinox, and summer of 1998.

gression fit increases suggesting that PCN_{KUV} could differ up to 50% from PCN_{THL}. The same conclusion can be made from comparisons between SVS and KUV: the correlation also becomes poorer ($r \sim 0.6$), though it is slightly better than that between THL and KUV. According to the slope and intercept values, PCN_{KUV} could differ up to 30% from PCN_{SVS}.

The standard PCN index is normalized to be positive in estimating variations in the transpolar electric fields through sensing magnetic perturbations caused by the ionospheric DP2 current system developed over the polar region during southward IMF. During summer, this DP2 system maintains stable, sunward transpolar current. In winter, the Region 1 FAC system would add the sunward magnetic perturbations to

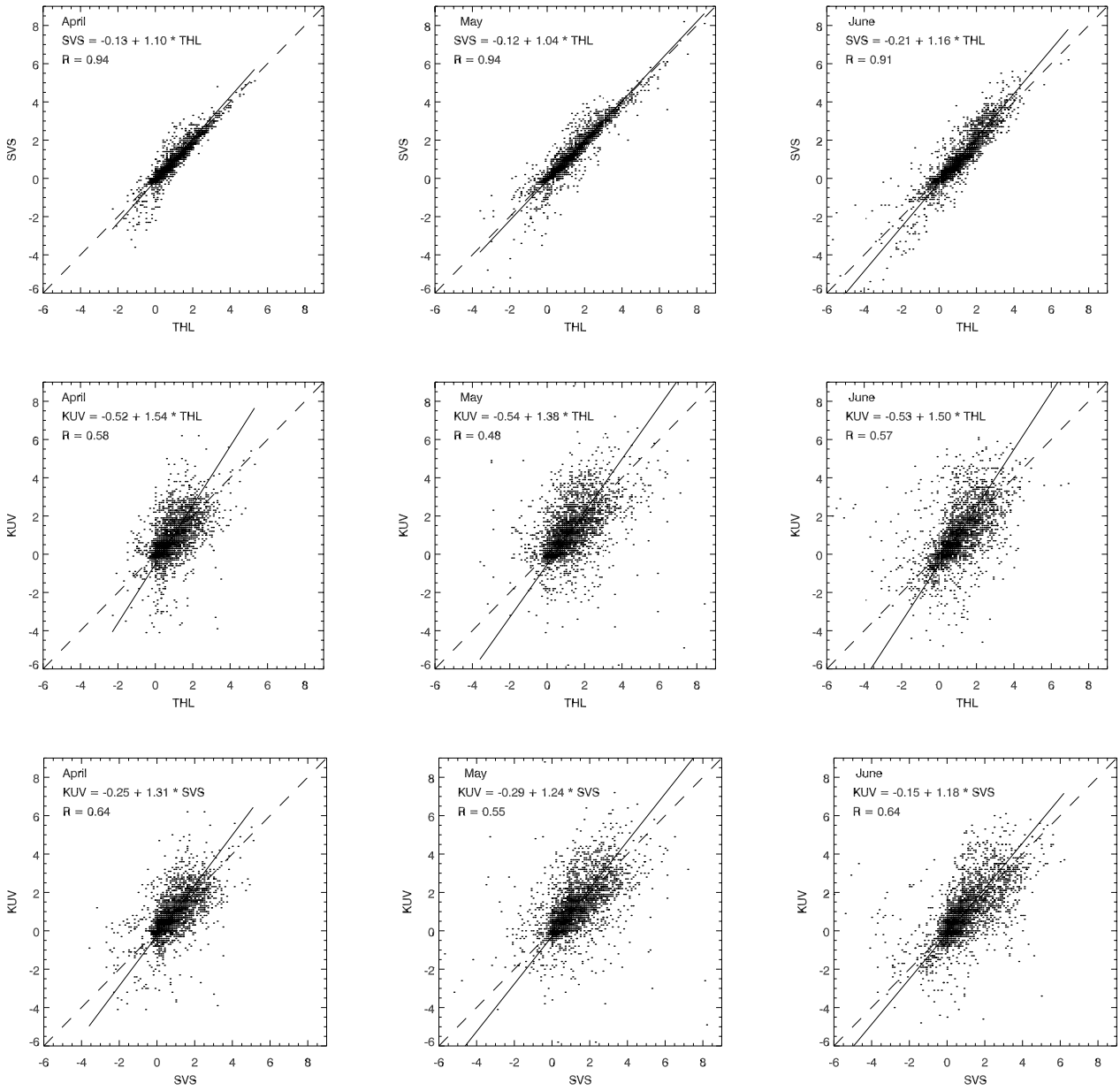

Figure 17. Correlation of the $PCN(DMI)_{sta}$ indices obtained from THL, SVS, and KUV for April–June 1998.

the DP2 magnetic disturbances [e.g., *Vennerstrøm et al.,* 1991].

It is known that the background convection (caused by the solar wind "quasi-viscous" interaction with the Earth's magnetosphere) is a two-cell system and the IMF B_y-related ionospheric convection is generally circular around the magnetic pole [e.g., *Papitashvili et al.,* 1994]. As $B_z \rightarrow 0$, the DP2 current system becomes asymmetric (shifted towards dawn or dusk) depending on the B_y-component direction and hemisphere. Therefore, a transpolar current of the combined convection system will be sunward in general, and one can expect that the PC index will also be positive. As the IMF turns northward and $B_z > B_y$, the dayside near-pole ionospheric electric field is reversed (from dusk to dawn) causing a reversal of the transpolar ionospheric current in the anti-sunward direction. In this case, the PC index would be negative while the station (used for derivation) rotates under that current; however, negative PC-index values are usually limited to the near-noon MLT hours. *Shue and Weimer* [1994] showed that the near-pole region (where the anti-sunward convection holds during southward IMF) is almost unaffected (at least, statistically) by geomagnetic activity and changes in the IMF azimuthal component. They estimate that the width of the sunward, transpolar current (i.e., the dusk-dawn distance between the foci of the DP2 system) could reach 30° during enhanced convection caused by moderate magnetic activity.

From the results of this study, we conclude that the index-effective area definitely includes Qaanaaq and Savissivik, but excludes Kullorsuaq. Therefore, taking into account the magnetometer "field-of-view" at SVS, the effective area for the northern PC index can be estimated as being ~15° in diameter centering at the geomagnetic pole. This area roughly corresponds to the lower estimates of the transpolar current width in the standard, two-cell convection pattern developed over the polar cap during southward IMF [e.g., *Papitashvili et al.,* 1994]. This effective area can be larger if new coefficients (similar to those we utilized from Thule) are determined for every new station. However, an ultimate criterion here should be preservation of the PCN_{THL} index over the area, for example, within 10% of a value.

7. Station-based PCN indices and their comparisons with the standard index

7.1 PCN index from the Greenland West Coast stations

In this section, we extended the study described in **Section 6** following the recommendation to derive the normalization coefficients and optimal directions from geomagnetic data recorded at all stations along the Greenland West Coast (**Figure 1**, http://www.dmi.dk/projects/chain/greenland.html) for better estimates of the actual effective area for the PCN index. We focused on the years 1994, 1995, and 1996, which have a good coverage of both the ground geomagnetic data from all stations and the IMF. The normalization coefficients are obtained from the correlation of hourly means geomagnetic and IMF data; the latter data are taken from http://nssdc.gsfc.nasa.gov/omniweb/. The hourly geomagnetic data were obtained from the 20-sec variation samples provided by DMI at the CD-ROM; these data are written in the

daily files `MY95mmdd.GDF` where `mm` and `dd` stand for months and days. We utilized the analysis technique described above in **Section 3**, that is, we used three years of data combined monthly to obtain the normalization coefficients for 1995. We mark below as "GDF" the PCN_{sta} indices obtained from these data.

First, we retrieved 20-sec variation data from the records of all twelve West Coast stations: Qaanaaq (THL, 85.3° CGM latitude, calculated for Epoch 2000); Savissivik (SVS, 83.6°); Kullorsuaq (KUV, 81.2°); Upernavik (UPN, 79.5°), Uummannaq (UMQ, 76.9°); Qeqertarsuaq (GDH, former Godhavn, 75.8°); Attu (ATU, 74.5°); Kangerlussuaq (STF, former Sondre Stromfjord, 73.2°); Maniitsoq (SKT, former Sukkertoppen, 72.0°); Nuuk (GHB, former Godthab, 70.5°); Paamiut (FHB, former Frederikshab, 68.0°), and Narsarsuaq (NAQ, 66.3°). Note that the daily "quiet level" in these variation data is defined for each month at DMI by utilizing the same approach as used for defining quiet days in winter at Thule (see **Table 2**); this level is subtracted from the magnetometers' readings in the files `MY95mmdd.GDF`.

Then we correlated the obtained hourly means at every station with the corresponding IMF data to obtain the normalization coefficients and optimal direction, combining data monthly for years 1994, 1995, and 1996. This approach allowed us to test the quality of variation data for Thule (after subtraction of

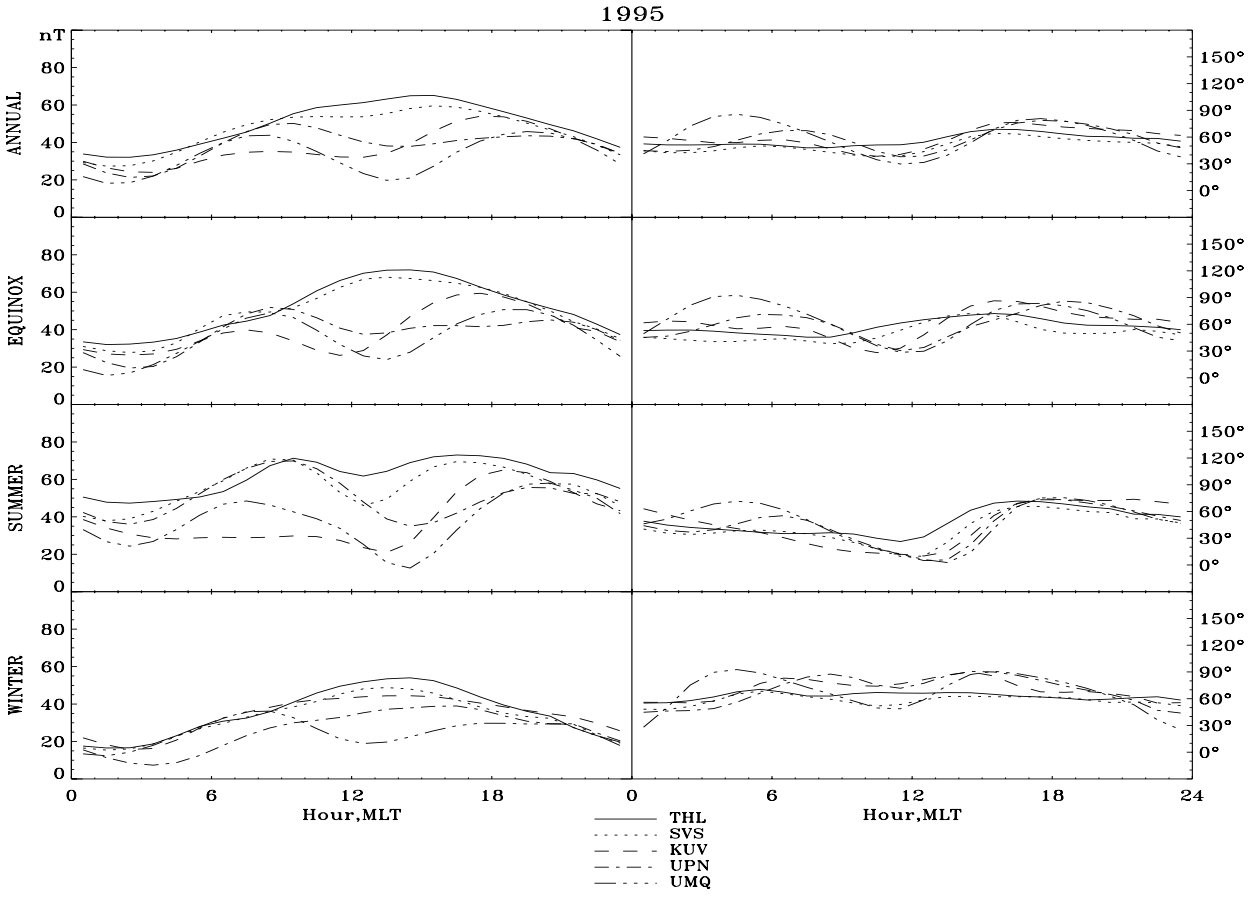

Figure 18. The UT variation of normalization coefficients (slope+intercept, left panel) and optimal directions (360°−Az), right panel) for five northernmost Greenland stations averaged through 1995 and by seasons.

quiet levels defined for each month rather than from interpolation between two consecutive winters) comparing the obtained "GDF" coefficients with the corresponding "DMI" (`coef24g3.dat`, 1977–1980, **Figure 4**) and "WDC" coefficients (1995, **Figure A15**).

Figures B1–B6 in **Appendix B** show annual time series of the normalization coefficients as well as the dial-plot diagrams derived from variation data recorded at all twelve West Coast stations for the year 1995. The first and most obvious observation is that the "WDC" and "GDF" plots for THL–1995 (**Figure A15** and **Figure B1**) are very similar; therefore, we are on sure ground in doing the analysis of GDF files for other stations. Another most obvious observation is that only five northernmost stations (THL, SVS, KUV, UPN, and UMQ) show similar behavior in their parameters; stations located equatorward of UMQ definitely break out of these four stations.

Figure 18 shows these parameters for five northernmost stations of the chain: THL, SVS, KUP, UPN, and UMQ. One can see that the parameters obtained for THL and SVS are almost identical through the entire year, though during summer the difference in the ionospheric response (i.e., slope+intercept) is most significant. The parameters for three northernmost stations (THL, SVS, and KUV) follow each other closely in winter; UPN shows similar behavior, but it is clear that UMQ breaks out of this list. During equinox, only two stations, THL and SVS, show similar behavior; the same is observed during summer. Thus, we can conclude from the analysis that the normalization coefficients are similar only for two northernmost stations THL and SVS during summer and equinox; in winter, the area where these coefficients stably preserve their values expands to KUV and even to UPN, but breaks at UMQ. Thus suggests that the width of transpolar ionospheric current is wider (~20° over-the-pole distance) in winter that during other seasons (~15° over-the-pole distance); this result is in agreement with the IZMEM modeling (http://www.sprl.umich.edu/mist/limie.html).

Figure 19 shows the PCN_{sta} indices for five northernmost stations THL, SVS, KUV, UPN, and UMQ, calculated on the base of obtained "GDF" coefficients for the first fifteen days of two summer (May and June) months, as well as for September (equinox) and December (winter) of 1995. Visual inspection of these plots shows that both the THL and SVS stations produce the same index through the year; in winter, the similarity between the index's time series goes equatorward including KUV and even UPN; during equinox and summer only THL and SVS produce the comparable indices.

To justify these findings, we decided to produce the scatter plots (similar to **Figures 16** and **17**) where we compared the PCN_{THL} indices with other PCN_{sta} indices calculated from variation data (GDF). First, we compared the standard $PCN(DMI)_{THL}$ with the newly obtained $PCN(WDC)_{THL}$ and $PCN(GDF)_{THL}$ indices for summer, equinox, and winter of 1995 (**Figure 20**); only then we proceeded with other stations.

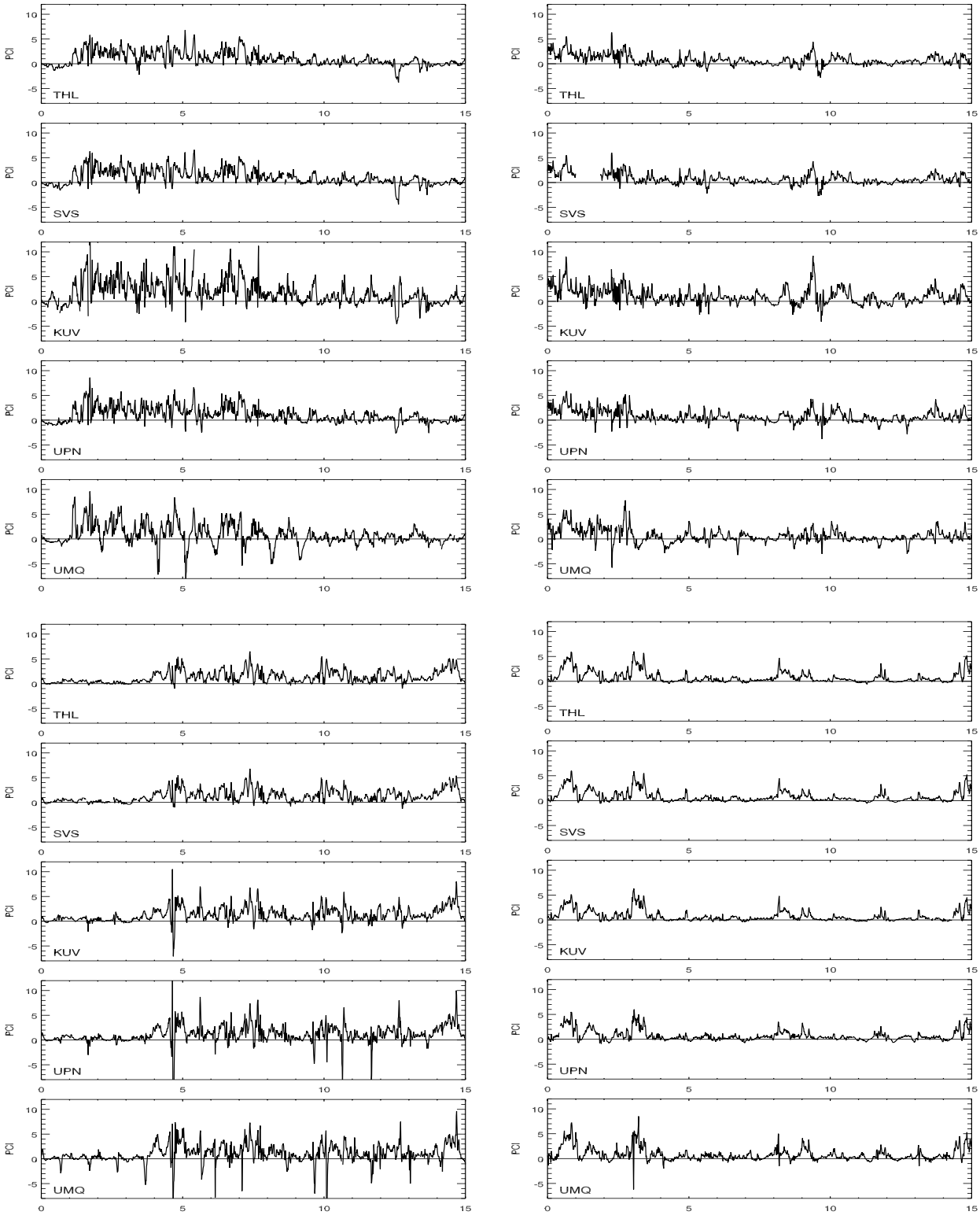

Figure 19. The PCN(GDF) indices derived from data of five northernmost Greenland West Coast stations for the first fifteen days of May (top left), June(top right), September (bottom left), and December (bottom right) of 1995.

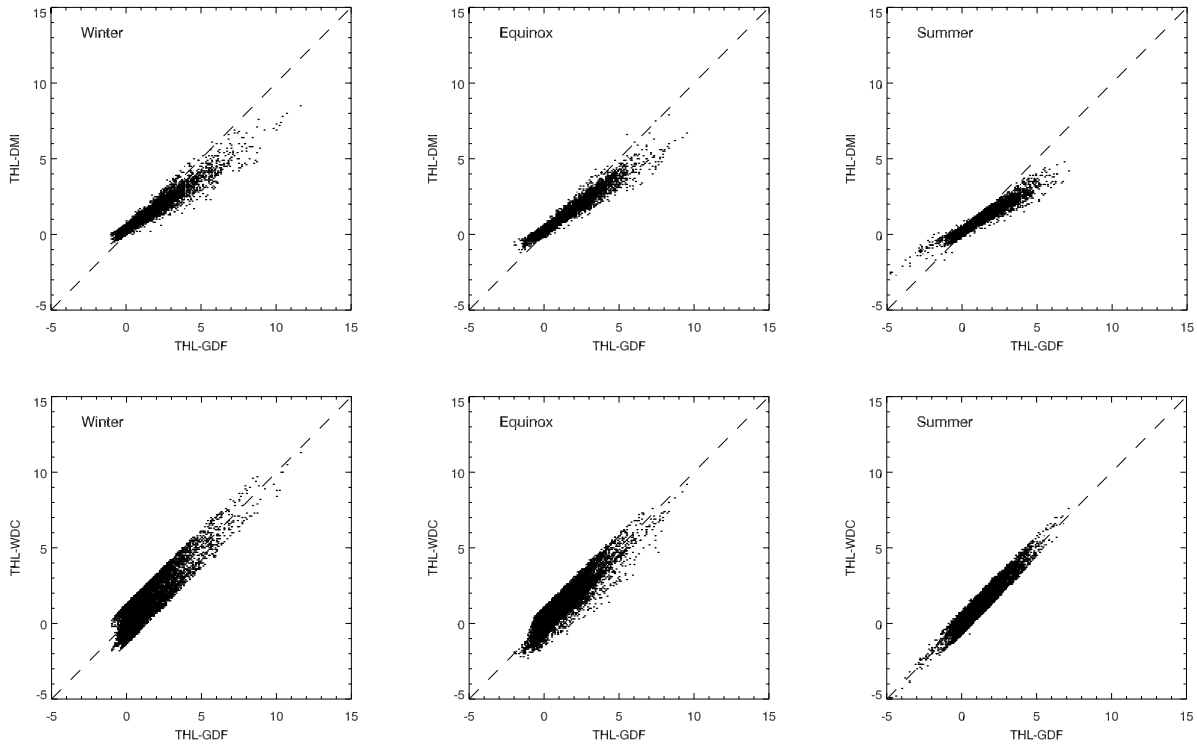

Figure 20. Correlation of the PCN indices obtained from THL for winter, equinox, and summer of 1995 from three different sets of coefficients: top panel - THL(GDF) and THL(DMI); bottom panel - THL(GDF) and THL(WDC) .

Visual inspection of **Figure 20** reveals that the standard PCN(DMI) index, derived from `coef24g3.dat`, is ~25% lower than the newly obtained indices PCN(WDC) and PCN(GDF), that is, the standard PCN may underestimate an "ideal" index. Two latter indices PCN(WDC) and PCN(GDF) match each other almost precisely.

Figure 21 shows comparisons of PCN(GDF) indices obtained for five northernmost Greenland West Coast stations. One can again see that only the PCN_{THL} and PCN_{SVS} indices (top row) match each other well enough in a course of the year. The PCN_{KUV} may contribute to the index derivation only in winter; all other stations are unable to match PCN_{THL}. The station Savissivik (SVS) is located at 83.6° CGM latitude (~700 km from the CGM pole) and Kullorsuaq (KUV) – at 81.2° (~1000 km). If we assume a radius for the observatory's "field-of-view" of the ionosphere as ~350 km (see **Section 5.2**), we can estimate the PCN effective area (that is, where the index stably preserves its value) as an area encircled by the CGM co-latitude 10° in summer and equinox; this area can be extended to 12° co-latitude in winter.

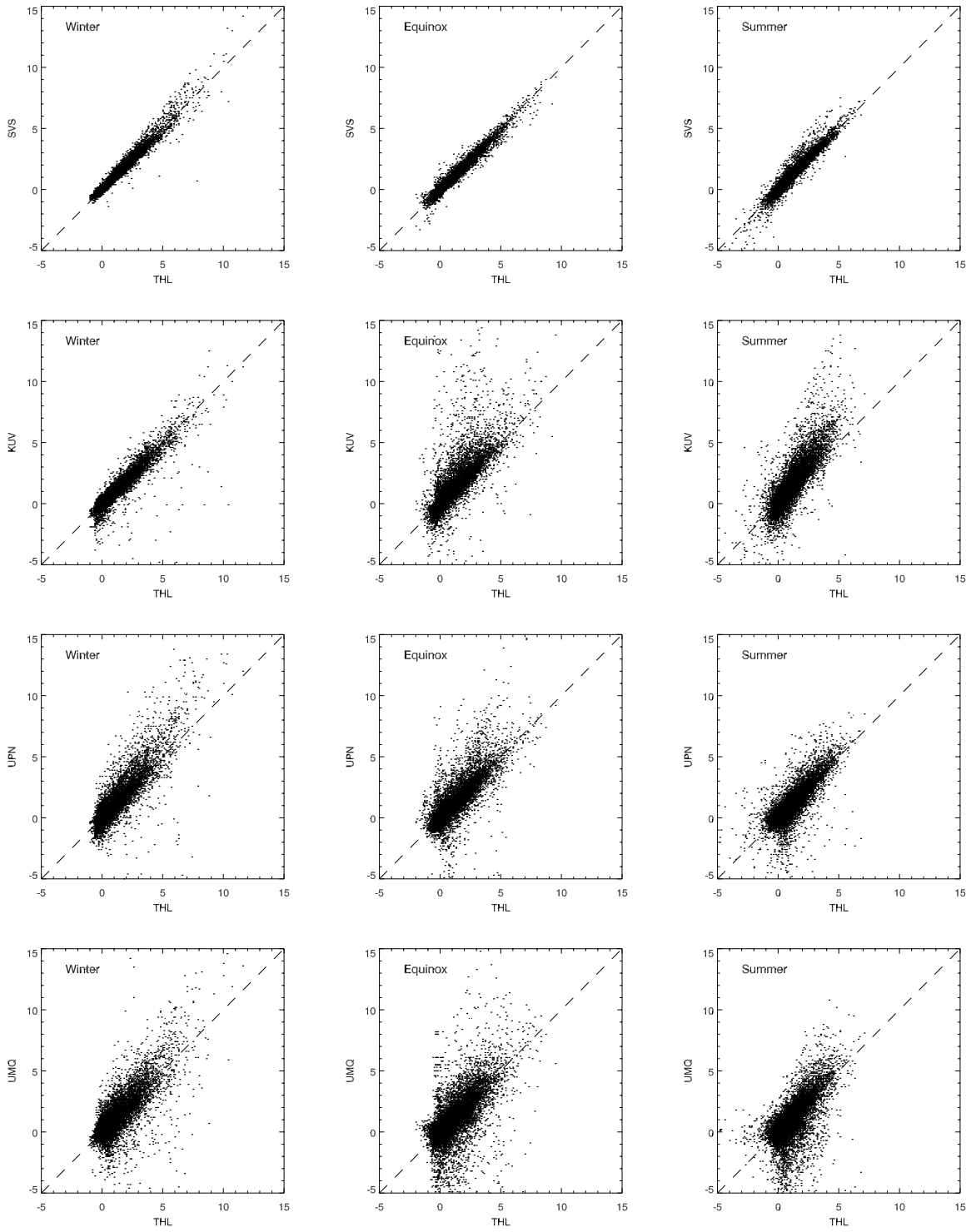

Figure 21. Correlation of the PCN(GDF) indices obtained five northernmost Greenland West Coast stations for summer, equinox, and summer of 1995: THL, SVS, KUV, UPN, and UMQ.

7.2 PCN index from the Greenland East Coast station Nord

The approach used in previous sections for estimation of the PCN effective area is applicable only if the stations are stretched along the geomagnetic meridian. However, according to **Table 1**, the Greenland East Coast station Nord (NRD, 81.0°) is located within the area where the PCN stably preserves its value, at least in winter. Here we test this assumption comparing the Nord's normalization coefficients and PCN_{NRD} index for 1995.

Figure 22 shows the normalization coefficients and optimal directions calculated from the variation data recorded at station Nord in 1994, 1995, and 1996, available from the DMI's CD-ROM as GDF files. This figure can be compared with the corresponding plots in **Appendix B**, for example, with **Figure B2** (left panel) where the coefficients are plotted for the West Coast station Kullorsuaq (KUV, 81.2°), located approximately at the same corrected geomagnetic latitude as Nord. In general, both these stations respond similarly to the IMF changes, although the optimal directions at Nord recognizably differ from those at Kullorsuaq during some months, for example, in February, May, June, July, and October.

Figure 23 shows the PCN_{sta} indices for the West Coast stations THL and KUV in comparison with the index derived from the East Coast station NRD (on the base of obtained "GDF" coefficients) for the first fifteen days of few months in 1995. Visual inspection of these plots shows that all three stations produce comparable PCN_{sta} indices, however, the best similarity is achieved during winter, as expected from the results plotted in **Figure 19**. Surprisingly, the PCN_{NRD} indices match well with the PCN_{THL} indices during winter and equinox.

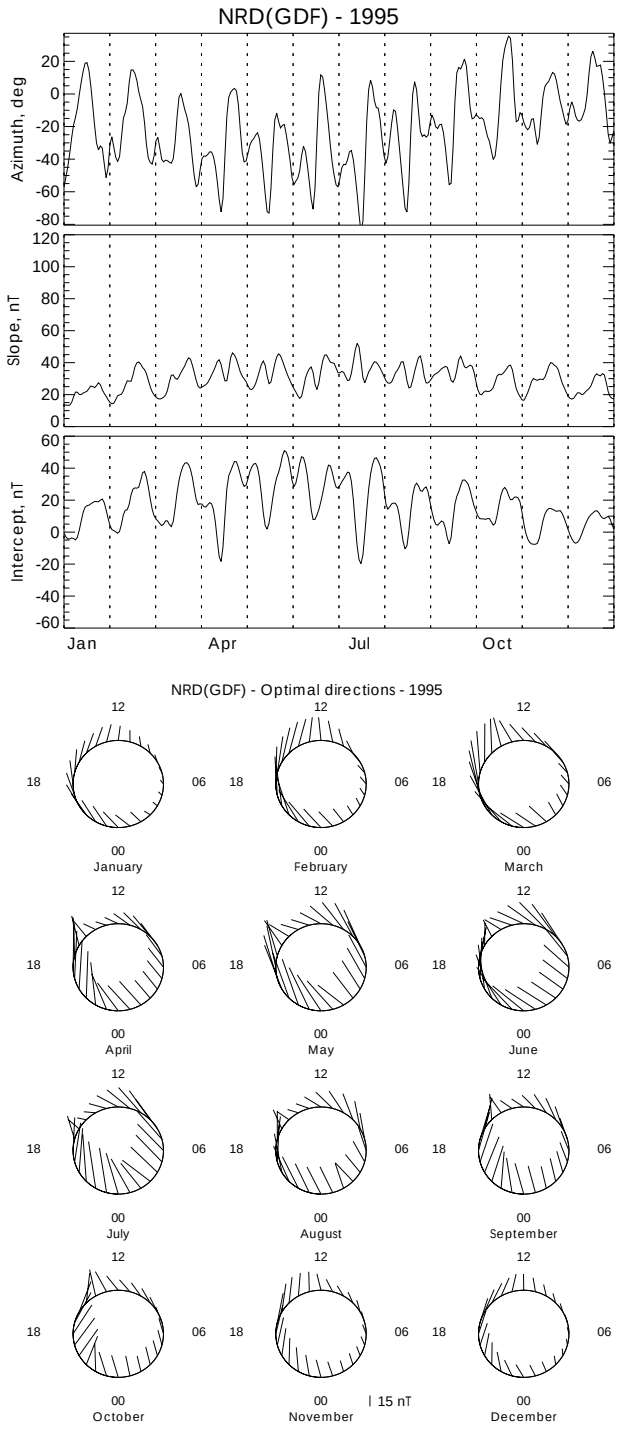

Figure 22. The normalization coefficients and optimal directions for the East Coast station NRD (GDF) – 1995.

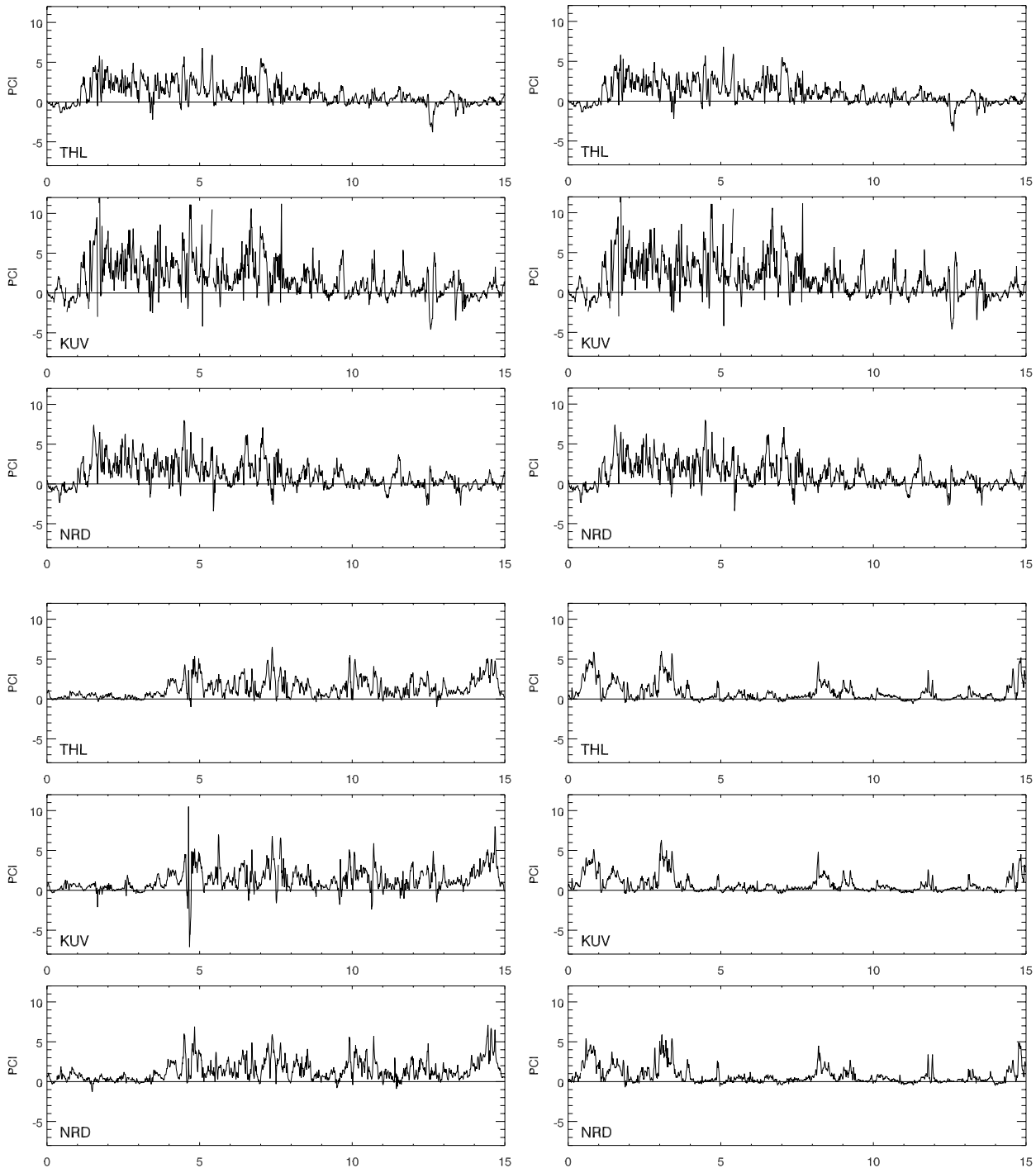

Figure 23. The PCN(GDF) indices obtained for stations THL, KUV, and NRD for the first fifteen days of May (top left), June (top right), September (bottom left), and December (bottom right) of 1995.

To justify this finding, we again produced the scatter plots (**Figure 24**) where we compare PCN_{NRD} with PCN_{KUV} and PCN_{THL}. As seen from the latter plots, PCN_{NRD} correlates well with PCN_{KUV} only during winter months; however, PCN_{NRD} matches again with PCN_{THL} during winter and equinox; this definitely expands the PCN effective area up to the 12° CGM co-latitude circle for the latter seasons.

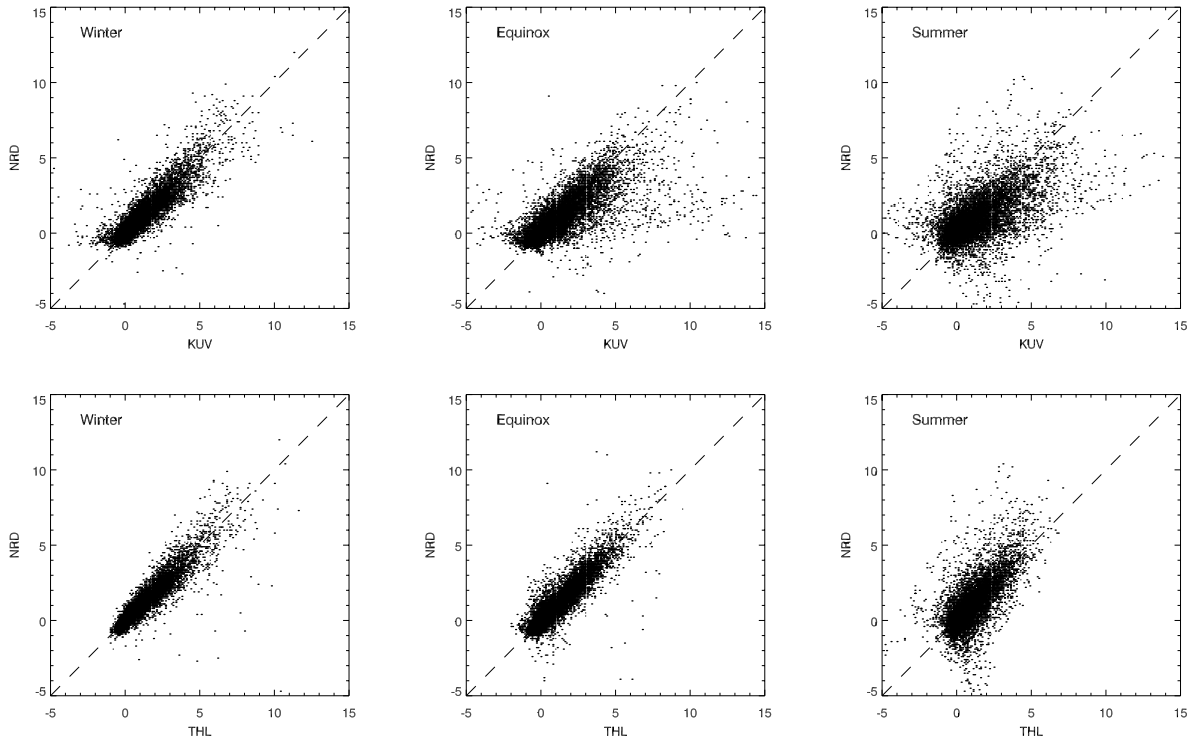

Figure 24. Correlation of the PCN(GDF) indices between the stations KUV and NRD (top panel) and THL and NRD (bottom panel) obtained for the winter, equinox, and summer months of 1995.

Thus, in this section, we firmly confirmed that the PCN effective area (where the index stably preserves its value) is confined within the CGM co-latitude 10° in summer; this area can be extended up to 12° co-latitude during equinox and winter. However, in case if data from Qaanaaq (THL) are inadvertently lost, we recommend using as a backup only the 1-min geomagnetic data from the West Coast station Savissivik (SVS); this should preserve the robustness of the PCN index time series.

8. Summary and recommendations

Although we tried to accomplish this investigation thoroughly looking for most of the properties of the standard PCN index currently derived at DMI, it is obvious that more studies are needed for better understanding of the index's physical meaning and its usefulness in a variety of practical applications. Therefore, we summarize the major results of our study and make the following recommendations:

1. The current (standard) PCN index is derived from 1-min geomagnetic data recorded at the standard magnetic observatory Qaanaaq (THL) using the set of normalization coefficients obtained from correlations of 15-min averages of ground and interplanetary data for 1977–1980, where the interplanetary parameters were delayed by 20 minutes. The results of this study show that the UT variation in PCN is almost negligible, the index's seasonal variation is weak (~25%), but the solar cycle variation is significant – up to 60%.

2. In this study, we propose a modified technique to calculate the index's normalization coefficients from hourly ground magnetometer and IMF data. This allowed us to investigate the solar cycle variations in the PCN normalization coefficients through 20^{th} – 22^{nd} solar activity cycles (1965–1998) and calculate the "corrected" (for the solar cycle effects) PCN index; we found that the latter index is larger than the standard PCN by ~25%.
3. The "corrected" PCN index shows the recognizable UT variation (~25%), which is comparable with its seasonal variation; the solar cycle variation of the "corrected" index is of the same order as for the standard PCN. From the analysis of **Figures 9–10** in **Section 5.1**, one can see that the averaged (over the cycles or over their minimums and maximums) annual time series of normalization coefficients may form a more universal set of coefficients valid for every year of the 11-year solar cycle.
4. We determined the PCN effective area (where the index stably preserves its value) as an area confined by the 10° CGM co-latitude in summer; this area can be extended up to the CGM 12° co-latitude during equinox and winter. These results are obtained from the analyses of the Greenland West Coast meridian chain data, as well as from the northernmost station Nord located at the Greenland East Coast (~5 hours apart of the West Coast). However, to be on sure ground with the PCN routine, standard calculations, we recommend limiting the PCN effective area to the circle of 20° in diameter, centered on the northern corrected geomagnetic pole. In case if the data from Qaanaaq (THL) are inadvertently lost, we recommend only the data recorded at the Greenland West Coast station Savissivik (SVS) as a backup for the standard PCN replacement.
5. One can see that all stations listed in **Table 1** are good candidates for validation of the effective area for the PCN and PCS indices. Although the subsurface magnetic anomalies in Northeastern Canada may make the data from Alert (and possibly from Eureka) suspect in that validation, we believe that data from all these stations should be utilized in validating the spatial extent of transpolar ionospheric currents in both hemispheres, ultimately defining the PCN and PCS effective areas. That would help in studying the coherence of geophysical information transmitted to the polar regions from the magnetosphere during different seasons and various solar wind and IMF conditions.

Acknowledgments. The Authors greatly appreciate Susanne Vennerstrøm and Eigil Friis-Christensen of DSRI, Torsten Neubert, Peter Stauning, Jurgen Watermann of DMI, and Kalevi Mursula of the University of Oulu for fruitful discussions and helpful comments. This work was mainly supported by the NATO Collaborative Research Grant EST.CLG.975033; a partial support was also received from the U.S. National Science Foundation awards OPP-9614175 and OPP-9876473 to the University of Michigan. V.O.P., L.I.G., and V.A.P. are grateful to DMI for the opportunity to undertake this study, help with data and facilities, and lavish hospitality.

References

Ahn, B.-H., H. W. Kroehl, Y. Kamide, and E. A. Kihn, Universal time variations of the auroral electrojet indices, *J. Geophys. Res., 105*, 267, 2000a.

Ahn, B.-H., H. W. Kroehl, Y. Kamide, and E. A. Kihn, Seasonal and solar cycle variations of the auroral electrojet indices, *J. Atmos. Solar-Terr. Phys., 62*, 1301, 2000b.

Ballatore, P., C. G. Maclennan, M. J. Engebretson, M. Candidi, J. Bitterly, C.-I. Meng, and G. Burns, A new southern high-latitude index, *Ann. Geophys, 16,* 1589, 1998.

Ballatore, P., and C. G. Maclennan, Significance of the high-latitude geomagnetic index AES-80: comparison with the PC index, *Earth, Planets and Space, 51,* No. 6, 425-430, 1999.

Chun, F. K., D. J. Knipp, M. G. McHarg, G. Lu, B. A. Emery, and O. A. Troshichev, Polar cap index as a proxy for hemispheric Joule heating, *Geophys. Res. Lett., 26,* 1101, 1999.

Couzens, D. A., and J. H. King, *Interplanetary Medium Data Book – Supplement 3a, 1977-1985*, Report NSSDC/WDC-A-R&S 86-04a, National Space Science Data Center, NASA Goddard Space Flight Center, Greenbelt, Maryland, 1986.

Fairfield, D. H., Polar magnetic disturbances and the interplanetary magnetic field, *COSPAR Space Res., VIII*, 107, 1968.

Gustafsson, G., N. E. Papitashvili, and V. O. Papitashvili, A revised corrected geomagnetic coordinate system for Epochs 1985 and 1990, *J. Atmos. Terr. Phys., 54*, No. 11/12, 1609-1631, 1992.

Kan, J. R., and L. C. Lee, Energy coupling function and solar wind-magnetosphere dynamo, *Geophys. Res. Lett., 6,* 577, 1979.

King, J. H., and N. E. Papitashvili, *Interplanetary Medium Data Book, Supplement 5, 1988-1993,* NSSDC/WDC-A-R&S 94-08, National Space Science Data Center, NASA Goddard Space Flight Center, Greenbelt, Maryland, 1994.

Kokubun, S., Relationship of interplanetary magnetic field structure with development of substorm and storm main phase, *Planet. Space Sci., 20*, 1033, 1972.

Maclennan, C. G., P. Ballatore, M. J. Engebretson, and L. J. Lanzerotti, A southern high latitude geomagnetic index: AES-80, *Antarctic J. of the U.S., 32*, No. 5, 193, 1997.

Papitashvili, V. O., and O. Rasmussen, Effective area for the northern polar cap magnetic activity index, *Geophys. Res. Lett., 26,* No. 19, 2917-2920, 1999.

Papitashvili, V. O., B. A. Belov, D. S. Faermark, Ya. I. Feldstein, S. A. Golyshev, L. I. Gromova, and A. E. Levitin, Electric potential patterns in the northern and southern polar regions parameterized by the interplanetary magnetic field, *J. Geophys. Res., 99*, 13,251, 1994.

Papitashvili, V. O., N. E. Papitashvili, and J. H. King, Solar cycle effects in planetary geomagnetic activity: Analysis of 36-year long OMNI dataset, *Geophys. Res. Lett., 27*, No. 17, 2797-2800, 2000.

Russell, C. T., and R. L. McPherron, Semiannual variation of geomagnetic activity, *J. Geophys. Res., 78*, 92, 1973.

Saroso, S., M. Sugiura, T. Iyemori, T. Araki, and T. Kamei, Derivation of polar cap AE indices, in *Proc. NIPR Symp. Upper Atmos., No. 5*, p. 35, National Institute of Polar Research, Tokyo, Japan, 1992.

Shue, J.-H. , and D. R. Weimer, The relationship between ionospheric convection and magnetic activity, *J. Geophys. Res., 99*, 401, 1994.

Takalo, J., and J. Timonen, On the relation of the AE and PC indices, *J. Geophys. Res., 103*, 29,393, 1998.

Troshichev, O. A., and V. G. Andrezen, The relationship between interplanetary quantities and magnetic activity in the southern polar cap, *Planet. Space Sci., 33*, 415, 1985.

Troshichev, O. A., N. P. Dmitrieva, and B. M. Kuznetsov, Polar cap magnetic activity as a signature of substorm development, *Planet. Space Sci., 27*, 217, 1979.

Troshichev, O. A., V. G. Andrezen, S. Vennerstrøm, and E. Friis-Christensen, Magnetic activity in the polar cap – A new index, *Planet. Space Sci., 36*, 1095, 1988.

Troshichev, O. A., V. G. Andrezen, S. Vennerstrøm, and E. Friis-Christensen, *Polar cap (PC) geomagnetic activity index for 1975–1982*, World Data Center B, Soviet Geophysical Committee, Academy of Sciences of the USS, Moscow, 142 pp., 1991.

Troshichev, O. A., R. Yu. Lukianova, V. O. Papitashvili, F. J. Rich, and O. Rasmussen, Polar cap index (PC) as a proxy for ionospheric electric field in the near-pole region, *Geophys. Res. Lett., 27*, 3809, 2000.

Troshichev, O. A., O. Rasmussen, and V. O. Papitashvili, Polar Cap (PC) Magnetic Activity Index, *IAGA News*, No. 40, 2001.

Vassiliadis, D., V. Angelopoulos, D. N. Baker, and A. J. Klimas, The relation between the northern polar cap and auroral electrojet geomagnetic indices in the wintertime, *Geophys. Res. Lett., 23,* 2781, 1996.

Vennerstrøm, S., *The geomagnetic activity index PC*, Ph. D. Thesis, *Scientific Report 91-3*, Danish *Meteorological* Institute, 105 pp., 1991.

Vennerstrøm, S., E. Friis-Christensen, O. A. Troshichev, and V. G. Andrezen, Comparison between the polar cap index PC and the auroral electrojet indices AE, AL and AU, *J. Geophys. Res., 96*, 101, 1991.

Vennerstrøm, S., E. Friis-Christensen, O. A. Troshichev, and V. G. Andrezen, Geomagnetic Polar Cap (PC) Index 1975-1993, *Report UAG-103, WDC-A for STP*, NGDC, Boulder, Colo., 274 pp., 1994.

Appendix A

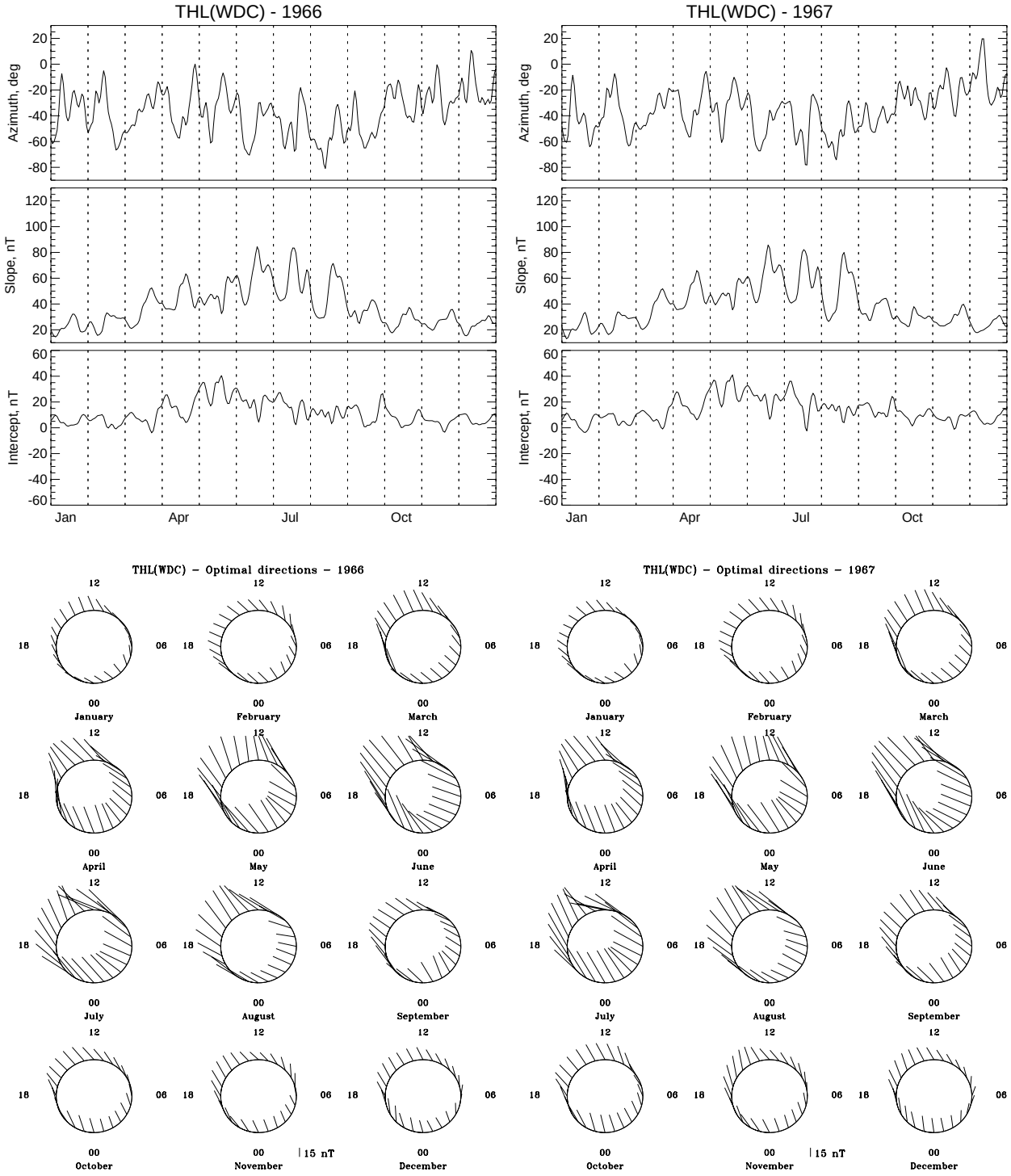

Figure A1. The same as in **Figure 4** (right panel) but plotted for years 1966 (left panel) and 1967 (right panel).

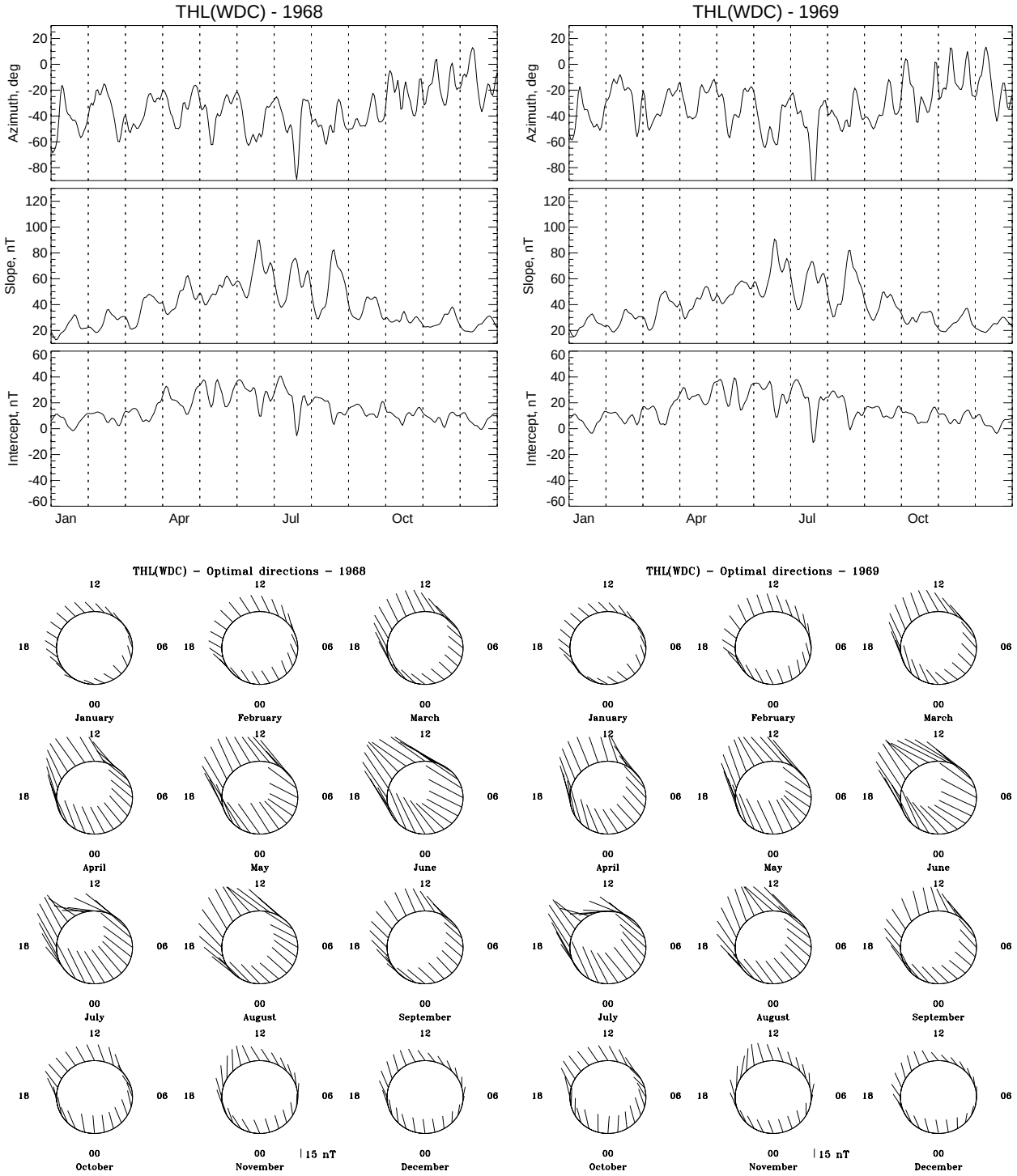

Figure A2. The same as in **Figure A1** but plotted for years 1968 (left panel) and 1969 (right panel).

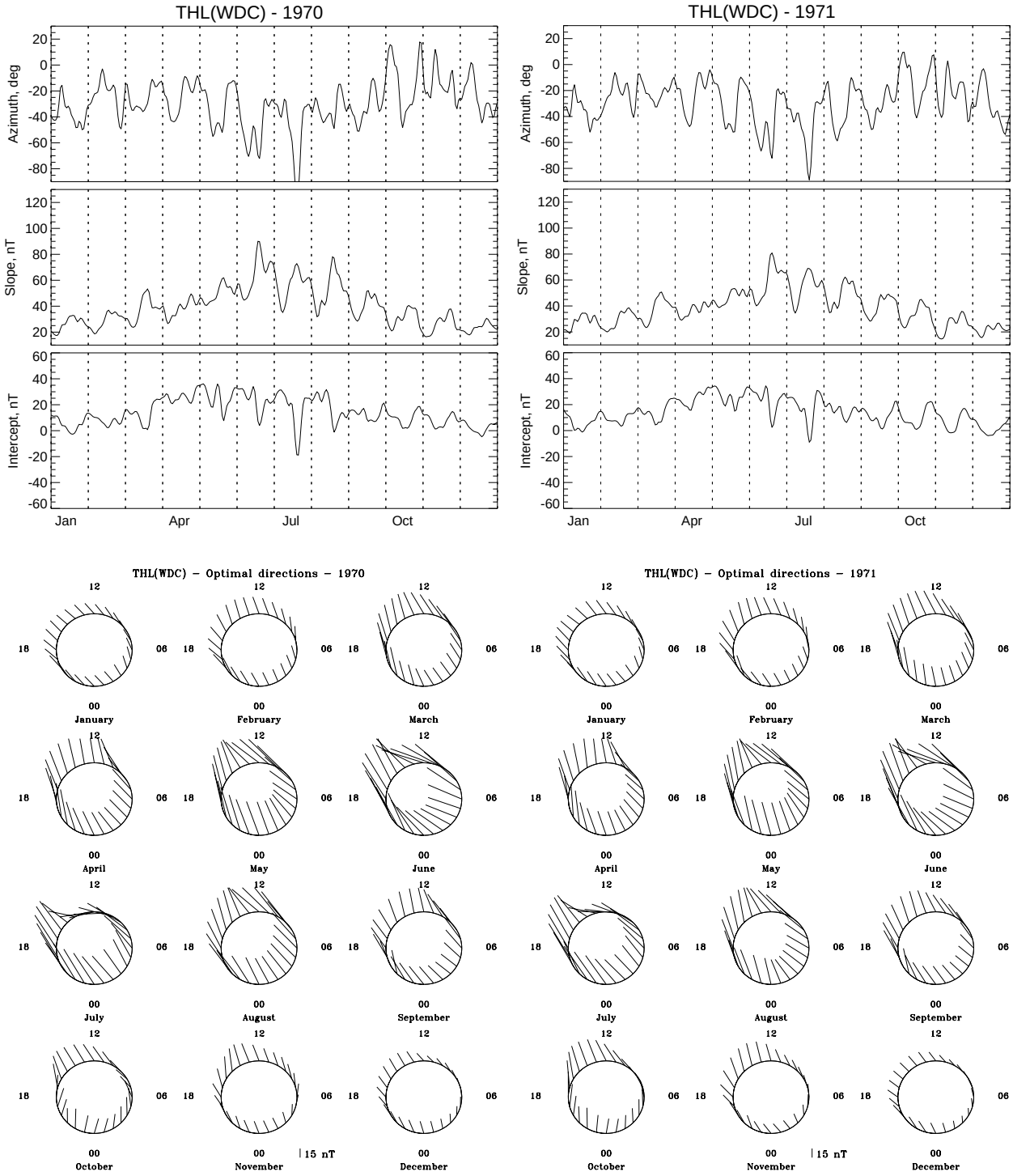

Figure A3. The same as in **Figure A1** but plotted for years 1970 (left panel) and 1971 (right panel).

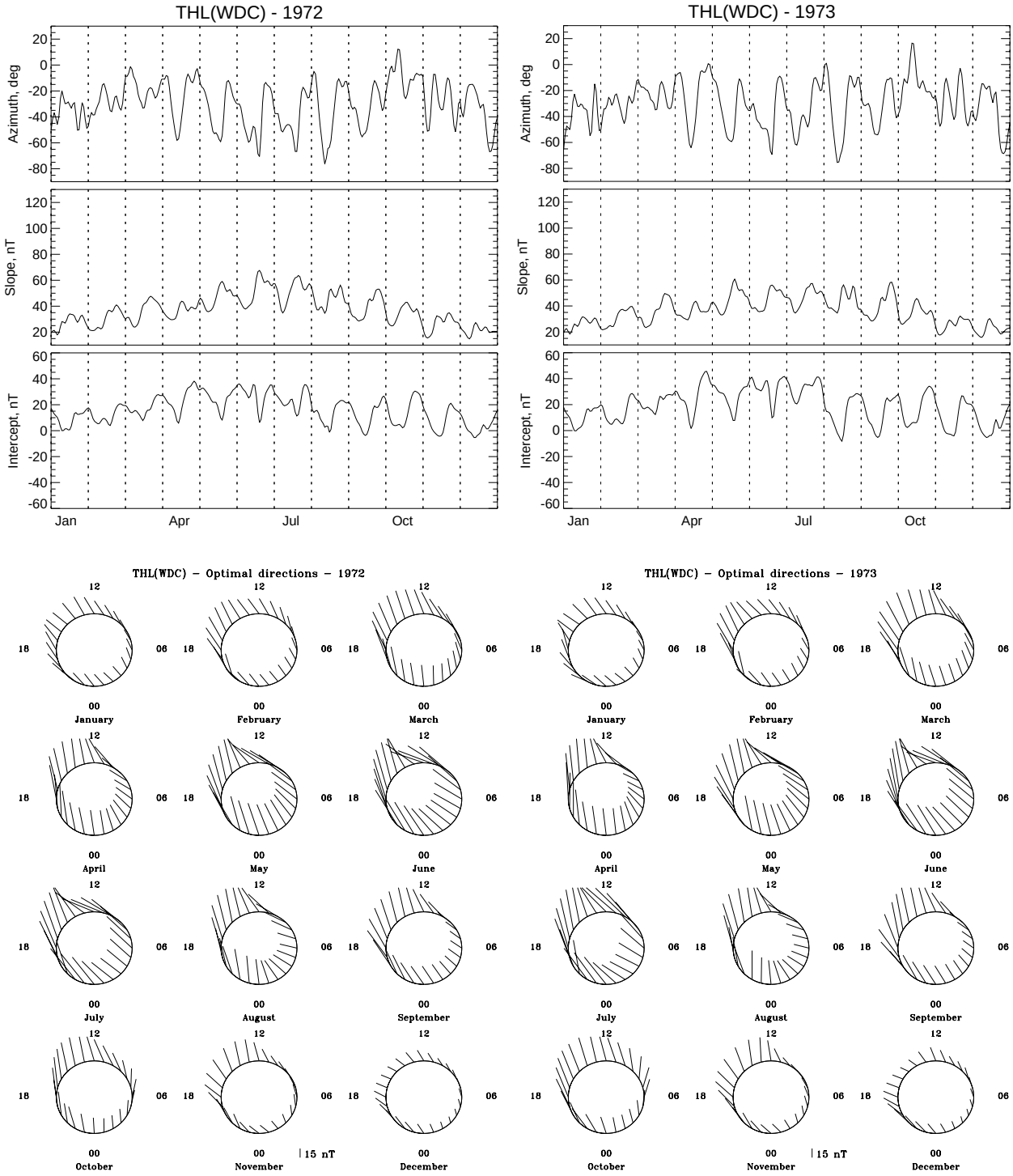

Figure A4. The same as in **Figure A1** but plotted for years 1972 (left panel) and 1973 (right panel).

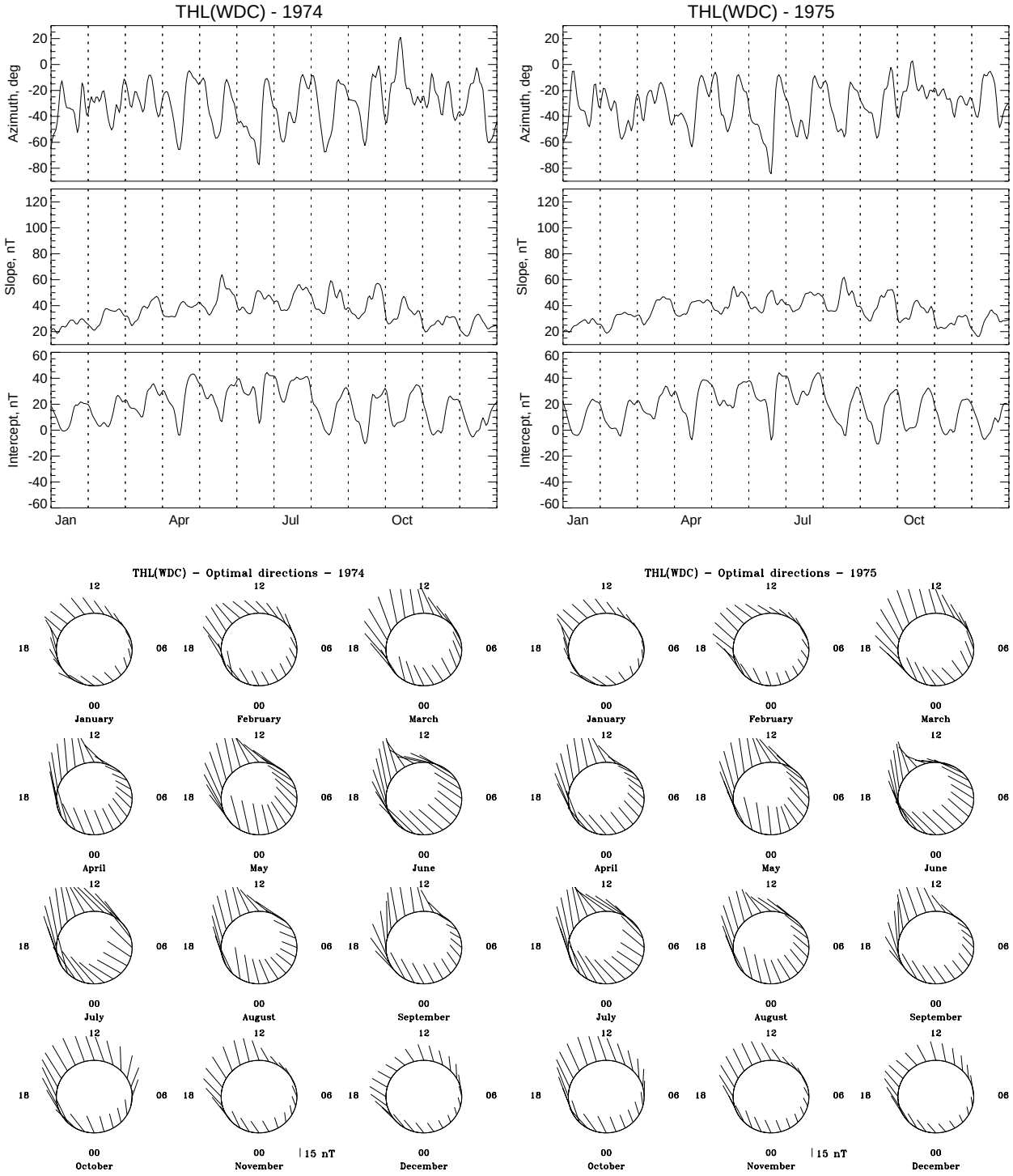

Figure A5. The same as in **Figure A1** but plotted for years 1974 (left panel) and 1975 (right panel).

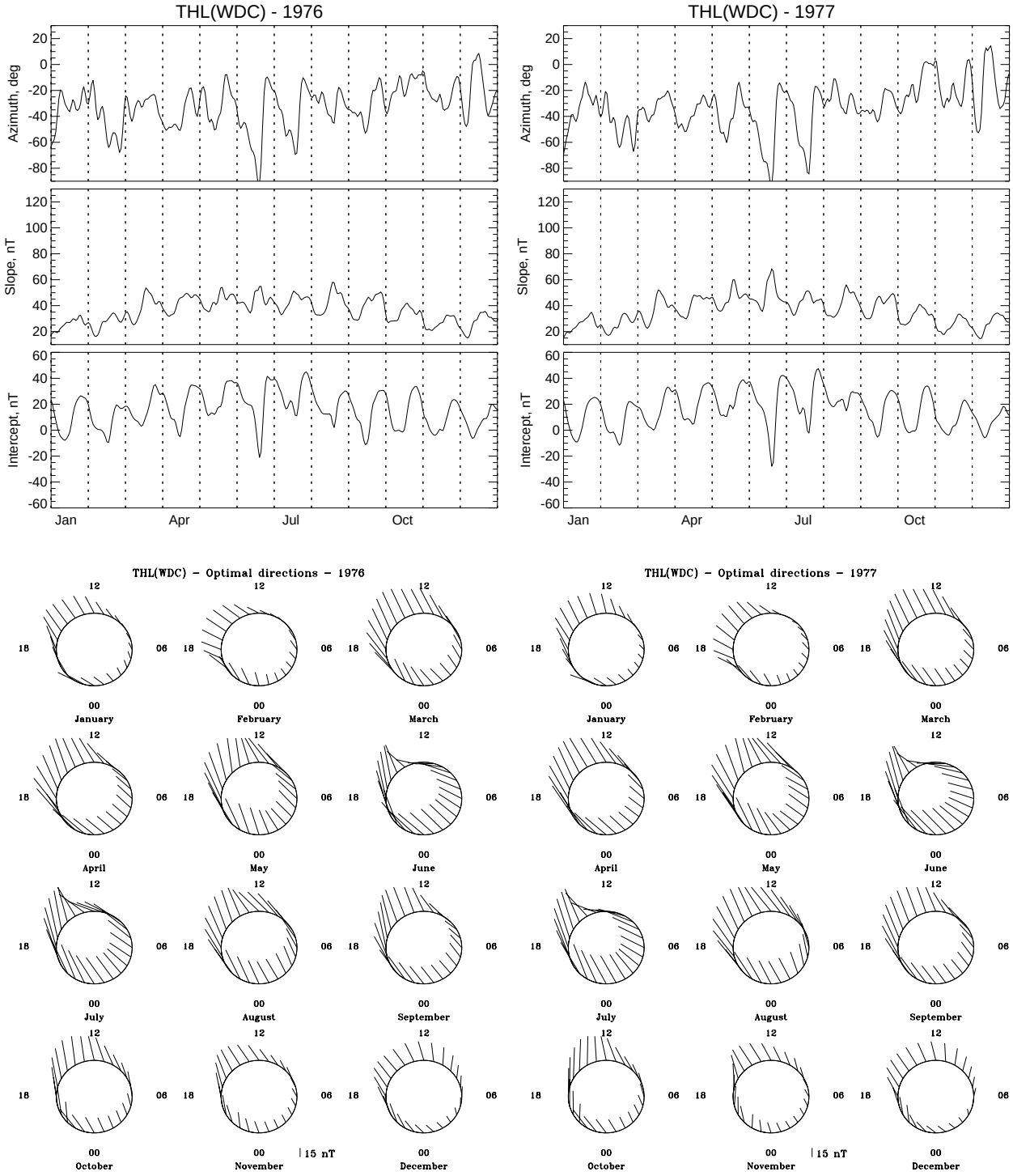

Figure A6. The same as in **Figure A1** but plotted for years 1976 (left panel) and 1977 (right panel).

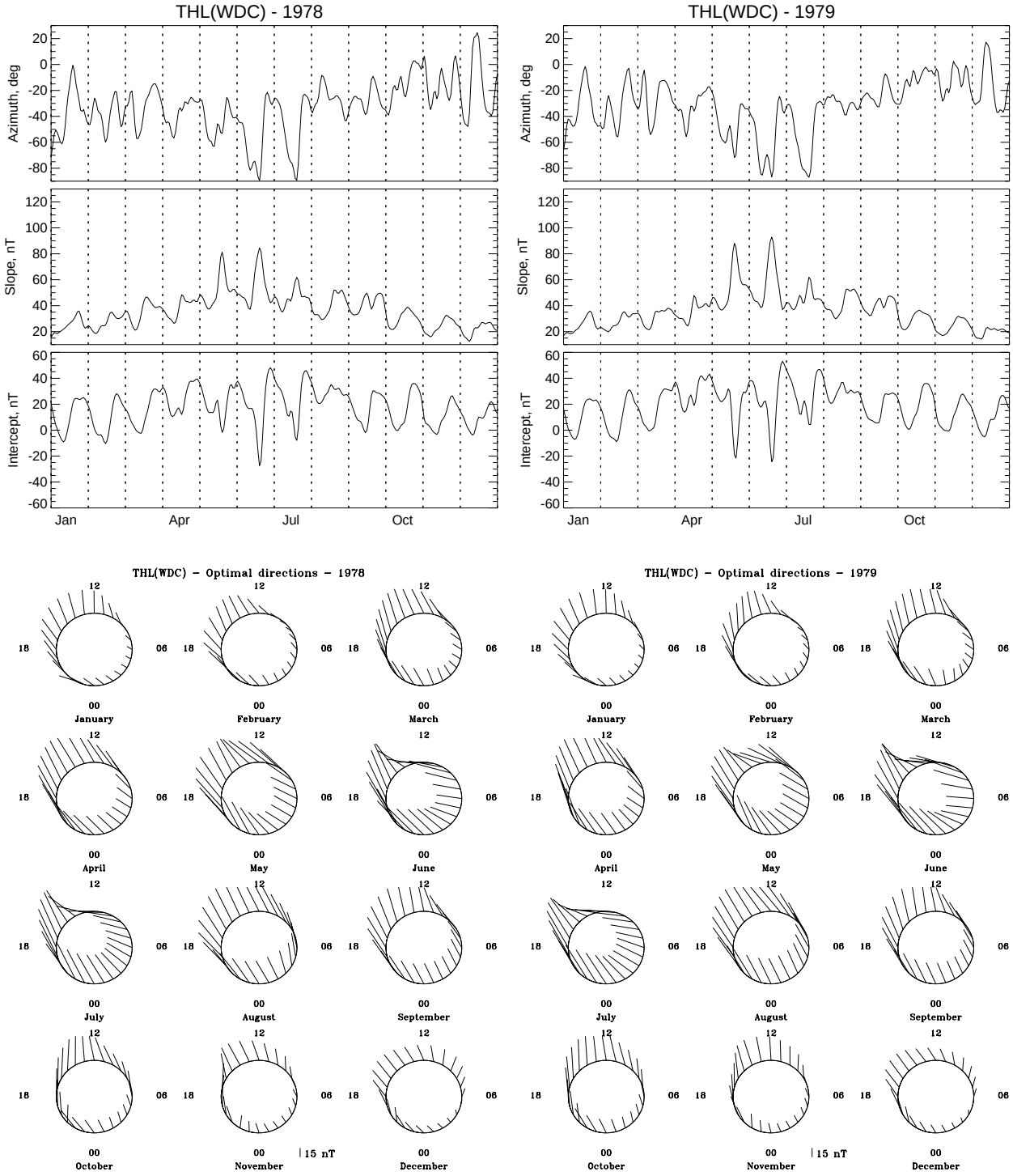

Figure A7. The same as in **Figure A1** but plotted for years 1978 (left panel) and 1979 (right panel).

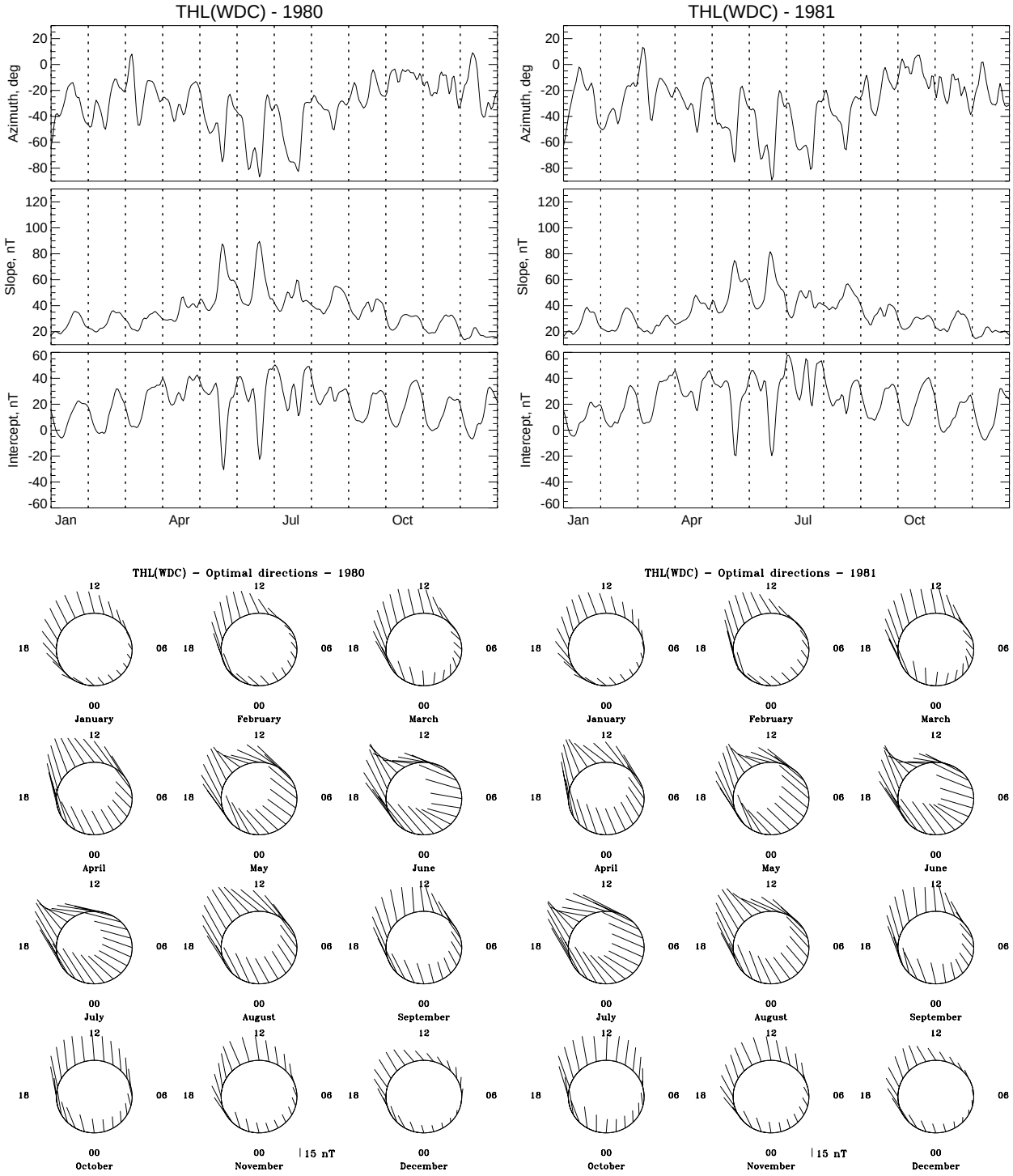

Figure A8. The same as in **Figure A1** but plotted for years 1980 (left panel) and 1981 (right panel).

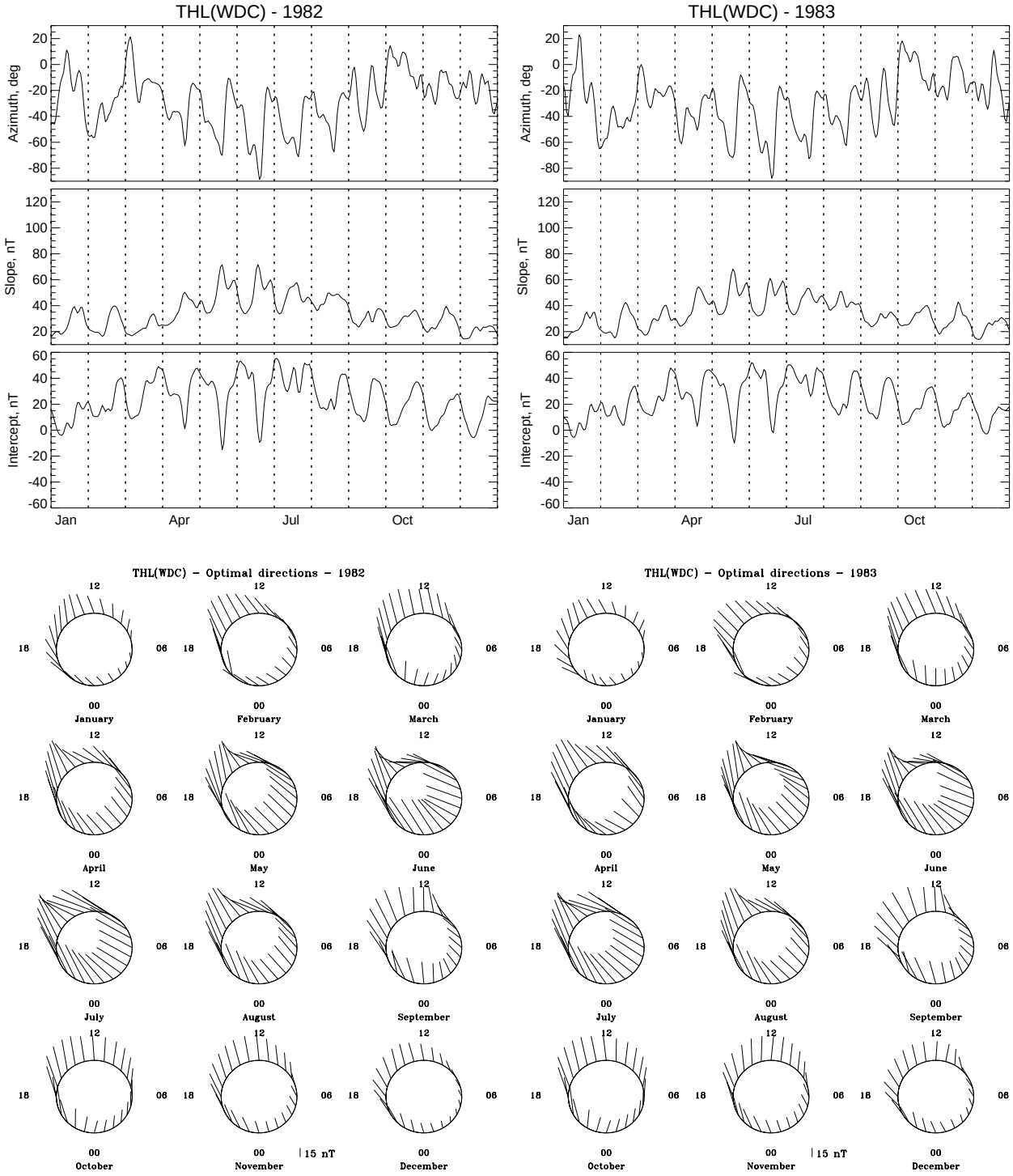

Figure A9. The same as in **Figure A1** but plotted for years 1982 (left panel) and 1983 (right panel).

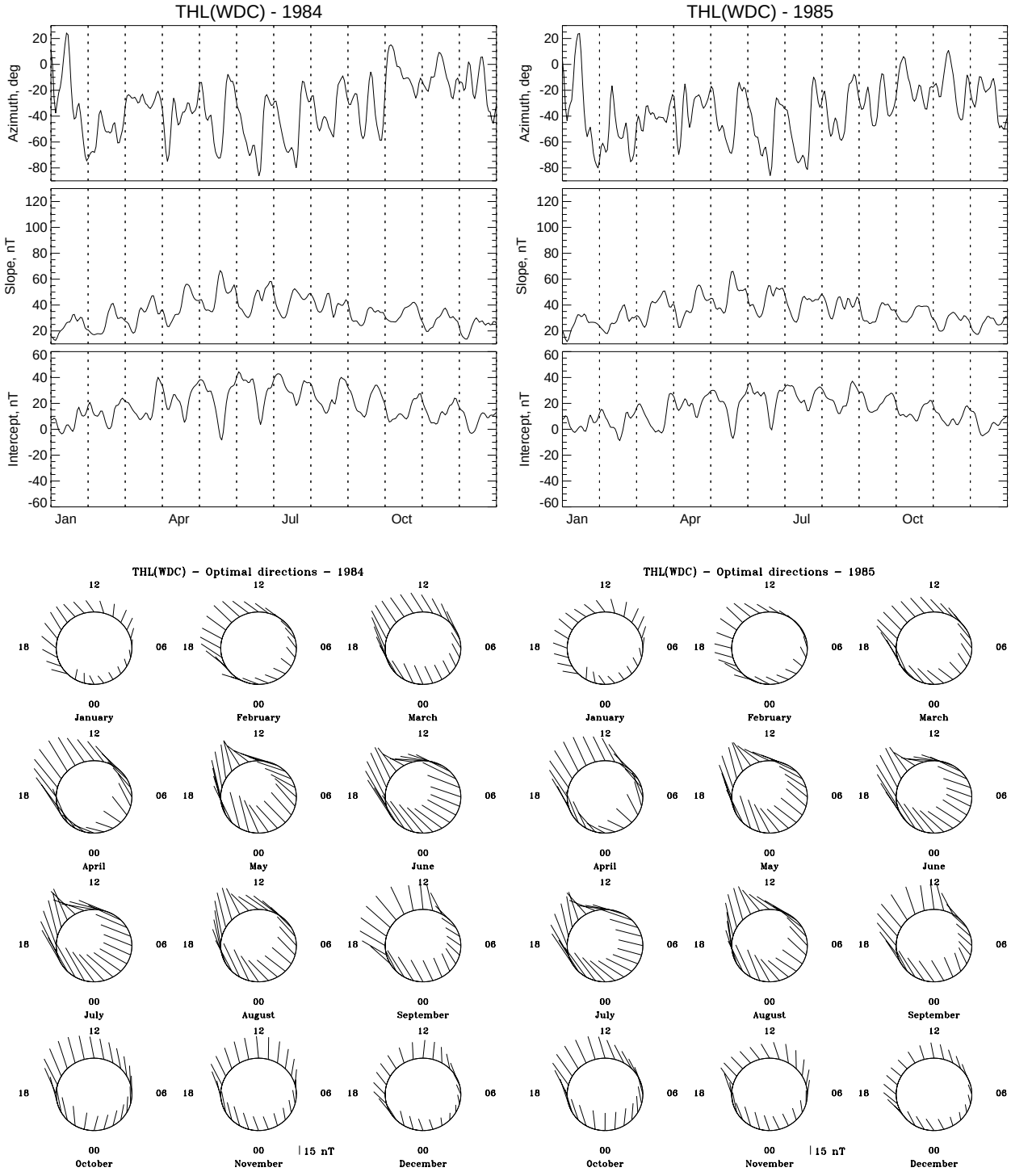

Figure A10. The same as in **Figure A1** but plotted for years 1984 (left panel) and 1985 (right panel).

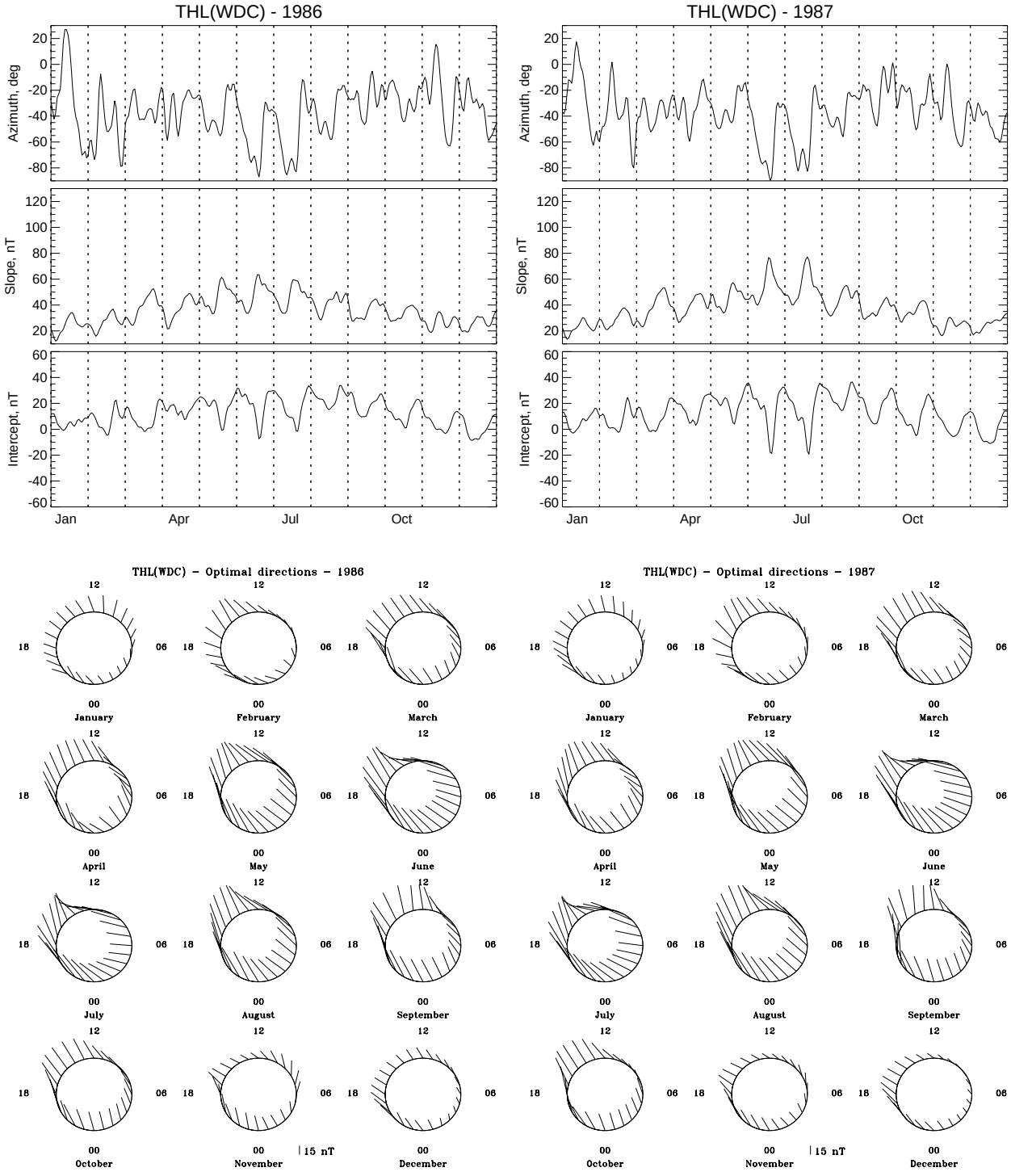

Figure A11. The same as in **Figure A1** but plotted for years 1986 (left panel) and 1987 (right panel).

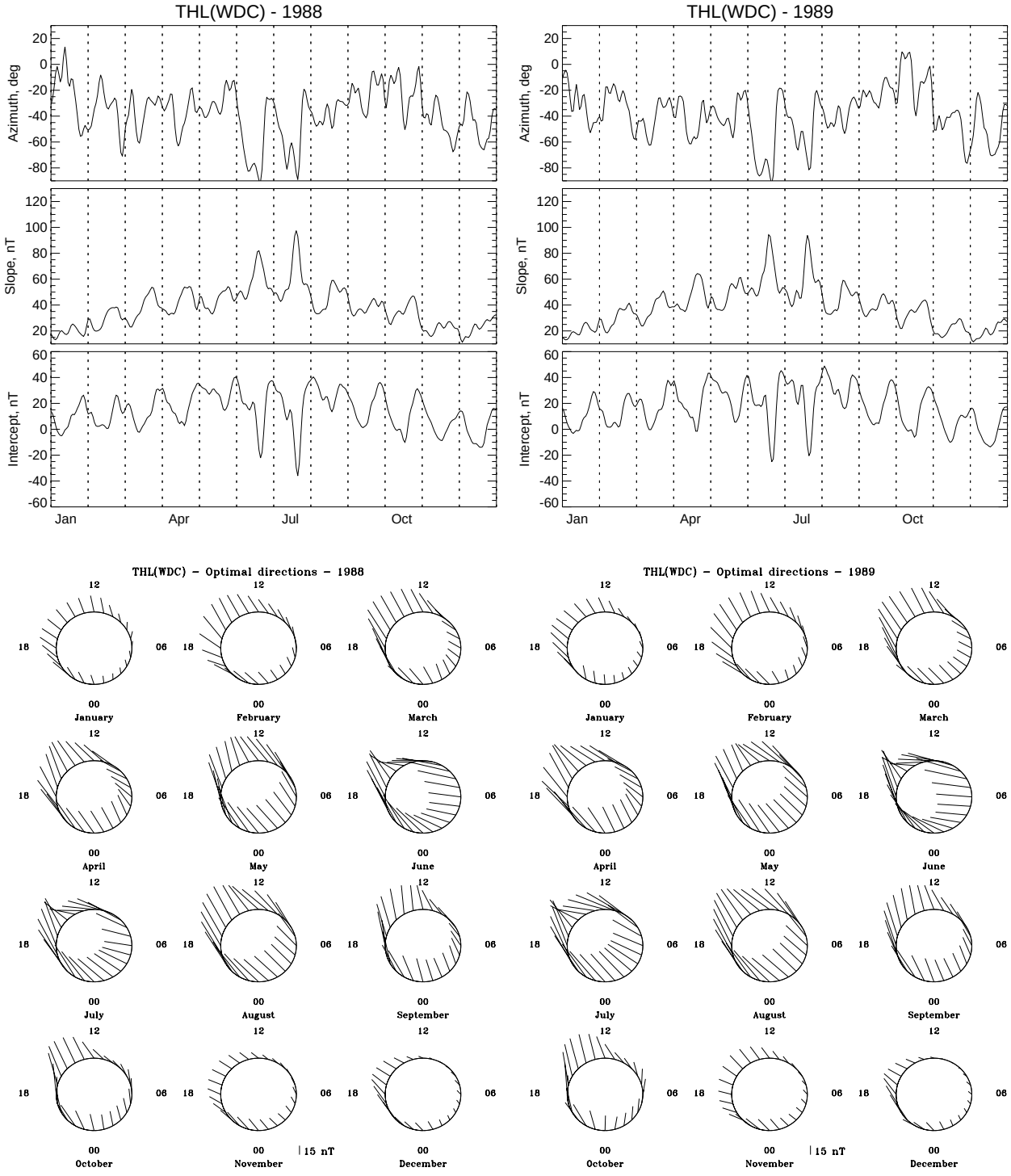

Figure A12. The same as in **Figure A1** but plotted for years 1988 (left panel) and 1989 (right panel).

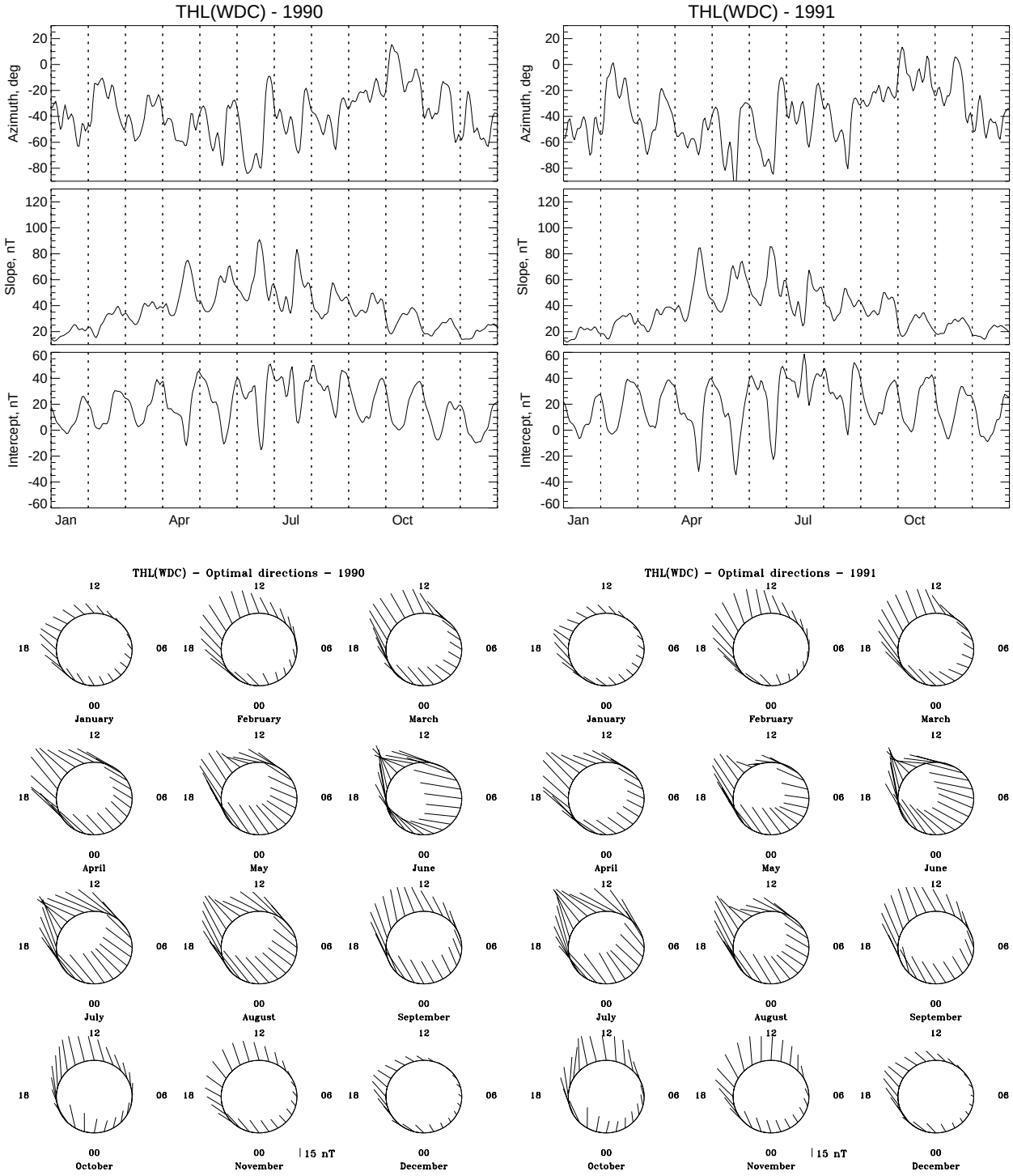

Figure A13. The same as in **Figure A1** but plotted for years 1990 (left panel) and 1991 (right panel).

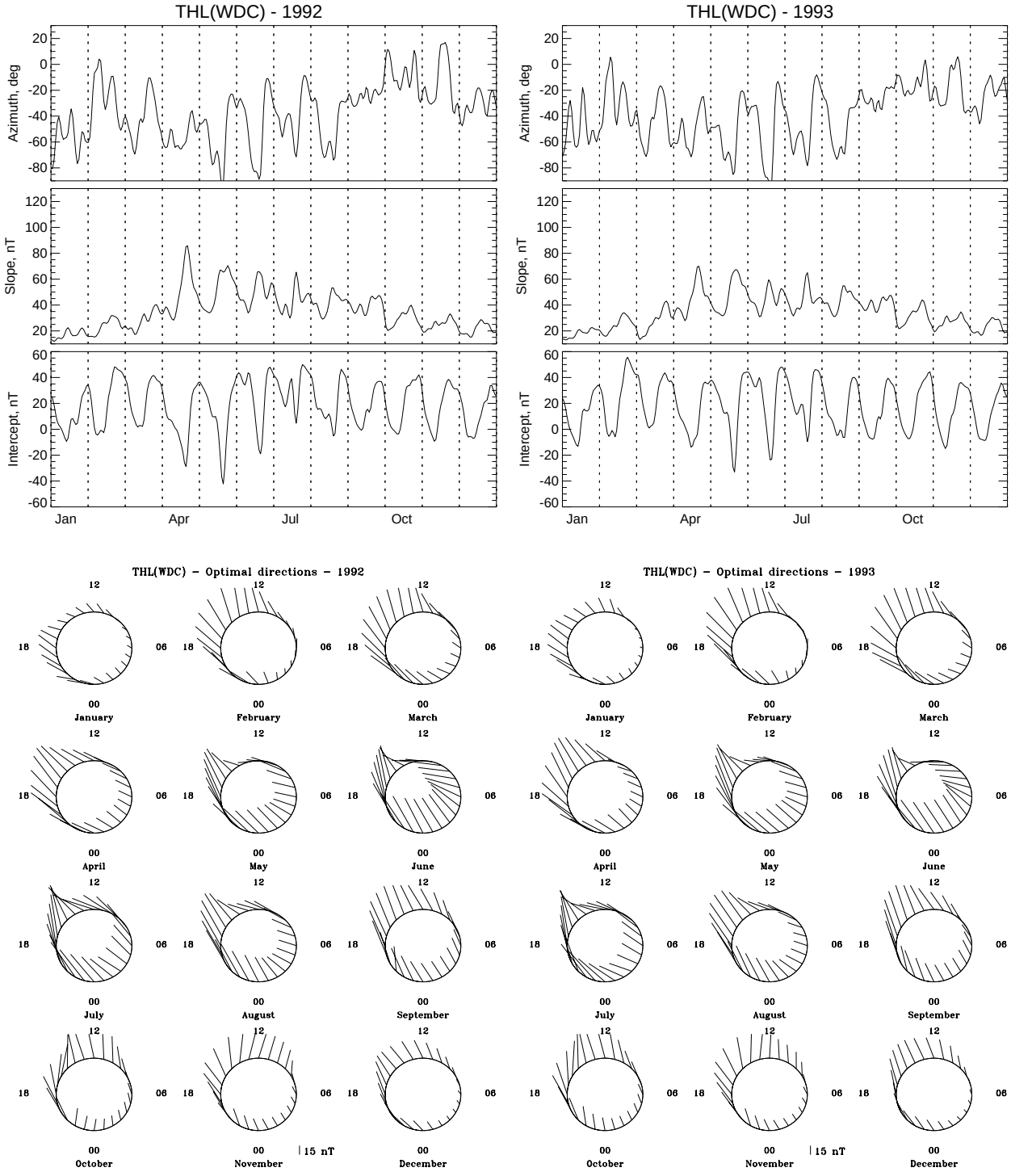

Figure A14. The same as in **Figure A1** but plotted for years 1992 (left panel) and 1993 (right panel).

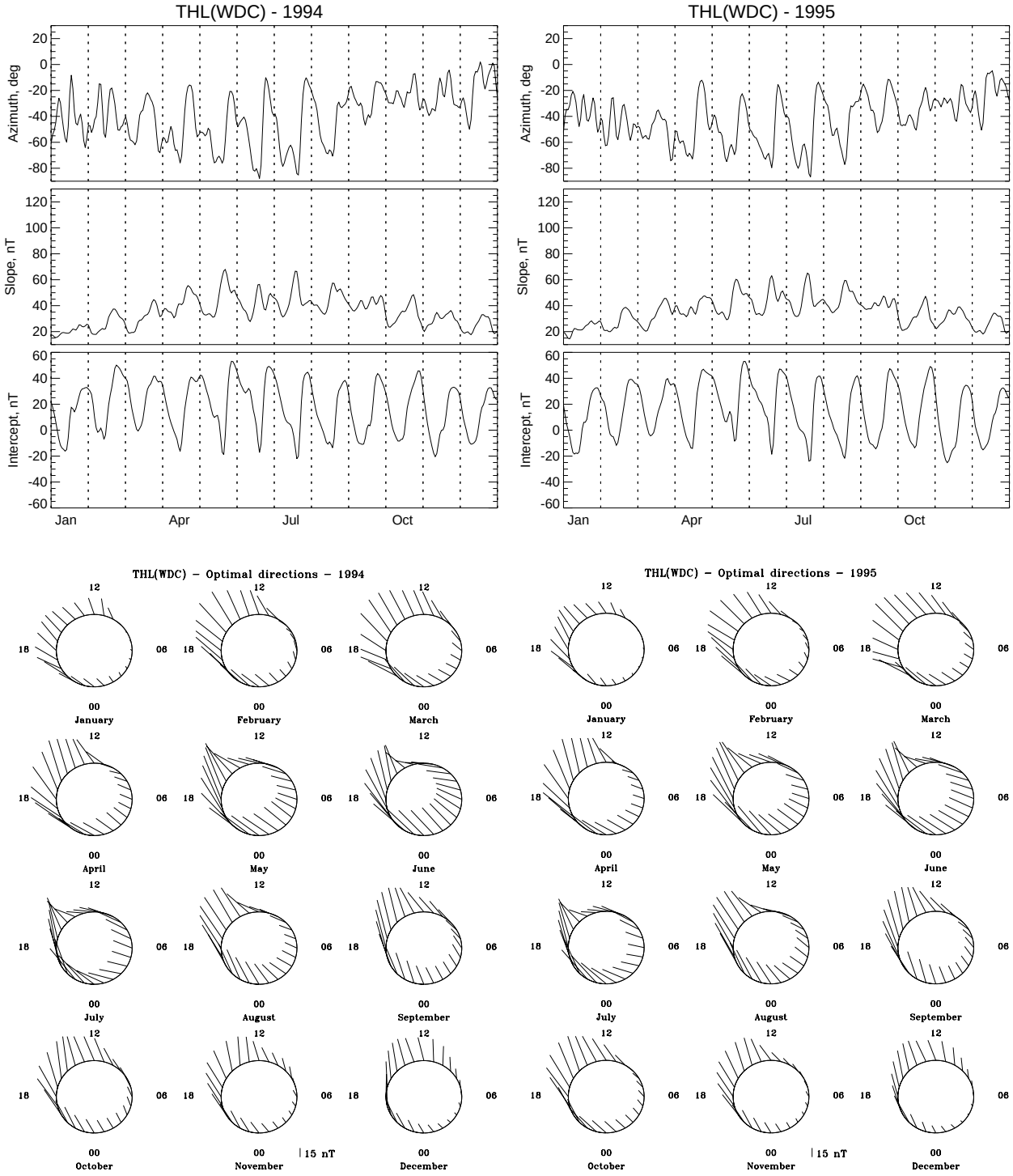

Figure A15. The same as in **Figure A1** but plotted for years 1994 (left panel) and 1995 (right panel).

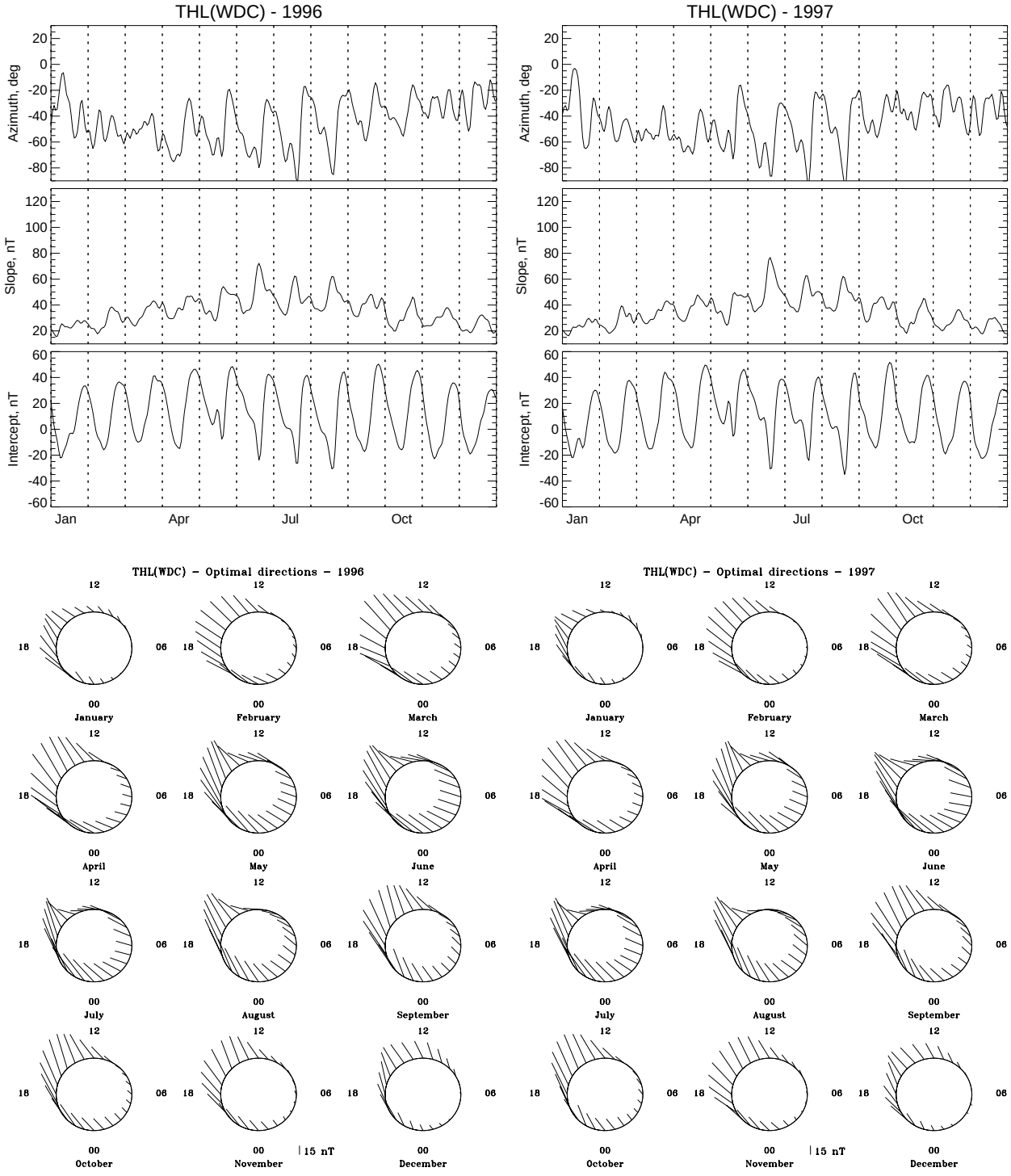

Figure A16. The same as in **Figure A1** but plotted for years 1996 (left panel) and 1997 (right panel).

Appendix B

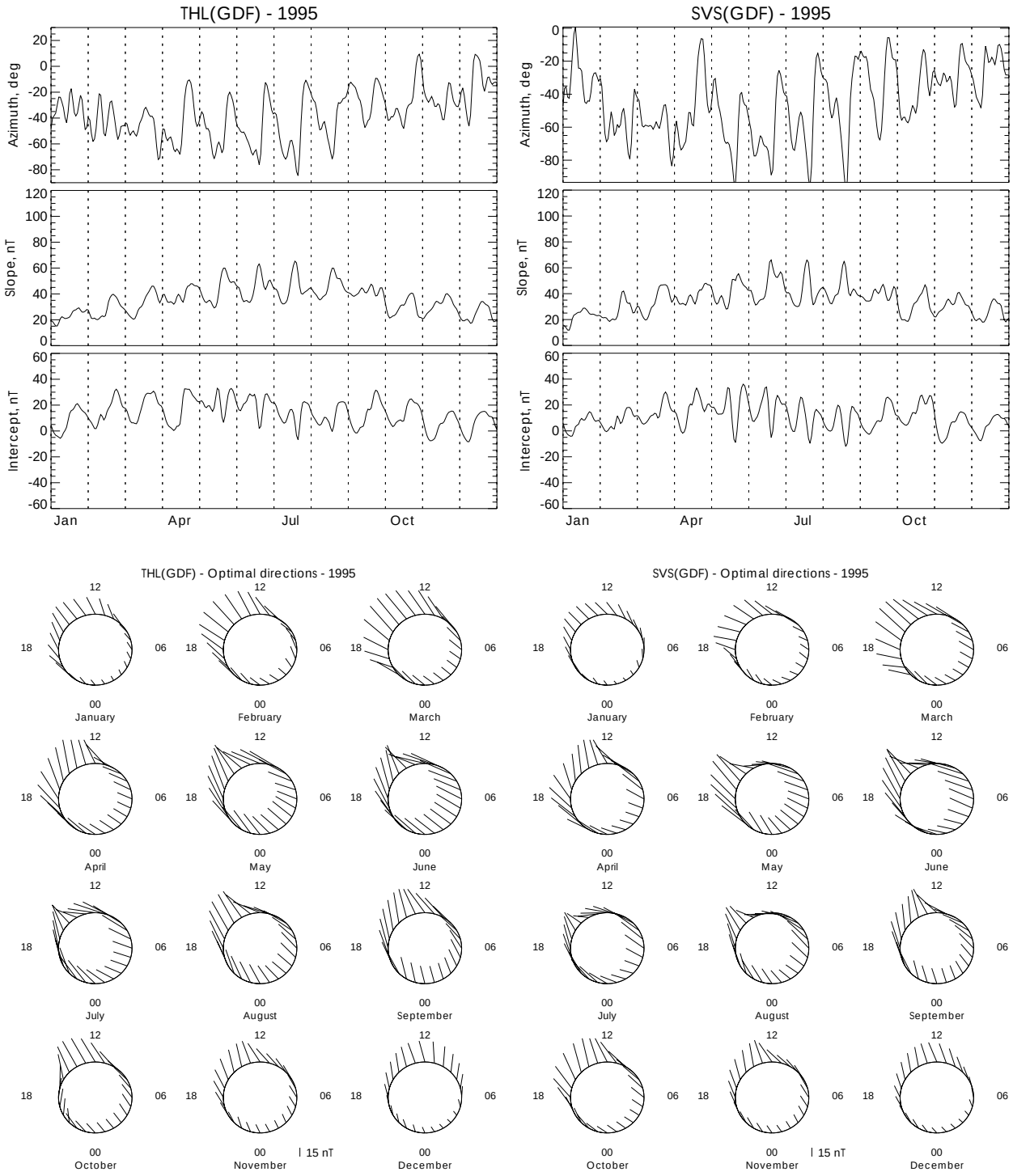

Figure B1. The normalization coefficients and optimal directions for THL(GDF) – 1995 (left panel – this plot is similar to the right panel in **Figure A15**) and SVS(GDF) – 1995 (right panel).

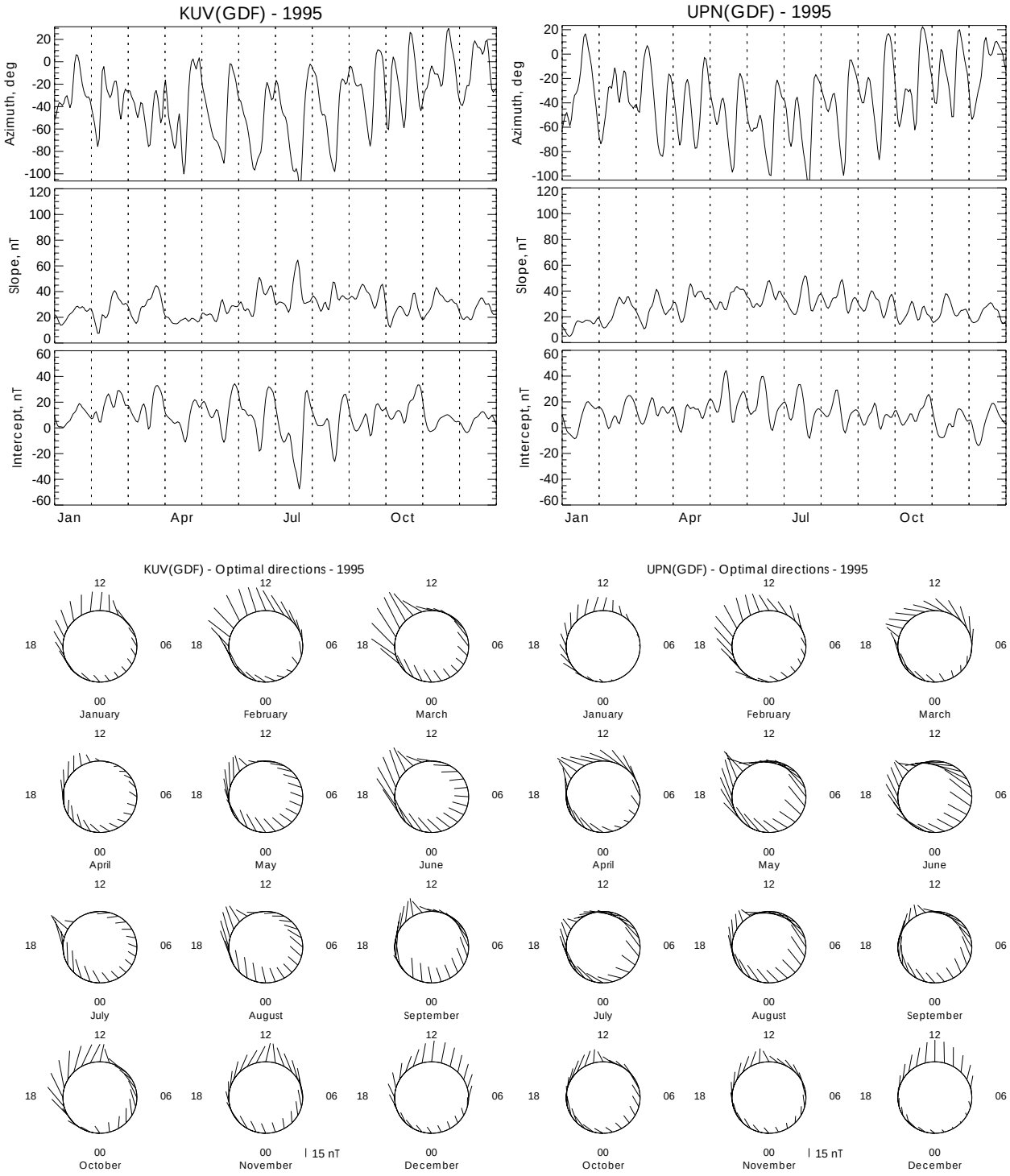

Figure B2. The same as in **Figure B1** but for KUV(GDF) – 1995 (left panel) and UPN(GDF) – 1995 (right panel).

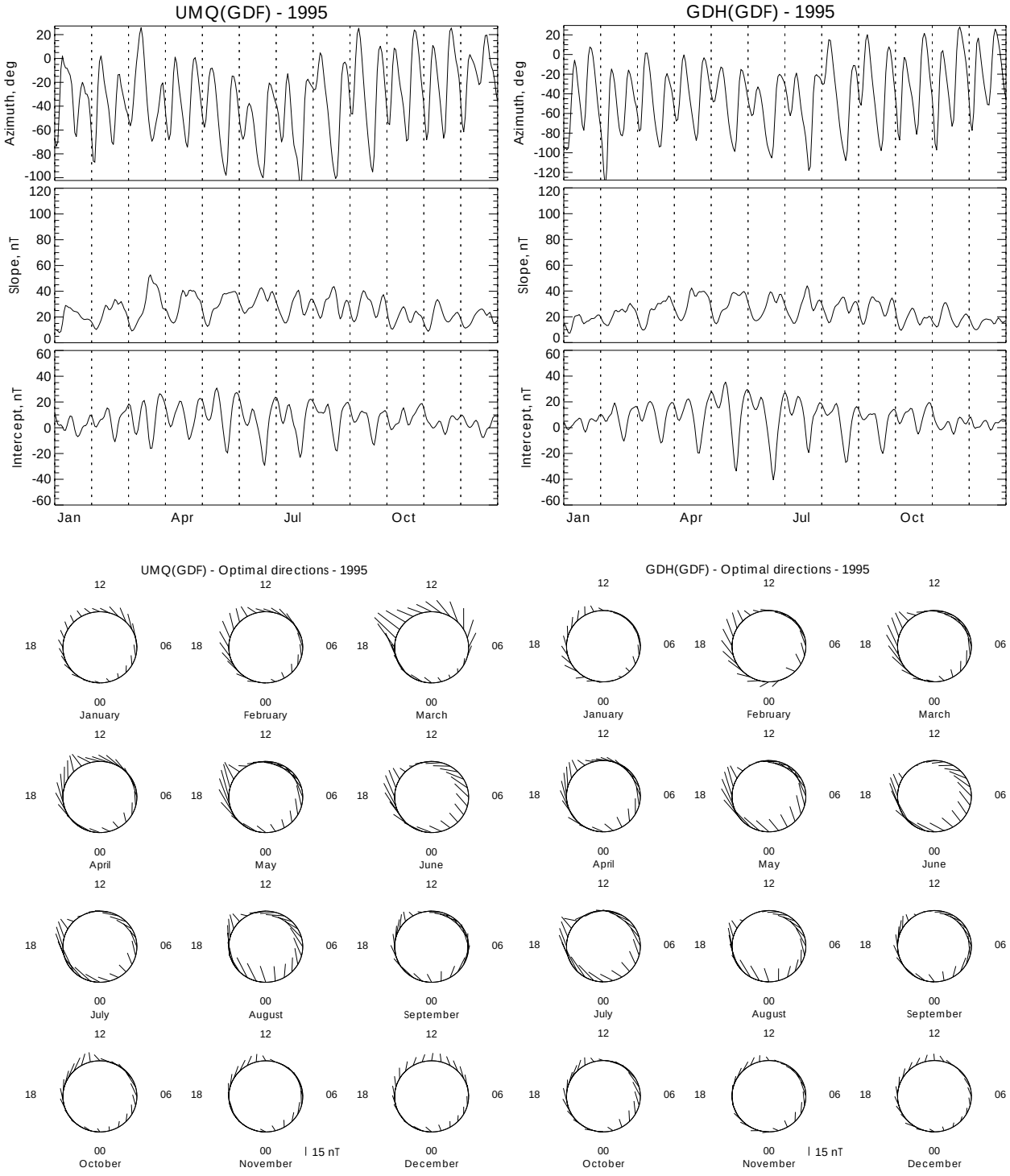

Figure B3. The same as in **Figure B1** but for UMQ(GDF) – 1995 (left panel) and GDH(GDF) – 1995 (right panel).

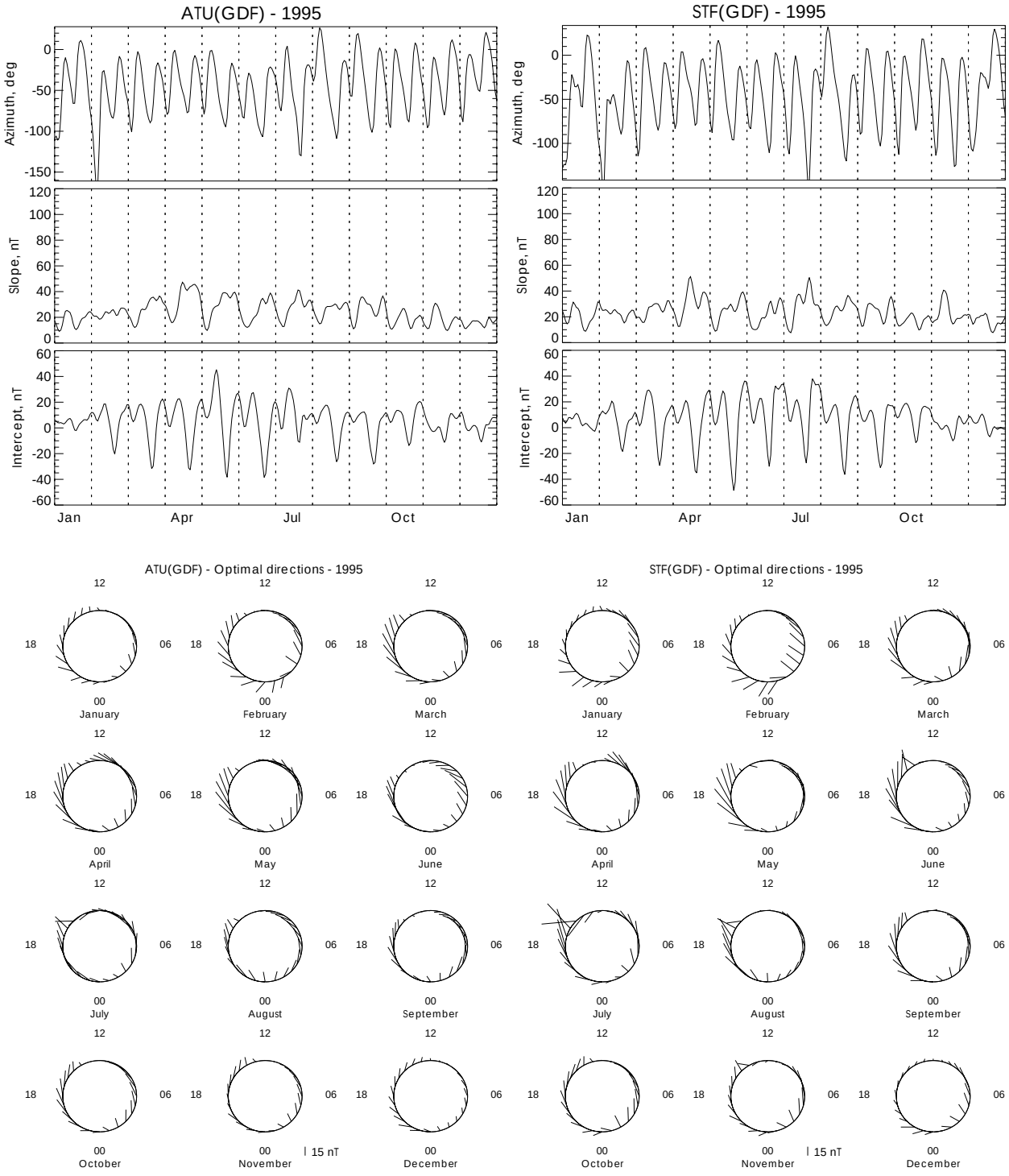

Figure B4. The same as in **Figure B1** but for ATU(GDF) – 1995 (left panel) and STF(GDF) – 1995 (right panel).

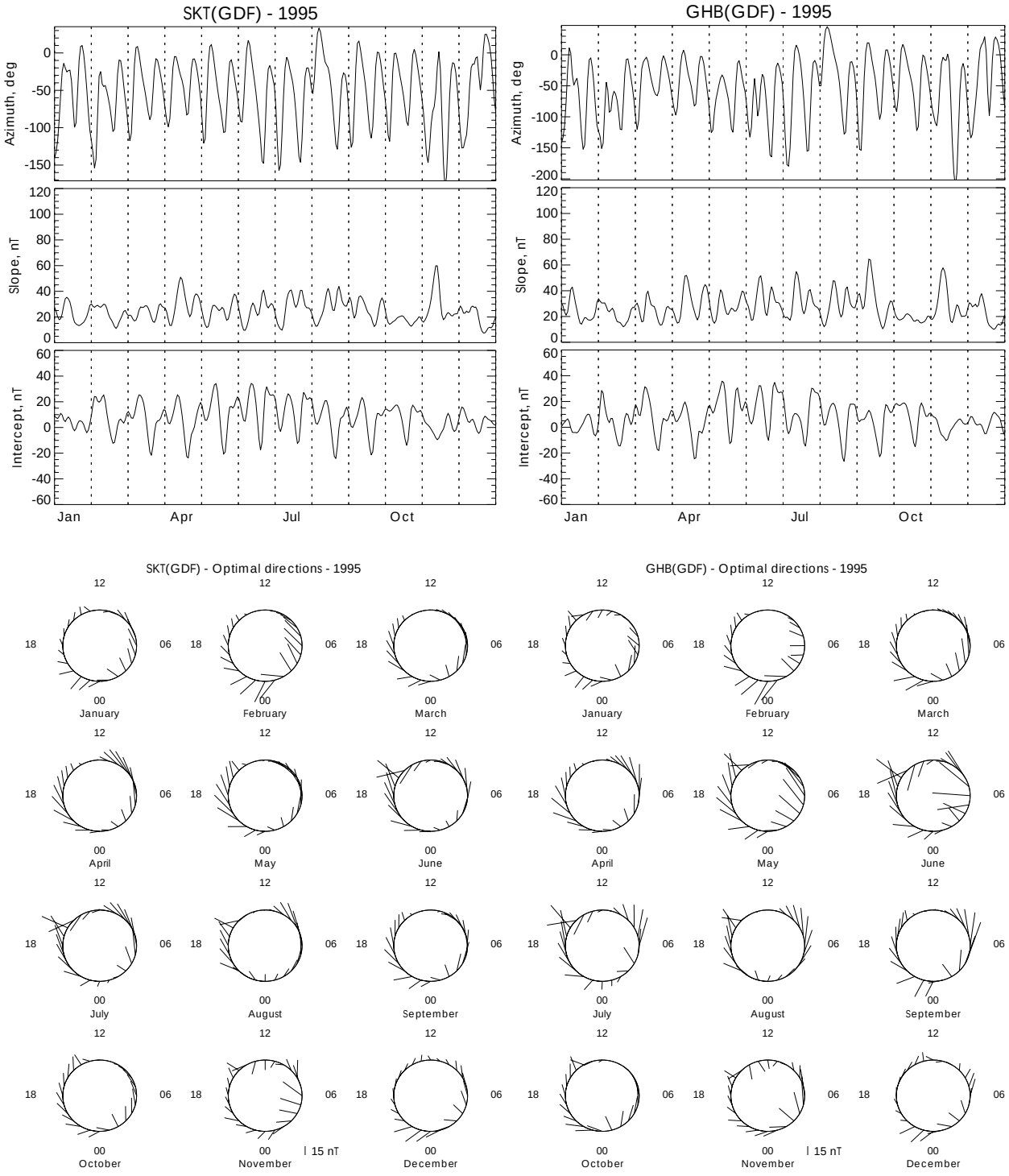

Figure B5. The same as in **Figure B1** but for SKT(GDF) – 1995 (left panel) and GHB(GDF) – 1995 (right panel).

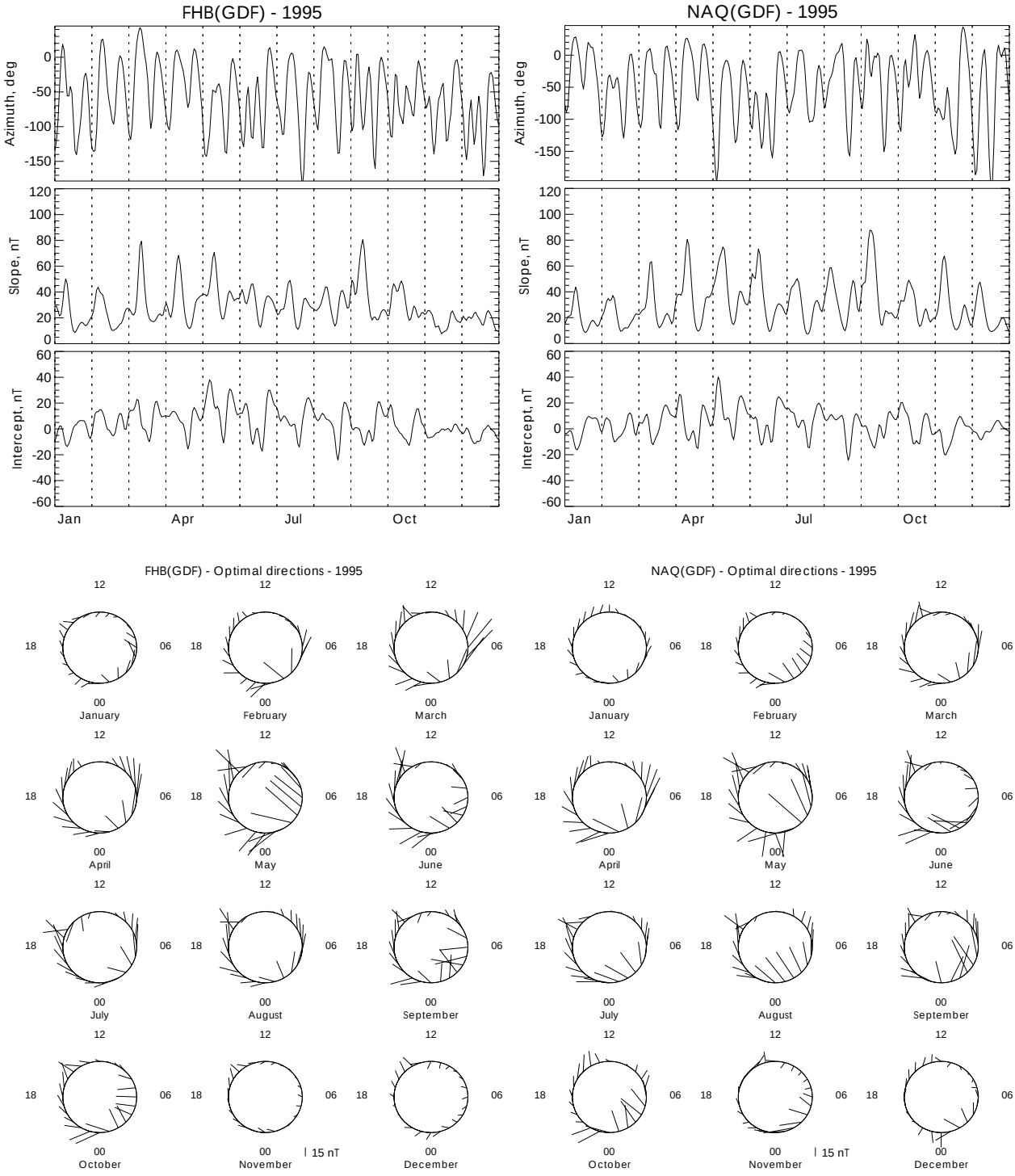

Figure B6. The same as in **Figure B1** but for FHB(GDF) – 1995 (left panel) and NAQ(GDF) – 1995 (right panel).

DANISH METEOROLOGICAL INSTITUTE

Scientific Reports

Scientific reports from the Danish Meteorological Institute cover a variety of geophysical fields, i.e. meteorology (including climatology), oceanography, subjects on air and sea pollution, geomagnetism, solar-terrestrial physics, and physics of the middle and upper atmosphere.

Reports in the series within the last five years:

No. 96-1
Poul Frich (coordinator)**, H. Alexandersson, J. Ashcroft, B. Dahlström, G. R. Demarée, A. Drebs, A. F. V. van Engelen, E. J. Førland, I. Hanssen-Bauer, R. Heino, T. Jónsson, K. Jonasson, L. Keegan, P. Ø. Nordli, T. Schmith, P. Steffensen, H. Tuomenvirta, O. E. Tveito:** North Atlantic Climatological Dataset (NACD Version 1) - Final report

No. 96-2
Georg Kjærgaard Andreasen: Daily response of high-latitude current systems to solar wind variations: application of robust multiple regression. Methods on Godhavn magnetometer data

No. 96-3
Jacob Woge Nielsen, Karsten Bolding Kristensen, Lonny Hansen: Extreme sea level highs: a statistical tide gauge data study

No. 96-4
Jens Hesselbjerg Christensen, Ole Bøssing Christensen, Philippe Lopez, Erik van Meijgaard, Michael Botzet: The HIRLAM4 Regional Atmospheric Climate Model

No. 96-5
Xiang-Yu Huang: Horizontal diffusion and filtering in a mesoscale numerical weather prediction model

No. 96-6
Henrik Svensmark and Eigil Friis-Christensen: Variation of cosmic ray flux and global cloud coverage - a missing link in solar-climate relationships

No. 96-7
Jens Havskov Sørensen and Christian Ødum Jensen: A computer system for the management of epidemiological data and prediction of risk and economic consequences during outbreaks of foot-and-mouth disease. CEC AIR Programme. Contract No. AIR3 - CT92-0652

No. 96-8
Jens Havskov Sørensen: Quasi-automatic of input for LINCOM and RIMPUFF, and output conversion. CEC AIR Programme. Contract No. AIR3 - CT92-0652

No. 96-9
Rashpal S. Gill and Hans H. Valeur: Evaluation of the radarsat imagery for the operational mapping of sea ice around Greenland

No. 96-10
Jens Hesselbjerg Christensen, Bennert Machenhauer, Richard G. Jones, Christoph Schär, Paolo Michele Ruti, Manuel Castro and Guido Visconti: Validation of present-day regional climate simulations over Europe: LAM simulations with observed boundary conditions

No. 96-11
Niels Larsen, Bjørn Knudsen, Paul Eriksen, Ib Steen Mikkelsen, Signe Bech Andersen and Torben Stockflet Jørgensen: European Stratospheric Monitoring Stations in the Artic: An European contribution to the Network for Detection of

Stratospheric Change (NDSC): CEC Environment Programme Contract EV5V-CT93-0333: DMI contribution to the final report

No. 96-12
Niels Larsen: Effects of heterogeneous chemistry on the composition of the stratosphere: CEC Environment Programme Contract EV5V-CT93-0349: DMI contribution to the final report

No. 97-1
E. Friis Christensen og C. Skøtt: Contributions from the International Science Team. The Ørsted Mission - a pre-launch compendium

No. 97-2
Alix Rasmussen, Sissi Kiilsholm, Jens Havskov Sørensen, Ib Steen Mikkelsen: Analysis of tropospheric ozone measurements in Greenland: Contract No. EV5V-CT93-0318 (DG 12 DTEE): DMI's contribution to CEC Final Report Arctic Trophospheric Ozone Chemistry ARCTOC

No. 97-3
Peter Thejll: A search for effects of external events on terrestrial atmospheric pressure: cosmic rays

No. 97-4
Peter Thejll: A search for effects of external events on terrestrial atmospheric pressure: sector boundary crossings

No. 97-5
Knud Lassen: Twentieth century retreat of sea-ice in the Greenland Sea

No. 98-1
Niels Woetman Nielsen, Bjarne Amstrup, Jess U. Jørgensen: HIRLAM 2.5 parallel tests at DMI: sensitivity to type of schemes for turbulence, moist processes and advection

No. 98-2
Per Høeg, Georg Bergeton Larsen, Hans-Henrik Benzon, Stig Synder-gaard, Mette Dahl Mortensen: The GPSOS project - Algorithm functional design and analysis of ionosphere, stratosphere and troposphere observations

No. 98-3
Mette Dahl Mortensen, Per Høeg: Satellite atmosphere profiling retrieval in a nonlinear troposphere (Previously entitled: Limitations induced by Multipath)

No. 98-4
Mette Dahl Mortensen, Per Høeg: Resolution properties in atmospheric profiling with GPS

No. 98-5
R. S. Gill and M. K. Rosengren: Evaluation of the Radarsat imagery for the operational
mapping of sea ice around Greenland in 1997

No. 98-6
R. S. Gill, H. H. Valeur, P. Nielsen and K. Q. Hansen: Using ERS SAR images in the operational mapping of sea ice in the Greenland waters: final report for ESA-ESRIN's: pilot projekt no. PP2.PP2.DK2 and 2nd announcement of opportunity for the exploitation of ERS data projekt No. AO2..DK 102

No. 98-7
Per Høeg et al.: GPS Atmosphere profiling methods and error assessments

No. 98-8
H. Svensmark, N. Woetmann Nielsen and A.M. Sempreviva: Large scale soft and hard turbulent states of the atmosphere

No. 98-9
Philippe Lopez, Eigil Kaas and Annette Guldberg: The full particle-in-cell advection scheme in spherical geometry

No. 98-10
H. Svensmark: Influence of cosmic rays on earth's climate

No. 98-11
Peter Thejll and Henrik Svensmark: Notes on the method of normalized multivariate regression

No. 98-12
K. Lassen: Extent of sea ice in the Greenland Sea 1877-1997: an extension of DMI Scientific Report 97-5

No. 98-13
Niels Larsen, Alberto Adriani and Guido DiDonfrancesco: Microphysical analysis of polar stratospheric clouds observed by lidar at McMurdo, Antarctica

No.98-14
Mette Dahl Mortensen: The backpropagation method for inversion of radio occultation data

No. 98-15
Xiang-Yu Huang: Variational analysis using spatial filters

No. 99-1
Henrik Feddersen: Project on prediction of climate variations on seasonel to interannual timescales (PROVOST) EU contract ENVA4-CT95-0109: DMI contribution to the final report:Statistical analysis and post-processing of uncoupled PROVOST simulations

No. 99-2
Wilhelm May: A time-slice experiment with the ECHAM4 A-GCM at high resolution: the experimental design and the assessment of climate change as compared to a greenhouse gas experiment with ECHAM4/OPYC at low resolution

No. 99-3
Niels Larsen et al.: European stratospheric monitoring stations in the Artic II: CEC Environment and Climate Programme Contract ENV4-CT95-0136. DMI Contributions to the project

No. 99-4
Alexander Baklanov: Parameterisation of the deposition processes and radioactive decay: a review and some preliminary results with the DERMA model

No. 99-5
Mette Dahl Mortensen: Non-linear high resolution inversion of radio occultation data

No. 99-6
Stig Syndergaard: Retrieval analysis and methodologies in atmospheric limb sounding using the GNSS radio occultation technique

No. 99-7
Jun She, Jacob Woge Nielsen: Operational wave forecasts over the Baltic and North Sea

No. 99-8
Henrik Feddersen: Monthly temperature fo-recasts for Denmark - statistical or dynamical?

No. 99-9
Thejll, K. Lassen: Solar forcing of the Northern hemisphere air temperature: new data

No. 99-10
Torben Stockflet Jørgensen, Aksel Walløe Hansen: Comment on "Variation of cosmic ray flux and global coverage - a missing link in solar-climate relationships" by Henrik Svensmark and Eigil Friis-Christensen

No. 99-11
Mette Dahl Meincke: Inversion methods for atmospheric profiling with GPS occultations

No. 99-12
Benzon, Hans-Henrik; Olsen, Laust: Simulations of current density measurements with a Faraday Current Meter and a magnetometer

No. 00-01

Høeg, P.; Leppelmeier, G: ACE: Atmosphere Climate Experiment: proposers of the mission

No. 00-02
Høeg, P.: FACE-IT: Field-Aligned Current Experiment in the Ionosphere and Thermosphere

No. 00-03
Allan Gross: Surface ozone and tropospheric chemistry with applications to regional air quality modeling. PhD thesis

No. 00-04
Henrik Vedel: Conversion of WGS84 geometric heights to NWP model HIRLAM geopotential heights

No. 00-05
Jérôme Chenevez: Advection experiments with DMI-Hirlam-Tracer

No. 00-06
Niels Larsen: Polar stratospheric clouds micro
physical and optical models

No. 00-07
Alix Rasmussen: "Uncertainty of meteorological parameters from DMI-HIRLAM"

No. 00-08
A. L. Morozova: Solar activity and Earth's weather. Effect of the forced atmospheric transparency changes on the troposphere temperature profile studied with atmospheric models

No. 00-09
Niels Larsen, Bjørn M. Knudsen, Michael Gauss, Giovanni Pitari: Effects from high-speed civil traffic aircraft emissions on polar stratospheric clouds

No. 00-10
Søren Andersen: Evaluation of SSM/I sea ice algorithms for use in the SAF on ocean and sea ice, July 2000

No. 00-11
Claus Petersen, Niels Woetmann Nielsen: Diagnosis of visibility in DMI-HIRLAM

No. 00-12
Erik Buch: A monograph on the physical oceanography of the Greenland waters

No. 00-13
Steffensen: Stability indices as indicators of lightning and thunder

No. 00-14
Bjarne Amstrup, Kristian S. Mogensen, Xiang-Yu Huang: Use of GPS observations in an optimum interpolation based data assimilation system

No. 00-15
Mads Hvid Nielsen: Dynamisk beskrivelse og hydrografisk klassifikation af den jyske kyststrøm

No. 00-16
Kristian S. Mogensen, Jess U. Jørgensen, Bjarne Amstrup, Xiaohua Yang and Xiang-Yu Huang: Towards an operational implementation of HIRLAM 3D-VAR at DMI

No. 00-17
Sattler, Kai; Huang, Xiang-Yu: Structure function characteristics for 2 meter temperature and relative humidity in different horizontal resolutions

No. 00-18
Niels Larsen, Ib Steen Mikkelsen, Bjørn M. Knudsen m.fl.: In-situ analysis of aerosols and gases in the polar stratosphere. A contribution to THESEO. Environment and climate research programme. Contract no. ENV4-CT97-0523. Final report

No. 00-19
Amstrup, Bjarne: EUCOS observing system experiments with the DMI HIRLAM optimum interpolation analysis and forecasting system